0261

REFERENCE COPY

NUSC Technical Document 7036
5 August 1991

The Near-Field Flow and Drag on Cylindrical Bodies Moving Concentrically Inside Very Long Tubes

Richard F. Hubbell
Launcher and Missile Systems Department

DTIC
SELECTED
JUN 1 5 1995
F

DTIC QUALITY INSPECTED 3

Naval Underwater Systems Center
Newport, Rhode Island • New London, Connecticut

Approved for public release; distribution is unlimited.

19950613 042

PREFACE

This document is a version of the author's Ph. D. dissertation, which was completed and published in 1989. This version is substantially identical in content to the original dissertation; some reformatting and some minor editing have been done.

REVIEWED AND APPROVED: 5 AUGUST 1991

W. A. McNally
Head, Launcher and Missile Systems Department

REPORT DOCUMENTATION PAGE

Form Approved
OMB No. 0704-0188

Public reporting burden for this collection of information is estimated to average 1 hour per response, including the time for reviewing instructions, searching existing data sources, gathering and maintaining the data needed, and completing and reviewing the collection of information. Send comments regarding this burden estimate or any other aspect of this collection of information, including suggestions for reducing this burden, to Washington Headquarters Services, Directorate for Information Operations and Reports, 1215 Jefferson Davis Highway, Suite 1204, Arlington, VA 22202-4302, and to the Office of Management and Budget, Paperwork Reduction Project (0704-0188), Washington, DC 20503.

1. AGENCY USE ONLY (Leave blank)	2. REPORT DATE	3. REPORT TYPE AND DATES COVERED
	5 August 1991	

4. TITLE AND SUBTITLE
The Near-Field Flow and Drag on Cylindrical Bodies Moving Concentrically Inside Very Long Tubes

5. FUNDING NUMBERS

6. AUTHOR(S)
Richard F. Hubbell

7. PERFORMING ORGANIZATION NAME(S) AND ADDRESS(ES)
Naval Underwater Systems Center
Newport Laboratory
Newport, RI 02841-5047

8. PERFORMING ORGANIZATION REPORT NUMBER
TD 7036

9. SPONSORING/MONITORING AGENCY NAME(S) AND ADDRESS(ES)

10. SPONSORING/MONITORING AGENCY REPORT NUMBER

11. SUPPLEMENTARY NOTES
Originally published in 1989 as the author's Ph.D. dissertation.

12a. DISTRIBUTION/AVAILABILITY STATEMENT
Approved for public release; distribution is unlimited.

12b. DISTRIBUTION CODE

13. ABSTRACT (Maximum 200 words)

A differential simulation based on the k- model of turbulence describing the flow field around a streamlined body traveling through fluid along the centerline of a closed-end tube has been used to predict drag coefficients for a range of Reynolds numbers and diameter ratios. The range of interest corresponds to torpedo/tube combinations of interest to the U.S. Navy. Pressure coefficients are also plotted as a function of axial position along the body. A finite difference solution of the inviscid flow field is also developed and presented. Comparison of inviscid pressure coefficients with viscous pressure coefficients reveals that the nose region displays essentially inviscid behavior. The viscous differential model verified the hypothesis that total drag on the body could be found by independent calculation of nose drag, cylindrical section drag and wake drag, proving that nose drag and tail drag are independent of the length of the cylindrical section. A one-dimensional control volume analysis was performed to predict drag coefficients as a function of Reynolds number. Experimental drop

14. SUBJECT TERMS
Fluid Mechanics Flow Theory
Hydrodynamics
Aerodynamics

DTIC QUALITY INSPECTED 3

15. NUMBER OF PAGES
194

16. PRICE CODE

17. SECURITY CLASSIFICATION OF REPORT	18. SECURITY CLASSIFICATION OF THIS PAGE	19. SECURITY CLASSIFICATION OF ABSTRACT	20. LIMITATION OF ABSTRACT
UNCLASSIFIED	UNCLASSIFIED	UNCLASSIFIED	SAR

13. ABSTRACT (cont'd)

tests were performed in water to benchmark the simulation. A brief analysis of and computer program for the unsteady portion of the body, assuming quasi-steady flow, are developed and presented.

Accesion For
NTIS CRA&I ☑
DTIC TAB ☐
Unannounced ☐
Justification .....
By .....
Distribution /
Availability Codes
Dist | Avail and / or Special
A-1

TABLE OF CONTENTS

	Page
LIST OF TABLES	iii
LIST OF ILLUSTRATIONS	iv
LIST OF SYMBOLS	vi
1 INTRODUCTION	1
1.1 Background	7
2 CONTROL VOLUME FORMULATION	25
2.1 Basic Assumptions	25
2.2 Application of Newton's Law	25
2.3 Solution for Constant Drag Coefficient	27
2.4 Drag Coefficient Estimate	28
2.5 Nose Drag Contribution	29
2.6 Tail Drag Contribution	30
2.7 Straight Section Drag Contribution	30
2.8 The Gap-Flow Analysis of Kotlow	32
2.9 A Numerical Analysis	33
2.10 Overall Drag Coefficient	34
2.11 Application to Design of the Experiment	34
2.12 Solution for Variable Drag Coefficient	36
Summary	37
3 EXPERIMENTAL FORMULATION	39
3.1 Methods of Obtaining High Model Reynolds Numbers	39
3.2 Feasibility of Testing in a Wind Tunnel	42
3.3 Drop Test Apparatus	46

3.4 Determination of Terminal Velocity..... 47
3.5 Determination of High Speed Movie Camera Settings... 48
3.6 Model Construction and Dimensions..... 49
3.7 Dimensionless Groups..... 52
3.8 Test Procedure..... 54
3.9 Reducing the Data..... 55
3.10 Presentation of Test Results..... 56
3.11 Curve-Fit Model..... 60
3.12 Experimental Accuracy..... 65
Summary..... 66

4 DIFFERENTIAL FORMULATION..... 69
4.1 Inviscid Analysis..... 69
4.2 Factors Affecting Viscous Differential Simulations.. 69
4.3 Numerical Approach..... 70
4.4 Basic Equations..... 71
4.5 Turbulence Model..... 73
4.6 Method of Solution..... 75
4.6.1 The Pressure-Correction Scheme..... 78
4.7 Discussion of Computer Simulation..... 79
4.8 Presentation and Discussion of Results..... 81
Summary..... 89

CONCLUSIONS AND RECOMMENDATIONS..... 91

REFERENCES..... 93

APPENDICES

A FLUID PROPERTIES AND EXPERIMENTAL CONSIDERATIONS..... 131

B DEFORING AND ACCELERATIUNG CONTROL VOLUME ANALYSIS... 149

C EXPERIMENTAL ACCURACY..... 151

D INVISCID ANALYSIS..... 157

E COMPUTER PROGRAMS:

E.1 UNSTEADY FORTRAN PROGRAM..... 167

E.2 INVISCID FORTRAN PROGRAM..... 169

E.3 TRI-DIAGONAL MATRIX FORTRAN PROGRAM..... 173

E.4 PRESSURE COEFFICIENT FORTRAN PROGRAM..... 174

BIBLIOGRAPHY..... 177

LIST OF TABLES

Table		Page
1	Displacement Thickness, Wind Tunnel and Water Tunnel.....	45
2	Model Specifications.....	51
3	Averaged Displacement of Models vs. Time.....	57
4	Comparison of Measured and Predicted Values.....	61
5	Comparison of Inviscid Hydrodynamic Mass with Experimentally Determined Values.....	64
6	RMS Experimental Errors.....	65
7	Diffusion and Source Terms.....	76
8	Grid Size and Inlet/Outlet Location Effects on Drag.....	80

LIST OF ILLUSTRATIONS

Figure		Page
1	Basic Torpedo Launch Configurations.....	98
2	Simplified Swimout Model.....	99
3	Velocity Profiles in the Annular Region, After Kotlow [10].....	100
4	Comparison of Experimental Drag Coefficients from Previous Studies.....	101
5	Boundary Layer on Tube Wall in a Wind Tunnel.....	102
6	Tube-Model Compared to Converging-Diverging Nozzle..	103
7	Drop Test Apparatus.....	104
8	Model Geometry.....	105
9	Distance, z, vs. Time, t, for the 625 Model.....	106
10	Distance, z, vs. Time, t, for the 750 Model.....	107
11	Distance, z, vs. Time, t, for the 875 Model.....	108
12	Control Volume with Accelerating Surface.....	109
13	Computed Drag Coefficients, C_d, vs. Gap Reynolds Number, Re_g.....	110
14	Free Body Diagram of the Model.....	111
15	Displacement, Velocity and Acceleration vs. Time for the 625 Model.....	112
16	Displacement, Velocity and Acceleration vs. Time for the 750 Model.....	113
17	Displacement, Velocity and Acceleration vs. Time for the 875 Model.....	114
18	Drag Coefficient vs. Time for the 625 Model.....	115
19	Inviscid Grid Layout for the 625 Model.....	116
20	Streamlines Used to Compute Pressure Coefficients for Inviscid Model.....	117
21	Inviscid Pressure Coefficient vs. Axial Position for the 625 Model.....	118

22 FLUENT Grid Layout for the 625 Model..... 119

23 FLUENT Grid Layout for the Short 625 Model..... 119

24 Pressure Coefficient vs. Axial Position for the Short 625 Model..... 120

25 Nose Pressure Coefficient vs. Axial Position for the Short 625 Model..... 121

26 Tail Pressure Coefficient vs. Axial Position for the Short 625 Model..... 122

27 Pressure Coefficient vs. Axial Position for the 625 Model..... 123

28 Nose Pressure Coefficient vs. Axial Position for the 625 Model..... 124

29 Tail Pressure Coefficient vs. Axial Position for the 625 Model..... 125

30 Velocity Profiles, Stations 13, 25, and 40 for the 625 Model..... 126

31 Velocity Profiles, Stations 56, 62, 74, and 100 for the Short 625 Model..... 127

32 Velocity Profile, Station 56 for the 625 Model Compared to Kotlow [10]..... 128

33 Profile Drag/Total Drag Ratio for the 625, 750, and 875 Models..... 129

LIST OF SYMBOLS

a.....area of model

A.....area of tube

a_o.....a constant defined in eq. 2-4a

a_{oe}.....an experimentally determined constant used in eq. 2-5

b_o.....a constant defined in eq. 2-4b

b_{oe}.....an experimentally determined constant used in eq. 2-4 and eq. 2-5

c.....speed of sound

C_d.....drag coefficient, $C_n + C_s + C_t$

C_{dt}.....drag coefficient at terminal velocity

C_n.....nose drag coefficient, eq. 2-9

C_s.....straight section drag coefficient, eq. 2-17

C_t.....tail drag coefficient, eq. 2-11

d.....diameter of model

D.....diameter of tube

D_e.....equivalent diameter, $D - d$

D_p.....profile drag also called pressure drag

D_τ.....shear drag

f_s.....modified Moody friction factor, eq. 2-15

F_b.....buoyant force, $\rho g \Lambda$

F_d.....drag force, $0.5 \rho C_d a V^2$

F_p.....pressure drag on straight section of the model

F_τ.....shear drag on straight section of the model

F_s.....drag on straight section of the model, $F_p + F_\tau$

F_t.....drag force on the tail of the model

g.....acceleration of gravity

h.....height of the annular gap, $D_e/2$

HL.....irreversible head loss

I.....moment of inertia

k.....turbulent kinetic energy

K_n.....pipe loss coefficient at nose

K_t.....pipe loss coefficient at tail

L.....length of model

L_e, L_{eff}.....effective length of model, Λ/a

L_n.....axial length of nose

L_s.....axial length of straight region

L_t.....axial length of tail

L_T.....length of tube

m.....mass of model, W/g

m_g.....mass of water in the annular gap, eq. 3-10

m_h.....hydrodynamic mass (of model), eq. 2-4c

M.....moment or molecular weight

p.....pressure

dp/dz.....axial pressure gradient

P.....power or production of turbulent kinetic energy

r.....radius

r^+.....dimensionless distance from wall, $\rho yw^*/\mu_l$

R.....gas constant

Re_β.....Reynolds number, annular tube flow, VD_e/ν

Re_d.....Reynolds number, based on model diameter, Vd/ν

Re_g, Re_w.....Reynolds number, annular gap, Vh/ν

Re_l.....Reynolds number, based on length, Vl/ν

Re_T.....Reynolds number in the tube, VD/ν

S.....displacement or surface area

S_ϕ.....source term in eq. 4-4

t.....time

T.....absolute temperature

T.....time to reach 98% of terminal velocity

u.....radial velocity component

u.....averaged gap velocity, $V/(\beta^2-1)$ in figure (12)

U.....time averaged velocity tensor

U_∞.....induced far field tube velocity (open tubes)

v.....theta velocity component,=0 axisymmetric flow

V, V_b.....model absolute velocity

V_g.....averaged gap velocity, same as u, eq. 3-11

V_t.....terminal velocity

w.....axial velocity

w*.....friction velocity, $(\tau_w/\rho)^{1/2}$

w.....averaged gap velocity, V/γ in figure (12)

W.....dry weight of model

W^+.....normalized axial velocity, w/w*

W_n.....net weight of the model, $W - F_b$

y.....radial distance from wall

z.....axial position

Z.....axial position of the model

C_1 = 1.44, C_2=1.92, σ_k=1.0, σ_ε=1.3 and C_μ=0.09, in eq. 4-3

Greek Symbols

α.....relaxation parameter

β.....diameter ratio, D/d

γ.....gap area/tube area, (A-a)/A

Γ_ϕ.....diffusion term in eq. 4-4

δ.....differential change

δ_T^*.....displacement thickness on tube wall

ε.....dissipation of turbulent kinetic energy

θ.....angle of attack

κ.....von Karman's constant

$\S$.....specific gravity of the model

Λ.....volume of model

μ.....molecular viscosity

ν.....kinematic viscosity

π.....pi

ρ.....density of fluid medium

τ.....shear stress

ϕ.....flow field property of interest, u,w,k or ε

ϕ.....potential function

ψ.....stream function

Ω.....net efflux of momentum

Subscripts

avg.....averaged (from data)

b.....body

c.....near wall point at which there is equilibrium

d.....drag or diameter

e.....experimental

g.....gap

h.....hydrodynamic

i.....inner, related to the surface of the model

i.....integer related to column number or inner

j.....integer related to row number

l.....laminar

L.....length

m.....measured or moment

n.....nose or net

o.....outer, related to the surface of the tube

p.....point (node) in the discretized flow domain

p.....pressure

s.....straight

t.....tail or terminal or turbulent

T.....tube

τ.....shear

v.....vehicle

w.....wall

Superscripts

*.....non-dimensional

n.....number of iterations

'.....correction term, e.g. p' is pressure correction

CHAPTER 1

INTRODUCTION

The purpose of this investigation was to extend present understanding of aerodynamic drag acting on cylindrical bodies traveling concentrically in circular tubes. The primary motivation for this study was that there existed a lack of detailed information related to the near flow field surrounding a vehicle moving through an incompressible medium within a very long concentric tube.

Considerable interest has been expressed within the mass transit research community (Dept. of Transportation) with respect to the near flow field encompassing a train during travel through a very long tube (tunnel). There is also interest in the U.S. Navy concerning the mathematically similar problem of pushing a torpedo out of a long over-sized tube. The work presented in this study has been tailored to the range of torpedo-tube combinations of most interest to the Navy.

Since much of the published literature on this subject is related to train-tunnels, a brief discussion of that application is presented. Several types of high-speed mass transit ground transport systems have been proposed. High-speed vehicles (usually trains) travel in enclosed guideways (usually tunnels) for significant distances. Since the vehicles travel at sufficiently low velocity it is

reasonable to regard the air medium as essentially incompressible (Mach number less than 0.2). The present analysis is then applicable.

The physics of the train-tunnel and torpedo-tube are such that fluid is forced (by the naturally developing pressure drop) to flow down the annular gap between the vehicle and the guideway to fill the void created at the back of the vehicle. Motion of the fluid is strongly coupled to the motion of the vehicle through the conservation mechanisms of mass and momentum. Specifically, an estimate of aerodynamic drag on the vehicle is desired. Since total drag is composed of two separate parts, i.e., shear drag and pressure drag, the relative contribution of each is also sought. It is anticipated that future work will investigate methods of reducing drag by understanding the predominant mechanisms using insight gained from this study.

Three main investigations were carried out to address the problem:

1. Integral Formulation, presented in Chap. 2
2. Experimental Formulation, presented in Chap. 3
3. Differential Formulation, presented in Chap. 4.

Let us discuss these three approaches here briefly.

INVESTIGATION #1

INTEGRAL FORMULATION

A simplified control volume approach was initially taken. Drag results are readily obtainable but lack the desired local detailed information about the velocity and pressure fields since this method forces one to deal with averaged quantities. It is certainly useful, however, to estimate the terminal velocity and tube length required to conduct a drop test using a particular tube-model pair.

A simplified engineering model, using hydraulic loss coefficients and pipe friction factors, was constructed. Since this simplified model assumed that vehicle drag coefficient was constant, i.e., not a function of velocity, the model was called the constant-C_d model. The constant-C_d model was based on Bernoulli type pressure drops in the nose region (very little shear losses), Kotlow's [10] integral method in the straight annular region, and Hoerner's [1] loss coefficient model for the tail. Total drag was obtained by adding the independently calculated drag components of the separate regions. The result is a simplified engineering model capable of reasonably reproducing the drag predicted in the more exact differential approach described in Investigation #3, with an enormous savings of time and effort.

INVESTIGATION #2

EXPERIMENTAL FORMULATION

Wind tunnel testing is not practical due to the requirement that the body move with respect to the fixed wall. A fixed body within the wind tunnel violates similarity of boundary conditions. Experimental studies were conducted using cylindrical bodies with hemispherical noses and conical tails to verify the analytical work. A suitable drop test apparatus, using a water filled tube, was designed and fabricated, similar to Hoppe and Gouse [11] and later by Nayak et al. [12]. By closing the end of the tube it is possible to simulate an infinitely long tube. This is because in an infinitely long tube there is no induced axial flow in the tube due to its infinite resistance to flow. A suitable guideway and release mechanism was designed and constructed. Results were obtained for gap Reynolds numbers (based on the annular gap) up to 2E4. High speed photography was used to construct a position vs. time history for the model from rest to terminal velocity. Terminal velocity was sufficiently high to ensure that turbulent flow had been established in the annular clearance.

INVESTIGATION #3

DIFFERENTIAL FORMULATION

The first step was a finite difference analysis to solve the axisymmetric inviscid velocity and pressure fields surrounding the body.

The main analytical effort was to conduct a differential analysis of the viscous flow field over a range of laminar and turbulent Reynolds numbers using the finite difference approach. After the velocity and pressure fields were determined the data were postprocessed to obtain forces on the surface of the body.

From the known velocity field, local shear stresses on the vehicle were obtained and integrated over the surface of the vehicle to obtain the overall axial component of the shear forces, briefly called shear drag. From the pressure field the axial component of overall pressure drag, also called form or profile drag, was obtained. Total drag was found by adding the overall shear and form drag.

Several simplifying assumptions were made during this study:

1. Incompressible flow
2. Quasi-steady flow past the body
3. Infinite tube length
4. Axisymmetric flow

At terminal velocity, the drag on the body equals the net

weight (weight in fluid minus weight of displaced water). Conversely, the differential analysis, in which the body is at the terminal velocity, should predict a drag force equal to the net weight from the drop-test experiment and, in fact, excellent agreement was obtained.

Drag coefficients for hydraulically smooth, streamlined bodies may be extrapolated with confidence for turbulent Reynolds numbers of 2E4 up to prototype values of 5E6 using a power-law relation.

A curve-fit of C_d versus Reynolds number has been proposed in this study for the closed environment of a tube-vehicle for the range of diameter ratios and turbulent Reynolds numbers of interest to the Navy.

1.1 Background

The problem of immediate interest to the U.S. Navy is the development of an accurate engineering model capable of predicting fluid drag on a torpedo during a "swimout" launch from a submarine torpedo tube. Swimout simply means the torpedo engine is started and the torpedo powers itself down the tube and exits into the ocean as shown[1] in figure 1a . figure 1b schematically shows a torpedo launching system, with a pump providing an external pressure gradient to push the torpedo out of the submarine. The external pressure gradient problem was not addressed in this study. This investigation was concerned with the flow problem shown in figure 1a only, a simplified model of which is presented in figure 2.[2]

This study features a differential computer model that incorporates a hemispherical nose and a conical tail fixed to the straight cylindrical section and thus complements and considerably extends all previous work. In addition, this study included the design of an experimental drop test apparatus that was built and utilized to collect time vs.

---

1. Figures are collected at the back of this document.

2. Later, in figure 8 , there is shown a cylinder of diameter, d, and length, L, having a hemispherical nose and conical tail on the centerline of a closed-end tube of diameter, D, and length, L_T. Other relevant parameters, such as absolute vehicle velocity, V, and average flow velocities, u and w, are shown and related in figure 12 .

distance data for actual scale models in the geometrical ratios of interest to the Navy. Before progressing into the details of this analysis, a historical background and the significance of a number of previous studies are presented, most of which have been on the subject of trains traveling through long tunnels.

Gouse [7] provides an excellent review of the early German work on the train-tunnel problem. The following discussion is offered with credit to [7]. One of the earliest German papers is by Weismann [14], who assumed that for an open tunnel drag would be proportional to $(V^2 - U_\infty^2)$ where U_∞ is an induced far- field velocity in the open tunnel (U_∞=0 for a very long tube). We now know, however, from Davidson [8] or Hammitt [20] and [35], that drag is proportional to $(V - U_\infty)^2$. Prandtl and some fellow researchers also did work on train-tube aerodynamic drag. Tollmein et al. published a paper [15] on the subject in 1927, as did Langer [16]. As discussed in [7], this group placed model train cars in a stationary wind tunnel. They made the assumption that drag could be found:

$$F_d = \frac{1}{2} \rho \, a \, C_d \, (V - U_\infty)^2 ,$$

where

F_d = model drag force

ρ = density of fluid medium

a = model cross-sectional area

C_d = model drag coefficient

V = model absolute velocity

U_∞ = induced far-field velocity in the tunnel.

They assumed C_d was only a function of train and tunnel geometry and Reynolds number based on $(V - U_\infty)$. They ignored the fact that they had violated the boundary condition of a moving inner wall, which, as discussed in Sect. 3.2, is very significant. They also ignored friction on the walls of the tunnel in the vicinity of the train, which turns out to be a fairly reasonable assumption, but they did not try to estimate its relative importance. They went on to relate pressure drops using the steady flow energy equation with pipe loss coefficients down the tunnel, which has subsequently been shown by a number of researchers to be acceptable. Some of these early deficiencies were addressed by Sutter [4]. He estimated the relative importance of wall friction in the vicinity of the train and found it to be negligible for large clearances and short tunnels. However, Kotlow [10] has shown that wall friction plays an important role for small clearances in both the open- and closed-end tunnels. Sutter also improved upon Tollmein's work by including the velocity in the gap, w, in his analysis. Sutter also did extensive testing involving trains entering and exiting tunnels. He then generalized his simple loss coefficient theory to include the transient as well as the steady state case. It is interesting to note from Sutter's work that maximum drag occurs approximately when the rear of the train enters the tunnel and then decreases to a steady value. For a 180 meter

train traversing a 3300 meter tunnel, approximately 2200 meters of travel are required to reach the steady value. Drag was calculated by measurement of engine power output. Rolling losses were predetermined by running the train in open spaces so that the tunnel effect could be isolated. Unfortunately, Sutter did not run the train into a very long tunnel that was completely blocked off on the far end and let it coast/brake to a stop after reaching steady state. Under these circumstances steady state would be reached very soon after the rear of the train entered the tunnel so that good data would be easily and safely collected. There was probably no reason to perform such a test since a long tunnel in Europe is 2 miles long. The present study examines the limiting case of zero induced flow, which remains to the present untested at full scale Re_d of 10^7. Scale model tests such as Davidson [8] in 1974 have been done up to Re_d of 200,000, and in 1972 the Jet Propulsion Laboratory at Caltech in Pasadena, California [17], reported scale model results up to Re_d=3E6.

Abramovich [5] and Hara [6] also developed loss coefficient models based on Sutter's data. More recently analytical work has been done by Gouse et al. [7], Davidson [8], Sud and Chaddock [9], and Kotlow [10]. Ref [7] and [8] used basic integral techniques combined with loss coefficient models to obtain drag. The significance of [8] was that compressibility effects were measured and analytically modeled. The integral technique applied to the incompressible

case was greatly improved by Sud [9] through use of an eddy viscosity model in the sublayer and von Karman's similarity hypothesis in the turbulent region. Sud extended the analysis to include the developing region. Kotlow [10] then extended Sud's analysis to include a wide range of blockage ratios and Reynolds numbers.

This investigation is essentially an extension of work done by Kotlow [10] concerning fluid dynamic drag on smooth cylindrical bodies traveling concentrically down very long fluid-filled tubes. Figure 3 shows the shapes of the velocity profile at various points in the flow field. Kotlow assumed the flow was steady and incompressible and that all walls were hydraulically smooth. This study makes the same assumptions. Whereas Kotlow assumed that flow enters the straight annular region in a rectangular velocity profile as in figure 3 , this study allowed for the simultaneous solution of the flow field in all regions, producing a realistically skewed velocity profile at the entrance to the straight annular region.

Experimental efforts to understand concentric turbulent annular tube flow were recorded as early as 1907, by Becker [50]. Quarmby [18] was successful in predicting friction factors for fully developed concentric turbulent annular tube flow. The theoretical results presented were for the range $6E3 \leq Re_{\beta} \leq 4.5X10^{4}$, for six values of β, ranging from 1.05 to 50, $Re_{\beta}=V(D-d)/\nu$. Quarmby [18] developed a basic approach

that was successfully extended to the case of the inner wall moving with respect to the outer wall. The technique is to use Deissler's equation for eddy diffusivity to obtain velocity profiles for the sublayer and von Karman's similarity hypothesis to obtain profiles in the turbulent layer. Quarmby [18] succeeded in obtaining reasonable agreement with his experimental results. Wilson and Medwell [19] extended the Quarmby [18] analysis by modeling the hydrodynamic boundary layer growth in the entry region for concentric turbulent annular tube flow using the momentum integral technique. The velocity profiles were determined by use of Reichardt's expression for eddy diffusivity which was adjusted for calculations near the wall by implementation of Van Driest's [32] damping factor. The successful analytical models of Quarmby [18] and of Wilson and Medwell [19] were combined and extended by Sud and Chaddock [9] to provide for a moving inner boundary. The drag coefficient predicted by Sud and Chaddock at $Re_d=10^6$ was adjusted using the 1/6 power law relation suggested by Gouse [7] to obtain a value corresponding to $Re_d=10^5$. The predicted coefficient was about 15% lower than the value given by Davidson [8], which was based on a compilation of independent experimental results produced by Grittner, Smith, JPL, Hoppe and Gouse. Davidson reduced and correlated these results to a common plot of drag coefficient versus area blockage ratio, shown in figure 4 . Sud and Chaddock speculated that neglect of entrance effects

and the use of a simplified model for the wake region in their analysis may have contributed to the discrepancy between their results and the correlation of Davidson.

In the author's opinion the work of Kotlow [10] is the best available analytical work done on this subject. Therefore, a brief description of Kotlow's analysis and the computer algorithm has been included. Kotlow [10] applied the model of turbulent flow developed by Sud and Chaddock [9] to obtain velocity profiles and pressure gradients at each axial station down the annulus. There are essentially two parts to the Kotlow analytical model, a fully developed region and an entry region. The fully developed model will be discussed first.

In the sublayer, Deissler's equation for eddy diffusivity was used to produce a first order ordinary differential equation in du^+/dy^+, including a damping factor, n^2, obtained from concentric tube experiments that accounts for the effect of the wall on turbulence. Runge-Kutta numerical integration was used to obtain the dimensionless velocity profiles in the sublayer. In the turbulent layer model Kotlow [10] used a second order ordinary differential equation in d^2u^+/dy^{+2}, obtained by Von Karman's similarity hypothesis combined with the Prandtl mixing length. Runge-Kutta was employed to perform the integration and produce dimensionless velocity profiles. Integration is continued as far as the axis of zero shear. Once the dimensionless velocity profile was found in

the fully developed region, local vehicle shear stress is calculated. Profile or pressure drag was found using a force balance on the fluid in the annular gap.

The momentum integral technique was used to locate each profile in the entry region, producing shear stress as a function of axial position. Entry shear drag was found by integrating local stresses over the surface area. Profile drag in the entry region was found by determining the local pressure gradient, computed by assuming irrotational flow in the inviscid core region, and assuming zero radial pressure gradient.

There are several important advantages of the differential approach used in this study over the integral techniques employed by Kotlow [10]. The main advantage is that by solving the entire flow field around the body in a single operation it is not necessary to make many of the assumptions necessary to carry out an integral analysis. For example, the velocity profile at the entrance to the straight annular region was assumed by Kotlow to be "slug" flow, figure (3). This study showed that the velocity profile at this location is actually skewed due to shear effects from the nose. This skewing produces the effect of shortening the developing or entry length. The differential calculations done in this study also do not require the assumption of irrotational flow in the inviscid core in the entry region, in order to calculate the pressure gradient. There are many other

assumptions that can be avoided in the matching and checking of velocity profiles, the details of which are very involved.

In the wake region, a pressure coefficient was calculated by Kotlow [10] similar to Sud and Chaddock [9] and Hammitt [20] based on Hoerner's data [1] of a model in free field flow. Wake drag was calculated by multiplying this pressure drop (rise) by the projected vehicle area. This study uses a sudden-expansion-in-pipe-flow analogy of the wake, in the integral analysis in Chap. 2. The differential solution in Chap. 4 of this study has the distinct advantage of not requiring the use of open environment data, or the pipe-flow analogy.

Kotlow's entry analysis showed that wall shear stresses start high at the inlet and rapidly decay in the axial direction. The developing pressure gradient also is quite high at the inlet but decays more slowly than shear stress. Consequently profile drag is more significant than shear drag in the entry length. Kotlow concludes that, quantitatively, the entry length is nearly negligible, since it raises the total drag by an inconsequential 3.0%. Based on this important conclusion it was assumed, in Chap. 2, that the flow was fully developed in the entire annular region.

Between 1920 and 1960 there was essentially no progress made until interest in smaller clearances and higher speeds started to arise. Much experimental work has been done, especially by the Japanese, who are interested in high speed

streamlined trains. Hoppe and Gouse [11] provide an excellent summary of early Japanese, French and Russian work. The following discussion is provided with credit to [11]. In the first important Japanese analysis, Kawaguti [21] used the Rayleigh analogy in an incompressible laminar flow analysis to obtain the drag of a train concentric to the tunnel. Kawaguti then extended the laminar analysis to the turbulent case by the use of the eddy viscosity concept. This general approach was later followed by Gouse [2]. Kawaguti used the experimental data of Miki [22] to obtain the proper eddy diffusivity coefficient. Hara [23] analytically predicted the aerodynamic forces acting on a train entering a tunnel. Actual drag data presented by Kawamura and Ono [24] had been previously taken. A transient one-dimensional inviscid flow problem taking into account compressibility was solved. A pressure wave propagates to the opposite end of the tunnel (and is then reflected back) when the nose of the train enters the tunnel. The solution by Hara continues until either the reflected pressure wave comes back to the nose of the train, or the rear of the train has entered the tunnel. By assuming a value for the train skin friction coefficient, taken to be constant and equal to the free environment value, the pressure drag coefficient and pressure distribution along the train axis was determined. Pressure data were taken by Hara and Okushi [25] while pulling a cylinder (d= 0.63 in, L= 2 ft) through a tube (D= 1.1 in, L_T= 19 ft). The model was

suspended on a piano wire that was stretched down the centerline of the tube. Measurements of static pressure along the wall of the tube were taken and correlated with various train nose and tunnel entrance shapes. Having the pressures along the wall allows for direct prediction of profile drag. Hara's original analytical model underpredicted profile drag since it was based on the lower value of free environment skin friction coefficient.

Hara [6] set out to improve the original analytical model by getting a better estimate of the transient skin friction coefficient as the model enters the tube. To accomplish this the pressure data mentioned above were used together with a one-dimensional analysis of the annular flow between the model and the tube. This method turned out to be very successful and Hara [26] presented pressure data and skin friction coefficients for specific Japanese railroad train-tunnel combinations. To complete his drag model Hara [27] incorporated the results of Miki [22] and Tanaka [28] for wind tunnel measurements of train afterbody drag. Hara [27] then offers an empirical drag coefficient equation, developed for the unique Japanese geometry (β=1.75).

Another Japanese author of note is Fukuchi [29], who studied drag on trains in very long tunnels. The one-dimensional approach of Hara was utilized. A drag coefficient model of reasonable accuracy was presented. The difficulty was in getting data for very long tubes, so the

model, being inherently empirical, was less accurate than Hara's model. Fukuchi [30] used the Hara approach to calculate drag on trains passing through underground train stations, and for the case of trains traveling in opposite directions inside the tunnel.

Similar one-dimensional models have been made for the French railroad by Nouvion [31], and for the Russian railroad by Abramovich [32]. All reported results are empirical and highly specific to the actual train-tunnel being tested.

Cromack [33] obtained data on $1/24^{th}$ scale slot cars in the open and going through tunnels in air. He was able to measure the instantaneous electrical power, P, required by the car and he obtained instantaneous velocity, V. Aerodynamic drag, F_d, was then calculated from, $F_d = P/V$. The result is good qualitative trends between different configurations but quite low quantitative predictions. Perhaps the fault is that the physical relation of the car to the track is too eccentric to be expected to conform to the standard concentric predictions. Eccentric tubes tend to require less pressure drop to produce the same flow rate through the annulus.

Experiments done by Gregorek and Engle [34] involve the deceleration of cylindrical models in a long horizontal tube. The models were propelled into the tube and the deceleration was measured. Drag force is then inferred from the deceleration of the model. Three model diameters were tested

(d=1.806 in, d= 2.089 in, d= 2.414 in) and three L/d ratios (10,20,30). The tube (D= 2.8 in, L_T= 180 ft) produced β=1.55, 1.34, 1.16 respectively. The models all had a streamlined boat tail afterbody and either a flat or ellipsoidal nose. The results of this experiment agree with the generally accepted results shown in figure 4 .

Hammitt [35] presents a basic one-dimensional analysis for the induced flow produced by a train traveling through a tunnel for both the steady and accelerating cases. He assumes that the vehicle drag coefficient is constant, i.e., unaffected by changing vehicle velocity. This assumption neglects the important Reynold's number dependence, which most investigators take as an axiom.

Perhaps the most impressive experimental effort to date as discussed by Kurtz [17] was the VICS (Vehicles in Confined Spaces) study conducted by Caltech, JPL in 1971-1973, for the DOT (Dept of Transportation). The VICS facility consists of three elaborately instrumented long vertical tubes, all D= 2.0 in, the VICS-32, VICS-70 and VICS-120, where the number denotes tube height, L, in feet. The VICS-70 is capable of producing Re_d up to 10^5. The investigators at JPL recognized that the actual near flow field is far more complicated than the usually employed one-dimensional analysis allows. Their idea was to develop a long vertical test facility so that terminal velocity could be measured with a high degree of precision. They also wanted detailed pressure data. In the

VICS-70 models are launched from a spring powered short stroke catapult accelerator to a velocity close to the terminal velocity. The first 50 feet of travel allows for small variations in model velocity to disappear and the model to settle down to the terminal velocity. The final 20 feet of travel are where most of the wall pressure and velocity readings are taken. In order to maintain pressure integrity in the tube during pressurized runs, a system of copper wire coils was placed around the outside of the tube. Permanent magnets were placed in the model in order to induce a voltage in the coil as the model passed by. Velocity was found from V= (distance between coils)/time. Static wall pressure was found from very accurate pressure transducers capable of giving a pressure profile as the model passed by. Test Reynolds numbers were increased by using CO_2 and Freon-12. More information on this method of increasing Re_d is contained in Appendix A. The facility was hydrostatically tested to 300 psig but operated only up to 165 psia (11 atm). Use of Freon at 70 psig and 70°F is delicate because it will liquefy, so a toggle valve was installed at the bottom of the tube to check for this possibility. Models typically weighed 25 pounds and were released with no spin. Their fall was guided by molded plastic runners to remain concentric (or eccentric, if desired). A special arrestor was constructed of cellulose sponge sections to absorb the model's kinetic energy at the end of the run.

In order to achieve Re_d = 3E6, for incompressible flow, the VICS-120 was constructed. It is attached to the outside of the 9 story Space Sciences Building (Bldg. 183) at the JPL. It is in a class all by itself, even considering the impressive VICS-70 just described. It is capable of operating at 50 atm and uses CO_2, N_2, Freon-12 or air as the working fluid. It is very flexible in terms of being able to test configurations requiring simultaneous movement of models in interconnecting tubes, as would be experienced in underground train systems. Porous wall sections can be added, as can wall elements with different roughness.

A gas gun catapult can launch a 50 pound model at 100 fps in 3 ft, with no spin. The model's travel was guided by plastic runners down the centerline of the tube (D= 2", L_T= 120 ft). Models typically travel at 10 - 100 fps. Velocity is measured by optical sensors used to form what Kurtz [17] calls speed traps created by the model breaking a light beam. The speed traps have a time resolution of 0.10 ms and an accuracy of 0.16 ms which allows precise velocity measurement up to 250 fps. Pressure signatures are produced by fast response (200 Hz) pressure transducers mounted on the wall of the tube. Great ingenuity went into the design of models intended to simulate actual train cars. Distributed roughness produced by coating the exterior of the model in 0.003 diameter polystyrene balls was used. Special grooving was fashioned to simulate door, windows and other openings.

The results of the JPL tests for the conditions assumed in the present study of infinitely long (closed-end) tubes are compared to the results of the differential section, Chap. 4, of this study. Good agreement was realized.

The author considers that many of the design concepts that went into the VICS-70 and VICS-120 are very significant with respect to the topic under study. The author researched most of the parameters that control the effectiveness of any experimental effort related to this topic. Significant topics include: choice of fluid medium, model design, guideways, release mechanisms, arrestors, velocity measurement and model stability considerations. The author of this report reached the conclusion that the JPL design is optimum in all these respects for steady state testing; however, it does have some important limitations which are briefly discussed.

The main objective of this study was to perform a detailed study of the flow field surrounding the model; this cannot be done by JPL, or any other test facility. The secondary objective of this study was to drop test models having specific geometries and values of dimensionless parameters to determine terminal velocity and drag. The drop test apparatus used in this study, Section 3.3, produced accurate, repeatable terminal velocity data, as verified by the differential simulation, Section 4.8. Since the Navy is interested in the launching of torpedoes, it is natural to be interested in transient velocity data. In this respect, the

drop test done in this study had the advantage over the steady-state-only-JPL in that transient model velocity data were collected and are presented in Section 3.10.

The JPL facilities, while capable of providing good tube wall pressure data, are not capable of providing pressure data at the model surface. In addition, JPL is incapable of directly providing detailed surface stress data on the model. The best they can do is back-calculate a total shear drag by subtracting pressure drag (assuming zero radial pressure gradient and using wall pressures) from total drag. Another major area that cannot be confidently addressed by JPL is the question of separation at the rear of the model.

The differential simulation done in this study overcomes all of the limitations just discussed, except the transient case, which was addressed experimentally. The author suggests that, by providing information on local surface distributions of pressure and shear as well as knowledge of separation, this study significantly contributes to the overall body of knowledge.

CHAPTER 2

CONTROL VOLUME FORMULATION

Sect. 2.1 Basic Assumptions

The purpose of this chapter is to present the first of three studies, a control volume formulation of the basic equation of motion for a cylindrical body falling through fluid in a long tube. This differential equation will then be solved both analytically and numerically and subsequently compared with both the experimental and numerical (differential) formulations.

The basic assumptions mentioned in Chap. 1 will be adopted here:

1. The flow is incompressible and viscous.
2. All surfaces are hydraulically smooth.
3. Unsteady hydrodynamic effects are modeled by a hydrodynamic mass term, m_h, developed in Appendix D.
4. The body falls vertically and concentrically.

The shear and pressure forces on the body will be approximated by simple one-dimensional flow arguments.

Sect. 2.2 Application of Newton's Law

A schematic of the geometry of the falling body is shown in figure 12 . Newton's second law, figure 14 , states that the summation of vertical forces on the body is proportional to its vertical acceleration:

$$\Sigma F = W_n - F_d = (m + m_h) \frac{dV}{dt} , \qquad 2\text{-}1$$

where W_n = net weight = $W - F_b$

F_d = drag force = see eq. 2-2

F_b = buoyant force = $\rho g \Lambda$

m = body mass = W/g

m_h = hydrodynamic mass = see eq. 2-4c

V = body velocity.

The body drag force can be modeled in terms of an overall drag coefficient referred to body velocity and cross-sectional area:

$$F_d = C_d \, a \, \frac{\rho}{2} V^2 . \qquad 2\text{-}2$$

In general, for a smooth surface, C_d is a function of body shape, Reynolds number, and tube-to-body diameter ratio, β, where $\beta = D/d$.

Combining eq. 2-1 and 2-2, the basic differential equation for body motion becomes

$$W_n = \frac{1}{2} \rho \, a \, C_d \, V^2 + (m + m_h) \frac{dV}{dt} , \qquad 2\text{-}3$$

subject to the initial condition $V=0$ at $t=0$. Eq. 2-3 may be solved analytically, if C_d is assumed constant, and numerically, if C_d varies with Reynolds number. These solutions may then be used to fix design conditions for the experimental formulation.

Sect. 2.3 Solution for Constant Drag Coefficient

Assume that the drag coefficient, C_d, is constant and equal to the drag coefficient, C_{dt}, at terminal velocity, V_t. Eq. 2-3 may then be solved in closed form by separation of variables and integration:

$$V = V_t \tanh(b_o t). \qquad 2\text{-}4$$

The parameter V_t is the terminal velocity of the falling body, which is reached within 99.5% when $b_o t > 3$.

$$V_t = a_o\, b_o = \left[\frac{2W_n}{C_{dt}\ \rho\ a}\right]^{1/2},$$

and

$$a_o = \frac{2(m + m_h)}{\rho\ C_{dt}\ a}, \qquad 2\text{-}4a$$

$$b_o = \frac{(W_n\ \rho\ C_{dt}\ a/2)^{1/2}}{m + m_h}; \qquad 2\text{-}4b$$

a value for m_h may be found from Appendix D:

$$m_h = \frac{\rho\ \Lambda}{\beta^2 - 1}, \qquad 2\text{-}4c$$

where Λ = volume of the model.

The displacement and acceleration are obtained from eq. 2-4:

$$S = \int V dt = a_o \ln[\cosh(b_o t)], \qquad 2\text{-}5$$

and

$$\frac{dV}{dt} = a_o \left[\frac{b_o}{\cosh(b_o t)}\right]^2.$$

Eq. 2-4 and 2-5 provide reasonable design estimates of body motion if combined with the next section, which develops an approximate method for predicting the (nearly constant) body drag coefficient, C_d.

Sect. 2.4 Drag Coefficient Estimate

Return to figure 12 and consider cross-sections 2-3-4-5, which divide the near-body flow field into three regions: the nose region (2-3), the straight section (3-4), and the tail region (4-5).

It is proposed to model the overall drag coefficient as the sum of nose, straight-section, and tail contributions:

$$C_d = C_n + C_s + C_t . \qquad 2\text{-}6$$

For the simple estimates which follow, the flow is assumed one-dimensional and steady, in a frame relative to a fixed body. In this frame the fluid approaches section 2 at velocity V and flows into the straight (gap) section 3-4, at velocity, w, called gap velocity, given by continuity:

$$w = V/\gamma, \qquad 2\text{-}7$$

where

$$\gamma = \frac{A-a}{A} = \frac{\beta^2-1}{\beta^2} = \frac{\text{gap area}}{\text{tube area}} .$$

Sect. 2.5 Nose Drag Contribution

Write the one-dimensional steady flow energy equation across the nose section (2-3):

$$p_n = \frac{p_2}{\rho} + \frac{V^2}{2} = \frac{p_3}{\rho} + \frac{w^2}{2} + HL_{2-3} ,$$

where HL denotes the head loss. We approximate section 2-3 as a 'duct entrance' and use the well-rounded entrance head loss from, e.g., White [39]:

$$HL_{2-3} = K_n \frac{w^2}{2} (1 - \gamma)^2 , \quad K_n \simeq 0.05 . \qquad 2\text{-}8$$

We neglect shear stress on the body nose and assume that the nose drag is given by $F_n \simeq (p_n - p_3)a$, where

$$(p_n - p_3) = \frac{\rho}{2} V^2 \left[\frac{1 + K_n (1-\gamma)^2}{\gamma^2} \right] .$$

This is equivalent to a nose drag coefficient of

$$C_n = \frac{2(p_n - p_3)}{\rho V^2} = \frac{1}{\gamma^2} + K_n \frac{(1-\gamma)^2}{\gamma^2} . \qquad 2\text{-}9$$

For example, when $\beta = D/d = 1.6$, eq. 2-7 gives $\gamma = 0.6094$, and then eq. 2-9 gives $C_n \simeq 2.71$.

Sect. 2.6 Tail Drag

Write the steady flow energy equation across the tail section (4-5):

$$\frac{p_4}{\rho} + \frac{w^2}{2} = \frac{p_5}{\rho} + \frac{v^2}{2} + HL_{4-5} \cdot$$

For the tail section we may approximate the head loss as a 'sudden expansion' where, from White [39]:

$$HL_{4-5} = K_t \frac{w^2}{2} (1 - \gamma)^2 \quad , \quad K_t \approx 1.0 . \qquad 2\text{-}10$$

In a similar manner to the nose-drag estimate, we approximate the drag on the tail as $F_t \approx (p_4 - p_5)a$, where

$$(p_4 - p_5) = \frac{\rho}{2} V^2 \left[\frac{(\gamma^2-1) + K_t (1-\gamma)^2}{\gamma^2} \right] .$$

This is equivalent to a tail drag coefficient of

$$C_t = \frac{2 (p_4-p_5)}{\rho V^2} = \frac{\gamma^2-1}{\gamma^2} + K_t \frac{(1-\gamma)^2}{\gamma^2} . \qquad 2\text{-}11$$

Continuing our example of β=1.6, $\gamma \approx 0.6094$, then eq. 2-14 predicts that $C_t = -1.28$, where the negative sign indicates a thrust or forward force.

Sect. 2.7 Straight Section Drag Contribution

A control volume enclosing the fluid within the gap

section (3-4) in figure 12 shows that there is no average momentum change because the entrance and exit velocities are equal, $v_3=v_4=w$. Then the net pressure force on the gap fluid is balanced by shear forces on the inner and outer surfaces of the gap fluid:

$$(p_3 - p_4)(A - a) = \pi d \int_{z_3}^{z_4} \tau_i \, dz + \pi D \int_{z_3}^{z_4} \tau_o \, dz . \qquad 2\text{-}12$$

This pressure drop, induced by flow through the gap, causes a pressure drag on the body, $F_p = (p_3 - p_4)a$. In addition, there is a shear force on the body, $F_\tau = \pi d \int \tau_i dz$, caused by the inner shear stress, τ_i. The total drag on the straight section is then $F_s = F_p + F_\tau$.

$$F_s = (p_3 - p_4)a + \pi d \int_{z_3}^{z_4} \tau_i \, dz . \qquad 2\text{-}13$$

To complete the analysis of the straight section requires correlations for (p_3-p_4) and τ_i. A simple approximation would be to form a Reynolds number based on gap velocity, w, and use the Moody chart, e.g., White [39], to estimate both pressure drop and wall shear. However, Kotlow [10] has made an extensive study of this gap flow, using a developing-flow analysis combined with a turbulent eddy viscosity formulation. His results are thought to be the most accurate available in the literature.

Sect. 2.8 The Gap-Flow Analysis of Kotlow

First, Kotlow [10] determines that little error is incurred by taking τ_i equal to a constant. Thus, the integral in eq. 2-13 is replaced by $(\pi d \tau_i L_s)$, where L_s is the length of the straight section, figure 12 . He then gives correlations involving two different Reynolds numbers:

1. For the body: $Re_d = Vd/\nu$,
2. For the gap flow: $Re_g = wD_e/\nu = \beta^2 Re_d/(\beta+1)$, 2-14

where $D_e = (D-d)$ is the hydraulic diameter of the gap. Kotlow correlates the pressure drop in the style of a Moody friction factor:

$$p_3 - p_4 = \frac{L_s}{D_e} \frac{\rho}{2} V^2 f_s , \qquad 2\text{-}15$$

where

$$f_s = \left[\frac{\beta^2+1}{2(\beta^2-1)}\right]^2 \left[0.001 + \frac{2.8}{(\log_{10} Re_g)^{3.1}}\right]$$

Meanwhile, Kotlow correlates the inner wall shear stress in terms of both body and gap Reynolds numbers, as follows:

$$\tau_i = \frac{\zeta(\beta+1)}{4(\beta+\zeta)} f_s \frac{\rho}{2} V^2 , \qquad 2\text{-}16$$

where $\zeta = 1.005\ \beta^{\chi}$,

and $\chi = 1.477 + 0.2195 \log_{10} Re_d$.

Kotlow [10] states that these correlations are accurate to ±3% in the range $10^5 < Re_d < 10^8$ and $1.0 < \beta < 2.0$. Once $(p_3 - p_4)$ and τ_i are computed from eq. 2-15 and 2-16, the straight section drag coefficient is, by definition,

$$C_s = \frac{2 F_s}{a \rho V^2} . \qquad 2\text{-}17$$

These correlations are somewhat complex, but their evaluation is straightforward.

Sect. 2.9 A Numerical Example

Continuing our example of $\beta = 1.6$, or $d/D = 0.625$, let us assume, guided by experimental considerations, a body of diameter $d = 0.625$ in. moving in a tube of diameter $D = 1.0$ in. at a velocity of 56 in/s or 4.67 ft/s, in water with $\rho = 1.94 \text{slug/ft}^3$ and $\nu = 1.07\text{E-}05 \text{ft}^2/\text{s}$. Then the gap velocity, w, is 7.67ft/s, whence $Re_d = 22700$ and, since $D_e = 0.375$ in., $Re_g = 22400$. Let the straight section length be $L_s = 5.43$ in.

From eq. 2-15, $f_s = 0.0396$, whence $(p_3 - p_4) \simeq 12.1 \text{ lbf/ft}^2$. From eq. 2-15, $\zeta = 3.15$, whence $\tau_i \simeq 0.361 \text{ lb}_f/\text{ft}^2$. Then the drag on the straight section is, from eq. 2-13,

$$F_s = (12.1) \frac{\pi}{4} \frac{0.625^2}{144} + \pi \frac{0.625}{12} (0.361) \frac{5.43}{12}$$

$$= 0.0258 + 0.0267 \simeq 0.053 \text{ lb}_f . \qquad 2\text{-}18$$

This is equivalent, from eq. 2-17, to a gap-section drag coefficient of $C_s \simeq 1.17$. By comparison, a calculation using

these same input values in Kotlow's eddy-viscosity computer code gives F_s=0.058 lb_f and C_s=1.29, or 10% higher. The primary reason for the error is that the body Reynolds number of 22700 is below the value of 10^5 specified by Kotlow, whose correlations were intended for large-scale bodies.

Sect. 2.10 Overall Drag Coefficient

Combining the nose, tail, and gap sections, we estimate the overall drag coefficient of the body from eq. 2-9 and 2-11 to be

$$C_d = C_n + C_s + C_t ,$$

$$C_d = \frac{\gamma^2 + (K_n+K_t)(1-\gamma)^2}{\gamma^2} + C_s \ . \qquad 2\text{-}19$$

For the models tested here, K_n≈0 and K_t≈1, so:

$$C_d = \frac{\gamma^2 + (1-\gamma)^2}{\gamma^2} + C_s , \qquad 2\text{-}20$$

where C_s must be computed from Kotlow's correlations eq. 2-15 to 2-17.

For our continuing example with β=1.6, eq. 2-20 predicts that the overall C_d≈2.58. We will compare this estimate in Chap. 3 with the experimental results.

Sect. 2.11 Application to Design of the Experiment

The running numerical example used here approximates a body-tube combination proposed for experimental formulation:

d=0.625 in., D=1.0 in., L_s=5.43 in., made of aluminum, with W=0.164 lb_f and volume Λ=1.64 in^3. We wish this body, when dropped in water, to reach 98% of terminal velocity, V_t≈56in/s, in a distance of about 2 ft - to stay within the field of view of the high speed movie camera.

We have estimated above for this body that C_d≈2.58 at V=56in/s. We now use this value in the constant-drag-coefficient formulas, eq. 2-4 and 2-5, to check our estimates. The net weight of the body in water is:

$$W_n = W - \rho g \Lambda = 0.164 - (1.94)(32.2)(1.64/1728) = 0.105\ lb_f.$$

The hydrodynamic mass, m_h, is estimated from eq. 2-4c, the formula developed in Appendix D:

$$m_h \approx \rho\Lambda/(\beta^2-1) = (1.94)(1.64/1728)/(1.6^2-1) = 0.00118\ slug,$$

or

$$m + m_h = 0.164/32.2 + 0.00118 = 0.00627\ slug.$$

The body cross-section area is 0.00213 ft^2. Eq. 2-4 may be used to predict body terminal velocity:

$$V_t = \{2(0.105)/[(2.58)(1.94)(0.00213)]\}^{1/2} \approx 4.44 ft/s = \underline{53 in/s}.$$

This estimate is about 5% less than our initially guessed value of 56 in/s. If necessary, one could iterate to find a new Reynolds number and repeat the procedure. Or one could modify body weight, etc., to meet these conditions.

From eq. 2-4, the parameters $a_o \approx 1.17$ ft and $b_o \approx 3.78$ s^{-1} for the proposed-design input values. We see from 2-4 that $V = 0.98\ V_t$ when $(b_o\ t) = 2.298$; that is, $\tanh(2.298) = 0.98$. Then, from eq. 2-5, the distance traveled to reach this velocity is

$$S = a_o \ln[\cosh(b_o t)] = 1.17 \ln[\cosh(2.298)] = 1.89 \text{ ft} = \underline{23 \text{ in.}}$$

This is within the 2-ft field of view of the camera. Therefore, the proposed design seems adequate, at least by this simple constant-C_d analysis.

This estimate of distance traveled should actually be conservatively large, since we have used $C_d \approx C_{dt} = C_d$ at terminal velocity, whereas the actual $C_d(t)$ begins higher than C_{dt} and continually decreases to C_{dt}.

Sect. 2.12 Solution for Variable Drag Coefficient

Since Kotlow's gap-section correlation predicts that C_d varies with Reynolds number, it is expected that more accuracy could be obtained by solving eq. 2-3 numerically using a variable C_d as predicted by eq. 2-15 to 2-20. A computer program that uses the Runge-Kutta method to integrate eq. 2-3 is given in Appendix E.1. It is readily adaptable for any tube/model configuration that is desired. This program was applied to the proposed design body-tube combination discussed above and will be compared in Chap. 3

with the experimental data and with the constant-C_d approximation.

Summary

This chapter has presented a control volume analysis of a cylindrical body falling concentrically in a vertical tube. Using one-dimensional flow approximations plus a turbulent-gap-flow study by Kotlow [10], simple formulas are proposed for overall body drag, and a simple solution is given for velocity and displacement of the body. These formulas are used to verify input parameters for a proposed test configuration. The control volume theory will be compared with experimental data in Chap. 3 and also with more accurate digital computer model results in Chap. 4.

CHAPTER 3

EXPERIMENTAL FORMULATION

The purpose of this chapter is to present the second of three studies, the experimental formulation of a cylindrical body falling through fluid in a closed-end tube. The results of this experimental effort are compared to the results predicted by the control volume formulation and will be subsequently compared to the numerical (differential) formulation.

A brief example helps clarify the dynamic scope of the experimental problem. The prototype could consist of either a 10 foot diameter train traveling at 100 mph (147 fps) in air, or a 21 inch diameter torpedo traveling at 55 fps in water. In both cases, $Re_d=Vd/\nu \simeq 9E6$. Unfortunately, the model test could not achieve this high Reynolds number. The highest Reynolds number actually achieved in testing was only 22700. As discussed in the next two sections, very few practical options are available to realize high test Reynolds numbers.

Section 3.1 Methods of Obtaining High Model Reynolds Numbers

There are five options available to increase $Re_d=Vd/\nu$. The first three involve increasing the terminal velocity. Terminal velocity, V_t, from the theory in Chap. 2, eq. 2-4, can be rewritten as follows:

$$V_t \simeq \left[\frac{2\Lambda(\S-1)g}{a\ C_{dt}}\right]^{0.5}, \qquad 3\text{-}1a$$

or $V_t = K\,[(\S - 1)g]^{0.5}$, with $K = \left[\frac{2L_e}{C_{dt}}\right]^{0.5}$, 3-1b

where d = model diameter

a = model frontal area = $\pi d^2/4$

Λ = model volume

L_e = equivalent model length = Λ/a

$\S$ = specific gravity of the model

g = acceleration of gravity

C_{dt} = drag coefficient at terminal velocity.

Examining eq. 3-1b it is clear that terminal velocity, V_t, in a drop test can be raised by

Option #1: increasing model specific gravity, $\S$

Option #2: increasing model equivalent length, L_e

Option #3: decreasing drag coefficient, C_{dt}.

Option #1 indicates that, all else being equal, a model made of stainless steel, $\S$=7.66, will have a terminal velocity 1.7 times larger than a model made of aluminum, $\S$=2.78. As discussed later in more detail, it was decided to use aluminum because it is much easier to machine and drill. The choice of $\S$=2.78 meant that option #1 was not fully utilized to increase terminal velocity.

Option #2 indicates that models with a long effective length, L_e (i.e., large Λ and small a) will have the highest terminal velocity. However, large values of model length, L, require long tube lengths, L_T, which is not practical. It was also decided to independently vary β=D/d and to fix L such

that certain dimensionless parameters would remain constant as discussed in Sect. 3.7, "Dimensionless Groups," later in this chapter. Option #2 was therefore not used to increase terminal velocity.

Option #3 was implemented by the use of a streamlined model geometry, as described in Sect. 3.6.

Option #4 is to increase $Re_d=Vd/\nu$ through large model dimensions,i.e.,large model diameter, d. This might partially compensate for lower terminal velocities arising from the choices made by the author as discussed under options #1, #2 and #3 above. The limitations associated with large model dimensions were discussed under option #2.

Option #5 is the last method to increase $Re_d=Vd/\nu$, which is to decrease the kinematic viscosity, ν, of the test fluid. This method would allow for the desired relatively small model dimensions and low terminal velocities. Given that the model might consist of a 1 in. diameter cylinder traveling at 5 fps, for Re_d=9E6 the fluid should have a viscosity on the order of 4.7E-8 ft^2/s, which is a factor of about 225 less than water. Appendix A contains several rather complete tables of kinematic viscosities for both gases and liquids and discusses methods of achieving low viscosities. The conclusion drawn in Appendix A is that there is no simple practical method available for producing such a low viscosity.

Based on the limited options to significantly raise

Re_d, given the choice of small streamlined aluminum models traveling at low terminal velocities, it was decided to use a simple drop test consisting of a wire-guided aluminum model with water as the working fluid.

The only other readily available experimental option open to the author was to consider wind tunnel testing. For reasons discussed in the next section wind tunnel testing was not used during this study.

Section 3.2 Feasibility of Testing in a Wind Tunnel

A brief calculation shows that in a wind tunnel (with V=100 ft/s, d=3.0" and ν=1.65E-4 ft^2/s) $Re_d=Vd/\nu=1.5E5$, which is about 6.7 times larger than the maximum Re_d=22700 achieved in the drop test. While this larger Reynolds number is obviously desirable, there are two main reasons why wind tunnel testing was not done.

Reason #1. Violation of Boundary Conditions

For kinematic similitude to exist, one must arrange for a moving wall in axisymmetric flow, which is essentially impossible. Therefore, wind tunnel data must be taken with stationary tube walls. These data will be reasonably good when $\beta=D/d$ is large, in which case the streamline pattern around the model is not adversely affected by the boundary layer growth on the tube walls due to the bulk flow in the tunnel. In the prototype there is no bulk flow through the tube. For the small values of β=1.14, 1.33 and 1.6 of

interest to this study, streamline displacement is sufficient to alter drag.

Reason #2. Distorted Approach Velocity Profile

In the prototype, the boundary layer on the tube wall due to the moving body is confined essentially to the annular gap between the body and the wall. The fluid is at rest everywhere in the field except in the near field surrounding the body. However, in a wind tunnel, the bulk flow through the tunnel causes a boundary layer to build along the entire length of the tube wall. At the point where the bulk flow in the wind tunnel accelerates into the annular gap, the presence of the tube boundary layer distorts the velocity profile of the flow past the model. This distortion will be less objectionable for large β's but for the small clearances of interest to this study the profile distortion will produce unreliable drag results.

The rest of this section discusses the tube boundary layer in a wind or water tunnel. Estimates of the streamline displacement and tube boundary layer height are made and compared to the gap height, h=(D-d)/2. A table is presented summarizing sample calculations.

Fluid is displaced away from the tube wall by a distance, δ_T^*, called the displacement thickness. Estimate δ_T^* on the tube[1] wall using flat plate turbulent flow relations from White [39], figure 5 :

1. subscript: T = Tube

$$\frac{\delta_T}{z} = 8\,\frac{\delta_T^*}{z}, \qquad 3\text{-}2a$$

$$\text{where } \frac{\delta_T^*}{z} \simeq 0.16\left[\frac{Vz}{\nu}\right]^{-1/7}, \qquad 3\text{-}2b$$

for V = free stream velocity entering the tube

δ_T = boundary layer thickness on the tube wall, defined to be the radial distance from the wall where the fluid velocity is equal to 99% of V

δ_T^* = displacement thickness on the tube wall = $\delta_T/8$

z = axial distance along the tube measured from the entrance of the tube

ν = kinematic viscosity of the fluid medium.

Multiply eq. 3-2b by z/D:

$$\frac{\delta_T^*}{D} \simeq 0.02\left[\frac{z}{D}\right]^{6/7}\left[\frac{VD}{\nu}\right]^{-1/7}, \qquad 3\text{-}3a$$

$$\text{where } Re_T = \frac{VD}{\nu} = \frac{V\beta d}{\nu} = \beta\, Re_d. \qquad 3\text{-}3b$$

Multiply eq. 3-2a by z/D:

$$\frac{\delta_T}{D} = 8\,\frac{\delta_T^*}{D}. \qquad 3\text{-}3c$$

Examine the gap clearance, h, where h=(D-d)/2:

$$\frac{h}{D} = \frac{\beta-1}{2\beta}. \qquad 3\text{-}4$$

$$\text{Then, } \frac{\delta_T^*}{h} = \frac{\delta_T^*/D}{h/D} = \frac{\text{eq. 3-3a}}{\text{eq. 3-4}}. \qquad 3\text{-}5$$

Multiply eq. 3-3c by D/h to get:

$$\frac{\delta_T}{h} = 8\,\frac{\delta_T^*}{h} . \qquad 3\text{-}6$$

Representative calculations from eq. 3-3 through eq. 3-6 for a wind tunnel and water tunnel are summarized in Table 1 .

Table 1. Displacement Thickness

Wind Tunnel and Water Tunnel

Variable	Equation	Air	Water
d		3.0 in.	3.0 in
β		1.6	1.6
D		4.8 in.	4.8 in
z/D		5.	5.
ν		1.65E-4 ft^2/s	1.07E-5 ft^2/s
V		100. fps	20. fps
Re_T	3-3b	2.4E5	7.5E5
δ_T^*/D	3-3a	1.35%	1.15%
δ_T/D	3-3c	10.8%	9.2%
h/D	3-4	18.8%	18.8%
δ_T^*/h	3-5	7.2%	6.1%
δ_T/h	3-6	57.6%	49.1%

Thus, for the values of d,β,D,z/D and ν of interest, the water tunnel tube boundary layer will occupy 49% of the annular gap and the wind tunnel 57%. The inlet profile distortion is apparently quite extensive. As β is further decreased from 1.6 down to 1.14, the inlet velocity profile engulfs the gap and there is total distortion.

The preceding considerations highlight the extremely difficult task of obtaining model data at prototype Reynolds numbers. The next section covers the actual model test consisting of a drop test, using water, with a short tube and three small wire-guided models.

Section 3.3 Drop Test Apparatus

The model started from rest and did a free-fall inside a water filled glass tube, figure 7 . Concentricity was ensured by the use of a guidewire passing down the centerline of the tube and threaded along the model centerline. The tube was made by Corning Glass Works and had a 1" inside diameter and was 6 ft. long (D=1.0", L_T=6.0 ft.).

The frame supporting the tube was built so that the tube could be made absolutely vertical to ensure that the body fell straight down to minimize any normal force (hence sliding friction) between the guidewire and the model. The frame was set on a pin at its base and then adjusted front-to-back by a set of turnbuckles. It was also adjusted right-to-left by a second set of turnbuckles. It was determined to be vertical by means of a carpenter's level held to the side of the tube.

At the bottom of the tube a hard rubber stopper with a small central hole for the guidewire was sealed into place by means of room temperature vulcanizing sealant (RTV). The top of the tube also had a similar hard rubber stopper with a

small central hole, which was firmly seated into the tube but was not sealed with RTV because it needed to be removed periodically to change models. The guidewire was 20 lb monofilament line that was stretched taut down the centerline of the tube by passing through the central holes of the hard rubber stoppers on either end of the tube. Another very small hole was made off the centerline in the top rubber stopper to allow a very small diameter (≈0.1mm) piece of monofilament line to pass through so that the model could be pulled back up the tube for the next run. This retrieval line was held by a solenoid operated plunger that was actuated at the beginning of each run to release the model. The solenoid mechanism and its power supply were built by the author out of standard parts available at retail electronics stores.

Section 3.4 Determination of Terminal Velocity

Various techniques were evaluated for determining terminal velocity, since it is such a critical parameter. In all cases the position of the model as a function of time was recorded. Velocity was inferred from accurate knowledge of distance and time. Using the constant-C_d model from Chap. 2, it was determined that the upper limit of terminal velocities was going to be about 5 fps. All position vs. time data presented in this report were taken using a high speed movie camera set at 100 frames/sec. The test set-up is schematically shown in

figure 7 .

The high speed movie camera had a built-in timing light and gave very repeatable position vs. time results, as presented in Sect. 3.10. It was attempted to get model location using an aluminum yardstick mounted to the wooden frame behind the glass tube containing the model. This method ended up providing only a rough check since the fine lines on the yardstick turned out to be unreadable on several of the films. Precise location of the model was determined by the technique described in Sect. 3.9. Elapsed time was precisely measured using a strobe light as a backup to the internal camera timing light.

Section 3.5 Determination of High Speed Movie Camera Settings

Reference is made to the case discussed in Sect. 2.11 "Application to Design of the Experiment." Equation 2-4 is used to calculate time, T=0.641 sec, required to reach 98% of terminal velocity. This is the time required to fall from rest to 23" of displacement. Also, solve V_t = 53 in./s from eq. 2-4, for use in determining camera speed. Through trial and error it was determined the model should move about 0.5 inches from one frame to the next frame to keep blurring to an acceptable minimum. Thus the camera was set at 100 frames per second. This setting happens to produce a convenient 0.01 sec/frame. The camera required 1 second to start up and reach a steady state film speed. Since T=0.641 sec, another

second was allowed to run the test, and one final second provided for the camera to coast to a stop. Thus, total camera time was 3 seconds or about 300 frames per run. At about 12 frames per foot of film length, this requirement translated into 25 feet of film per run. It also hints at the physical difficulty experienced manipulating large quantities of film to obtain position and time data.

Section 3.6 Model Construction and Dimensions

When building the models there was a problem drilling a very small diameter (0.02") hole down the length of the model to allow the guidewire to pass through, because small diameter drills have a very strong tendency to "wander" off the centerline and also to break. This problem was resolved by drilling a larger hole, d_h, down the centerline from each end, meeting in the middle. The larger drill "wandered" far less and didn't break like the small drills. Then at each end of the model a small bead was welded onto the model covering the 1/4" hole. The weld bead was then drilled to 0.02" to allow for the guidewire to pass through the centerline of the model. It was felt that this arrangement 1) created the least friction between the guidewire and the model since there was essentially only point contact at the ends vs. line contact through the entire model, 2) insured that the model was guided on its centerline, 3) was practical to implement.

An additional 0.017" diameter hole was drilled in each

model to accommodate the retrieval line. To minimize any adverse effects on the flow field, this hole was drilled perpendicular to the centerline about 3/8" from the apex of the cone, on the tail of the model.

Summarizing, figure 8 , three bodies (β=1.6, β=1.33 and β=1.14) were tested to get distance vs. time data while falling inside a 1.000" tube, figure 7 . They were called 625, 750 and 875, which corresponds to outside diameters of 5/8, 3/4 and 7/8 inches, respectively. All the bodies had a hemispherical nose, cylindrical mid-body, and a conical tail (also referred to as the nose, straight and tail sections respectively). Table 2 lists relevant model geometries and properties, which are sketched in figure 8 . Note that Λ is the volume of water the model displaced in a ready-to-run condition and that terminal velocities are the experimentally obtained values.

Table 2. Model Specifications[2]

	Body 625	Body 750	Body 875
Model Parameters			
Diameter, d (in.)	0.625	0.750	0.875
Center hole, d_h (in.)	0.125	0.125	0.125
L_n (in.)	0.313	0.375	0.438
L_s (in.)	5.433	3.453	1.588
L_t (in.)	1.38	1.375	1.485
$L=L_n+L_s+L_t$ (in.)	7.125	5.203	3.510
Frontal area, a ($in.^2$)	0.307	0.442	0.601
Displaced Vol., Λ ($in.^3$)	1.64	1.79	1.37
$L_e = \Lambda/a$ (in.)	5.33	4.05	2.27
Dry weight, W (lb)	0.1640	0.1796	0.1377
Buoyant force, F_b (lb)	0.0591	0.0646	0.0494
Net wt, $W_n = W-F_b$ (lb)	0.1050	0.1150	0.0884
Term. Vel., V_t, (in/s)	55.1	30.5	9.0
Primary Dimensionless Groups (evaluated at V_t)			
$\Pi_2 = \Lambda/D^3$	1.64	1.79	1.37
$\Pi_3 = gD/V_t^2$	0.123	0.413	4.88
$\Pi_4 = Re_T = V_tD/\nu$	3.63E4	2.E4	5.77E3
$\Pi_5 = \beta = D/d$	1.600	1.333	1.143
$\Pi_6 = S$	2.78	2.78	2.78
Secondary Dimensionless Groups (evaluated at V_t)			
$\Pi_1 = W_n/(\rho V_t^2 D^2)$			
$= \Pi_2\Pi_3(\Pi_6-1)$	0.358	1.32	11.9
$\Pi_7 = Re_d=V_td/\nu=\Pi_4/\Pi_5$	2.27E4	1.5E3	5.E3
$\Pi_8 = L_e/d = (\Pi_5^3\Pi_2)4/\pi$	8.53	5.40	2.60
$\Pi_9 = C_d = (\Pi_5^2\Pi_1)8/\pi$	2.34	5.97	39.6

A discussion of the dimensionless groups Π_1 through Π_9 is presented in the next section.

---

2. Fluid is water, ρ = 1.938 slugs/ft^3, ν=1.07E-5 ft^2/sec, μ = 2.074E-5 slug/ft-sec

Section 3.7 Dimensionless Groups

The problem of a model falling in a tube can be functionally described by $f(F_d, \S, \Lambda, g, \rho, \mu, D, d, V)=0$, where

F_d = drag force on the model (ML/t^2)

$\S$ = specific gravity of the model (1)

Λ = displaced volume of the model (L^3)

g = acceleration of gravity (L/t^2)

ρ = density of fluid (M/L^3)

μ = dynamic viscosity of fluid (M/Lt)

D = tube diameter (L)

d = model diameter (L)

V = model velocity (L/t).

Using ρ, V, D the following dimensionless groups appear:

$$\Pi_1 = F_d/(\rho V^2 D^2)$$

$$\Pi_2 = \Lambda/D^3$$

$$\Pi_3 = gD/V^2$$

$$\Pi_4 = Re_T = \rho VD/\mu$$

$$\Pi_5 = \beta = D/d$$

$$\Pi_6 = \S.$$

Functionally, the problem may be expressed as follows:

$$\Pi_1 = g(\Pi_2, \Pi_3, \Pi_4, \Pi_5, \Pi_6).$$

It is clear that Π_2, Π_5 and Π_6 are fixed through the choice of a model and a tube. For this study,

$\Pi_2 \approx 1.65$ for all cases. This value is of the greatest interest to the Navy, corresponding to a 21" diameter torpedo in a 27" diameter tube. The actual

experimental value varied ±15% due to the problem of drilling the central guidewire hole per Sect. 3.6.

D = 1.00" fixed tube diameter.

§ = 2.78, aluminum models.

d = 0.625", 0.750", 0.875" fixed model sizes, corresponding to β=1.6,1.33,1.14 defined by specific torpedo-tube combinations of interest to the Navy.

Examining Π_1, Π_3 and Π_4 it appears that the dimensional problem is to determine drag force, F_d, as a function of velocity, V, for a particular model (§,d,Λ) in a fixed tube (D) and predetermined fluid (ρ,μ).

It is possible to recast the dimensionless problem into more familiar terms.

Let $\Pi_7 = Re_d = Vd/\nu = \Pi_4/\Pi_5$,

and $\Pi_8 = L_e/d = \Lambda/ad = (\Pi_5^3\Pi_2)4/\pi$.

At terminal velocity, V_t, it is known that $F_d=W_n$, i.e., drag force equals the net weight of the model, where

$$W_n = g\rho(\S-1)\Lambda = \Pi_2\Pi_3(\Pi_6-1)\rho V^2D^2,$$

or $\Pi_1 = W_n/(\rho V_t^2D^2) = \Pi_2\Pi_3(\Pi_6-1)$, at V_t only.

It is customary to define a drag coefficient, C_d, in terms of model velocity, V, and model frontal area, $a=d^2\pi/4$:

$$\Pi_9 = C_d = 2F_d/(\rho V^2 a) \text{ , at all times,}$$

and $\Pi_9 = (\Pi_1\Pi_5^2)8/\pi$, at terminal velocity only.

The dimensionless problem then becomes finding the function, h, where

$$C_d = h(Re_d, \beta, L_e/d, \text{fluid}),$$

or $\Pi_9 = h(\Pi_2, \Pi_3, \Pi_4, \Pi_5, \Pi_6)$.

Experimentally, only one point of this function was obtained for each model. This point corresponded to the terminal velocity where the exact value of the drag force, F_d, is known. As discussed further in Chap. 4, the function h was predicted using the constant-C_d model and compared to predictions made by the more accurate numerical model.

Section 3.8 Test Procedure

A typical run proceeded as follows:

1. Initialize the model. Using the retrieval line the model would be gently pulled back up the tube to a preset position, at the top of the camera window. At this point the retrieval line would be placed under the solenoid operated release mechanism.

2. Lights. Proper light levels were critical to prevent under or overexposure of the film. Due to the short time each frame was exposed, high powered lights had to be used.

3. Camera. The high speed movie camera required about 1 second to come up to speed, so at this point the camera switch was manually activated.

4. Action. The model was released by activating the solenoid that held the retrieval line. At the same time a strobe light started up to mark the beginning of the run on the film.

5. End of run. Camera and lights were shut off.

6. Record run number and make notes of camera speed, body number, etc.

The camera had to be focused very precisely or else the nose of the model was in focus while the side of the model closest to the camera was blurry. Focus was an important consideration when reducing the data as described below.

Section 3.9 Reducing the Data

Data were obtained by examining the film using a microfiche machine. This allowed the developed film to be viewed one frame at a time on an enlarged screen. The nose of the model had to be in sharp focus and the level of film exposure was critical. A measurement was taken of the body length on the screen, which was compared to the precisely known actual model length, so that a scale could be made. Then for each frame the distance the nose moved from the previous frame, called δS, was measured to within 0.01 inch and was recorded. Each frame also had a timing mark on the border recorded by the internal strobe light in the camera. Elapsed time from the previous frame, called δ_t, was interpolated and recorded. This process continued frame-by-frame until the body disappeared off the screen. To ensure accuracy, the film was rewound to the beginning of the run and the whole process was repeated frame-by-frame. At the conclusion of the second reading the results were compared and differences were resolved by checking any frames in question. It was felt that

this procedure minimized self-error.

Section 3.10 Presentation of Test Results

After the data for each run had been tabulated into columns of δS and δT, as described above, they were entered in data files on the VAX 8600 super-minicomputer to facilitate graphing and presentation. It was found that the data were very repeatable for all three bodies. Tabulated displacement vs. elapsed time results for all three models are contained in Appendix A. The 625 model results are contained in Table A-4 . Table A-5 is a tabulation of results for the 750 model with Table A-6 tabulates results for the 875 model.

Table 3 presents a summary of time vs. average displacement for each of the three bodies, 625, 750 and 875. Asterisks are given for displacement when the model is at terminal velocity. For instance, it was estimated that the 875 model was at terminal velocity after it had traveled 2.05". However, the 750 model required 10.67 inches and the 625 a full 19.63 inches to reach terminal velocity. These results are compared to the constant-C_d model composed of eq. 2-5 and eq. 2-20, in Sect. 3.11.

There had been some concern that the model would fall at slightly different rates due to very small changes in angle of attack, θ, as it went down the guidewire, but there was no discernible hint of this in the data. It is probably a secondary effect.

Table 3. Averaged Displacement of Models vs. Time

Time sec.	Model 625 Z_{avg} in.	Model 750 Z_{avg} in.	Model 875 Z_{avg} in.
0.00	0.00	0.00	0.00
0.01	0.02	0.01	0.01
0.02	0.06	0.03	0.03
0.03	0.12	0.06	0.07
0.04	0.19	0.11	0.13
0.05	0.29	0.19	0.19
0.06	0.41	0.29	0.25
0.07	0.56	0.39	0.31
0.08	0.74	0.51	0.38
0.09	0.91	0.62	0.46
0.10	1.09	0.74	0.56
0.11	1.30	0.89	0.64
0.12	1.55	1.06	0.72
0.13	1.77	1.25	0.80
0.14	2.03	1.45	0.89
0.15	2.29	1.63	0.97
0.16	2.59	1.83	1.06
0.17	2.90	2.08	1.14
0.18	3.19	2.31	1.23
0.19	3.52	2.53	1.31
0.20	3.90	2.78	1.40
0.21	4.27	3.05	1.50
0.22	4.67	3.28	1.59
0.23	5.07	3.55	1.68
0.24	5.47	3.78	1.77
0.25	5.87	4.07	1.87
0.26	6.29	4.33	1.96
0.27	6.68	4.59	2.05
0.28	7.14	4.86	***

Table 3. continued

Time sec.	Model 625 Z_{avg} in.	Model 750 Z_{avg} in.	Model 875 Z_{avg} in.
0.29	7.58	5.15	***
0.30	8.03	5.44	***
0.31	8.52	5.73	***
0.32	9.05	6.00	***
0.33	9.51	6.27	***
0.34	9.97	6.56	***
0.35	10.48	6.86	***
0.36	10.98	7.15	***
0.37	11.47	7.44	***
0.38	11.99	7.73	***
0.39	12.49	8.02	***
0.40	13.01	8.31	***
0.41	13.53	8.60	***
0.42	14.06	8.89	***
0.43	14.59	9.19	***
0.44	15.13	9.50	***
0.45	15.69	9.79	***
0.46	16.25	10.08	***
0.47	16.82	10.37	***
0.48	17.40	10.67	***
0.49	17.97	***	***
0.50	18.54	***	***
0.51	19.11	***	***
0.52	19.63	***	***
0.53	***	***	***

The displacement vs. time data for the 625 model have been plotted in figure 9 . It is seen from figure 9 that the

data correlate very closely to the averaged displacement, Z_{avg}. The error bands on figure 9 embrace the maximum and minimum displacement values for any individual run. The data are totally contained within a ±4% band around Z_{avg}, with a standard deviation of ±3%. Figure 9 also compares the constant-C_d prediction made from eq. 2-5 with Z_{avg}. Eq. 2-5 is consistently low, but at the worst is only off by 6%. It is thought that the constant-C_d model under-predicts displacement because the use of $C_d=C_{dt}$ over-predicts drag in the early stages of the run, when the velocity of the model is very small.

A variable-C_d model was discussed in Sect. 2.12 where C_d was allowed to vary with velocity, figure 18 , as opposed to being fixed at the terminal velocity value, C_{dt}. The results of the variable-C_d model as computed by the Runge-Kutta based computer program in Appendix E.1 are also shown in figure 9 for comparison to data and the constant-C_d model from eq. 2-5. It is seen from figure 9 that the variable-C_d model consistently under-predicts the data and eq. 2-5, being as much as 8% lower than Z_{avg} at terminal velocity. A possible explanation of this result is that the variable-C_d model assumes turbulent flow for the entire run, i.e., from release through terminal velocity. The consequence of this assumption is that drag is over-predicted during the initial displacement, causing the variable-C_d model to under-predict displacement. This under-prediction is slightly worse than

the constant-C_d model because the variable-C_d model predicts $C_d > C_{dt}$ up to the terminal velocity. It is concluded that the constant-C_d model is acceptable and preferred over the variable-C_d for routine engineering calculations in the startup region.

Figure 10 graphically displays test results for the 750 model. The maximum and minimum data are entirely contained in an envelope ±4% around Z_{avg} with a standard deviation of ±3%.

Figure 11 presents the test results for the 875 model. The maximum and minimum displacement for any particular run are found to be contained in a ±5% band with a standard deviation of ±4% with reference to Z_{avg}.

In Chap. 4 the constant-C_d model will be compared to the numerical model over a wide range of Reynolds numbers for β=1.6, 1.33 and 1.14.

Section 3.11 Curve-Fit Model

Although the constant-C_d model adequately predicted displacement of the model as discussed in Sect. 3.10, it is nice to have a little more accuracy during the acceleration phase of travel in order to more accurately predict velocity and displacement. It is proposed to use a least-squares-curve fitting process to determine the constants a_o and b_o in the constant-C_d model, eq. 2-4 and eq. 2-5. The coefficients a_o and b_o will be called a_{oe} and b_{oe} respectively.

Table 4 contains values of a_o, b_o, V_t and C_{dt} from the

constant-C_d model of eq. 2-4, eq. 2-5 and eq. 2-20. Table 4 also lists the least-squares-curve-fit a_{oe} and b_{oe}. It is noted that the curve-fit for a_{oe} and b_{oe} is very stiff, i.e., a fairly wide range of values for a_{oe} and b_{oe} will fit the data. Values for Re_d and Re_g come from eq. 2-14 at steady state velocity. Values for C_{dte}, given in eq. 3-9 later in this section, are given for convenience to provide a comparison to C_{dt}.

Table 4. Comparison of Measured and Predicted Values

Model	a_{oe} / a_o inches	b_{oe} / b_o sec^{-1}	V_{te} / V_t in/s	C_{dte} / C_{dt}	Re_d	Re_g
625 Model						
measured	13.67	4.03	55.1	2.34	22700.	22400.
predicted	15.61	3.59	56.0	2.26		
750 Model						
measured	6.09	5.01	30.5	5.94	14800.	11300.
predicted	5.55	5.52	30.6	5.90		
875 Model						
measured	0.715	12.6	9.0	40.1	5100.	3100.
predicted	0.686	12.9	8.9	41.5		

Figure 9 compares Z_{avg} to the curve-fit model for the 625 model. The curve-fit model varies only ±1% from Z_{avg}. Figure 10 presents Z_{avg} and the curve-fit for the 750

model, with a ±1% deviation. Figure 11 shows the curve-fit model varying ±2% from Z_{avg} for the 875 model. Once the curve-fit model has been verified,it is possible to make very accurate predictions of displacement, velocity and acceleration during the acceleration phase, using a_{oe} and b_{oe} in eq. 2-4 and 2-5. This has been done for the 625 model and the results are given in figure 15 . For example, referring to figure 15 , when t=0.3 s the acceleration of the 625 model is about 39 in./s^2, velocity is roughly 46 in./s and the model has moved a total of approximately 8 inches from the time it was released. At t=0.6 s, the 625 model is at 54 in./s and has traveled 23 in. This result was predicted in Sect. 2.11 using the constant-C_d model.

Figure 15 is also useful for determining when the 625 model is at terminal velocity. It is noted, from eq. 2-3, that at the moment the model is released, acceleration is always equal to $W_n/(m+m_h)$. In the next instant after release, when the model has a velocity greater than zero, the acceleration begins to fall due to drag. Thus, it is possible to establish a criterion for terminal velocity defined as the model velocity when acceleration goes below 0.01g or about 4 in./s^2. Looking at figure 15 it is seen that the acceleration of the 625 model has fallen under 4 in./s^2 at t=0.6 sec.; similarly for the 750 model, figure 16 predicts terminal velocity of about 30.5 in./s occurring at t=0.46 sec when displacement is about 11 inches. The 875 model results

are given in figure 17 where the terminal velocity of 9 in./s occurs when t≈0.3 sec. and displacement is a little over 2 inches.

Once data are available it is possible to get an experimentally determined hydrodynamic mass and drag coefficient from the curve-fit constants a_{oe} and b_{oe}. Solve eq. 2-4a for hydrodynamic mass and eq. 2-4b for terminal drag coefficient, called m_{he} and C_{dte}, in terms of a_{oe} and b_{oe}.

Using eq. 2-4: $V_{te} = a_{oe} b_{oe}$, 3-7

$$m_{he} = \frac{W_n}{V_t b_{oe}} - \frac{W}{g}, \qquad 3\text{-}8$$

$$C_{dte} = \frac{2W_n}{\rho a V_{te}^2}. \qquad 3\text{-}9$$

From Appendix D, $m_g = m_h (\beta^2 - 1)^2$, 3-10

where m_g is the mass of the fluid in the annular gap created by the cylindrical section between the model and the tube wall. Comparing eq. 3-9 with eq. 2-3 indicates that the only difference between C_{dte} and C_{dt} is the choice of terminal velocity to be used, i.e., V_{te} or V_t respectively. Table 5 compares values for m_h found using simple inviscid theory, from eq. 2-4c, with values of m_{he} from eq. 3-8. Because of the stiffness of the equations resulting in a wide range of acceptable values of a_{oe} and b_{oe} causing a wide range in m_{he}, it is only possible to conclude qualitatively that as β

decreases m_{he} approaches m_h. Values for m_g, the mass of fluid in the gap, found using eq. 3-10, are given for comparison purposes.

Table 5. Comparison of Inviscid Hydrodynamic Mass with Experimentally Determined Values

Equation		2-4c	3-8	3-10			3-9
	m	m_h	m_{he}	m_g	m_h/m	m_{he}/m	
Model	slugs	slugs	slugs	slugs	%	%	C_{dte}
625	5.09E-3	1.18E-3	4.93E-4	2.87E-3	23.2	9.7	2.34
750	5.58E-3	2.58E-3	3.45E-3	1.56E-3	46.2	61.9	5.94
875	4.28E-3	5.00E-3	5.08E-3	4.70E-4	117.	119.	40.1

Since β is minimum for the 875 model and maximum for the 625 model, Table 5 clearly shows that as the gap decreases in annular height ($\beta \to 1$) the hydrodynamic mass of the model increases. This is due to the requirement that the fluid be accelerated to a higher gap velocity, V_g, where from continuity $(A-a)V_g = aV$, which gives

$$V_g = \frac{V}{\beta^2 - 1}, \qquad 3\text{-}11$$

which in turn requires a greater pressure drop.

Section 3.12 Experimental Accuracy

Details of the calculations used to determine the level of experimental accuracy are provided in Appendix C. The results are summarized in Table 6 for convenience:

Table 6. RMS Experimental Errors

Variable	RMS error
S, Z	1.4%
V, V_{te}	3.4%
C_{dte}	7.2%
Re_d	3.4%
β	0.5%
d	0.2%
a	0.4%
D	0.5%
A	1.0%
W	0.8%
W_n	2.4%
ρ	0.5%
ν	0.5%
Λ	2.2%
m	0.8%
m_h	2.5%
a_o	8.6%
b_o	11.2%
a_{oe}, b_{oe}	25.0%
m_{he}	25.4%

It is recommended that future investigators attempt to determine terminal velocity, V_{te}, as accurately as possible, since errors in V_{te} cause considerable problems estimating C_{dte}.

Because the model tends to approach V_{te} asymptotically, there is always a very slight acceleration at the end of any run. The present study was carried out using extreme care to minimize the error in V_{te}. This was done by using great care measuring ΔS over the greatest possible time, Δt, using data from the last several frames of a run.

Summary

This chapter has presented the experimental formulation of a cylindrical model falling concentrically in a vertical tube. It is shown that model Reynolds numbers (≈2E4) were more than two orders of magnitude less than the prototype (≈9E6). Dimensional analysis showed that the fundamental problem was to determine the variation of C_d with model Reynolds number. Test results from the drop test of three models, the 625, 750 and 875, have been presented. The test results show very repeatable displacement data vs. time for each model with a maximum ±5% spread with a standard deviation of ±4% around the average displacement, Z_{avg}. Test results also verify the simple constant-C_d model from eq. 2-4, eq. 2-5 and eq. 2-20 where $C_d=C_{dt}$. A simple curve-fit model was proposed for use in determining velocity,

displacement and acceleration during startup in a drop test. Experimentally determined values of hydrodynamic mass have been presented and compared to simple inviscid theory, eq. 2-4c. Experimental results and the constant-C_d model will be compared to more accurate digital computer model results in Chap. 4.

CHAPTER 4

DIFFERENTIAL FORMULATION

The purpose of this chapter is to present the third of three studies, the numerical or differential formulation of a cylindrical body falling through fluid in a closed-end tube. The results of this numerical effort are compared to the previous results predicted by the control volume formulation, i.e., the constant-C_d model from Chap. 2, and the experimental results of Chap. 3, as well as results obtained by other researchers.

Sect. 4.1 Inviscid Analysis

To the best of the author's knowledge there is no known closed form solution to the exact mathematical formulation for a body falling through an inviscid fluid in a closed-end tube. It was necessary then to make a finite difference inviscid analysis to determine the pressure field around the body. Appendix D contains the details of the inviscid analysis. It was anticipated that at the nose of the body the pressure field caused by the frictionless fluid would be very similar to the pressure field in water. After carrying out both investigations this result has been verified.

The next sections discuss the viscous flow field.

Sect. 4.2 Factors Affecting Viscous Differential Simulations

At the most basic level, one is very interested in the

spatial resolution of both the velocity and pressure fields surrounding the model as it travels down the centerline of the tube. Interest in computational methods derives from their ability to produce large quantities of detailed information about laminar and turbulent flows that is not readily available using experimental techniques. In addition, the computational results can be globally verified experimentally since total drag equals net weight at terminal velocity.

The exact mathematical formulations for conservation of mass, momentum and energy have been known for over 100 years. The ultimate may be the, as yet unknown, exact solution for these highly non-linear partial differential equations. Far short of that we obtain approximate solutions on a discretized domain, a procedure that has many theoretical and practical limitations. The present state of the art in computational fluid mechanics allows a reasonably good job modeling certain types of turbulent flows. A number of theoretical and practical considerations are briefly discussed next.

Sect. 4.3 Numerical Approach

Several types of numerical simulations presently exist [41]. Large Eddy Simulations (LES) model the small eddies and compute or resolve the large eddies. Also Direct Numerical Simulations (DNS) resolve eddies of all sizes. The DNS models

are limited to low Reynolds numbers because of limitations on computer size. Ref [36] points out that DNS requires the number of grid points to be proportional to Reynolds number to the 2.25 power. It is estimated in [36] that using DNS the highest Reynolds number that can be computed on a Cray 2 machine is between 5E3 and 1E4 on a 256 x 256 x 256 grid. It would take about 100 hours of Cray CPU time to get adequate convergence.

By comparison, a commercially available program called FLUENT [38], running on a Cray X-MP/28 with an 80 x 70 grid, to model flow around the 875 body, converged in 2 hours of CPU at Re_d=5E5. The same case required 60 CPU hours to converge on a VAX 8600.

Neither the LES or DNS approach was utilized in this study primarily because of the relatively low Reynolds numbers that could be examined in addition to their inherently large CPU requirements. The approach used in this study was to use FLUENT to calculate the flow field followed by some post-processing to obtain shear and profile drag on the body. A brief development of the analytical background behind FLUENT is presented next.

Sect. 4.4 Basic Equations

It was hypothesized that the field was steady, incompressible turbulent flow. The continuity and momentum equations [13] are

$$\frac{\partial U_j}{\partial x_j} = 0 ,$$

$$U_j \frac{\partial U_i}{\partial x_j} = -\frac{1}{\rho}\frac{\partial p}{\partial x_i} + \frac{\partial}{\partial x_j}\left[(\nu_l + \nu_t)\left(\frac{\partial U_i}{\partial x_j} + \frac{\partial U_j}{\partial x_i}\right)\right], \qquad 4\text{-}1$$

where ν_t is the eddy viscosity, ν_l is the molecular viscosity, and U_i is tensor notation for time mean velocity in the x_i direction. The first term on the left of the momentum equation is the convection term; the next term represents pressure gradient, followed by the diffusion term. Body forces such as gravity have been neglected. The continuity and momentum equations describe the mean or time-averaged flow when modeled numerically over a finite number of control volumes used to discretize the flow domain.

Because the flow is turbulent it is customary to decompose the velocity into separate terms for the mean and fluctuating components. This velocity splitting technique is called Reynolds decomposition. The approach is to use the averaged form of the Navier-Stokes equations. These two equations are given in the radial, r direction (V_r=u), and the axial, z direction (V_z=w), as follows:

$$r: \quad u\frac{\partial u}{\partial r} + w\frac{\partial u}{\partial z} = -\frac{1}{\rho}\frac{\partial p}{\partial r} + \nu\left(\frac{\partial^2 u}{\partial r^2} + \frac{1}{r}\frac{\partial u}{\partial r} - \frac{u}{r^2} + \frac{\partial^2 u}{\partial z^2}\right)$$

$$- \left(\frac{\partial}{\partial r}\overline{u'^2} + \frac{\partial}{\partial z}\overline{u'w'} + \frac{1}{r}\overline{u'^2}\right),$$

$$z: \quad u\frac{\partial w}{\partial r} + w\frac{\partial w}{\partial z} = -\frac{1}{\rho}\frac{\partial p}{\partial z} + \nu\left(\frac{\partial^2 w}{\partial r^2} + \frac{1}{r}\frac{\partial w}{\partial r} + \frac{\partial^2 w}{\partial z^2}\right)$$

$$- \left(\frac{\partial}{\partial r}\overline{u'w'} + \frac{\partial}{\partial z}\overline{w'^2} + \frac{1}{r}\overline{u'w'} \right). \qquad 4\text{-}2$$

The Navier-Stokes equations are similar to the momentum equations except for the addition of the Reynolds stress terms, given as the last term on the right-hand side.

The continuity equation for the axisymmetric case is

$$\frac{\partial}{\partial r}(ru) + \frac{\partial}{\partial z}(rw) = 0 .$$

It was assumed in this study that the flow was isothermal.

Sect. 4.5 Turbulence Model

Since the Reynolds number is large, a turbulence model must be simultaneously solved over the discretized domain. The popular two-equation k-ε model of turbulence was used to achieve closure [13]. The k-ε turbulence model is valid when all Reynolds stresses are of the same order (isotropic eddy viscosity). It was initially hypothesized that this problem did not have any highly swirling flows, so was isotropic. Excellent agreement between the numerical model and experiment subsequently verified this assumption.

In the k-ε model the mean velocity is the only velocity used. The effects of turbulence, contained in the Reynolds stress terms, are addressed through an "effective viscosity"

term, μ_t, that is added to the laminar or molecular viscosity, μ_l. The decomposition of viscosity into these two components is known as the "effective viscosity hypothesis." The implementation of this technique to any region dominated by inertial effects (high local Reynolds number) leads to the construction of the turbulent kinetic energy (TKE), which is represented by k, and the dissipation rate of TKE, called ε. The governing equations for k and ε are models of the Navier-Stokes equations and are solved outside of the viscous region. Rodi [13] gives the k-ε model in tensor form:

$$\frac{\partial(U_j k)}{\partial x_j} = P - \varepsilon + \frac{\partial}{\partial x_j}\left(\frac{\nu_t}{\sigma_k}\frac{\partial k}{\partial x_j}\right),$$

$$\frac{\partial(U_j \varepsilon)}{\partial x_j} = C_1 \frac{\varepsilon}{k} P - C_2 \frac{\varepsilon^2}{k} + \frac{\partial}{\partial x_j}\left(\frac{\nu_t}{\sigma_\varepsilon}\frac{\partial \varepsilon}{\partial x_j}\right), \qquad 4\text{-}3$$

where $$P = \nu_t \left(\frac{\partial U_i}{\partial x_j} + \frac{\partial U_j}{\partial x_i}\right)\frac{\partial U_i}{\partial x_j}.$$

P is the production of k. Also, ν_t is related to k and ε by the Prandtl-Kolmogorov relation:

$$\nu_t = C_\mu \frac{k^2}{\varepsilon},$$

where the empirical constants in the above are given by

$C_1 = 1.44$, $C_2 = 1.92$, $\sigma_k = 1.0$, $\sigma_\varepsilon = 1.3$, and $C_\mu = 0.09$.

Very close to the wall the flow is dominated by viscous effects. It was assumed that in the viscous region the logarithmic law-of-the-wall applied. The k-ε model was used only far from the wall, where $\nu_t >> \nu_l$. Very near the wall the approach was to use the logarithmic law-of-the-wall from the wall, y=0, out to $y = y_c$, just outside the viscous sub-layer. The values of k and ε obtained at y_c are the boundary conditions for eq. 4-3. At y_c it was assumed that the production of TKE was exactly equal to the dissipation of TKE; in other words there was local equilibrium. If k_c and ε_c denote the TKE and dissipation rate at point c, then Rodi has shown that

$$k_c = \frac{w^{*2}}{C_\mu^{1/2}} \qquad \text{and} \qquad \varepsilon_c = \frac{w^{*3}}{\kappa y_c},$$

where the friction velocity, $w^* = (\tau_w/\rho)^{1/2}$ and $\kappa = 0.41$ is von Karman's constant. The law-of-the-wall used in this study:

$$W^+ = 2.5 \ln(9r^+)$$

for W^+ = normalized axial velocity = w/w^*,

and $r^+ = \rho y w^*/\mu_l$

for y = radial distance from the wall out to a near-wall point P.

Sect. 4.6 Method of Solution

The differential equations are integrated over the computational cells (the finite control volumes) that

comprise the flow domain. That is why this method is known as the "finite volume" method. The core of the computer method is the program FLUENT [38], which is based upon the SIMPLE algorithm discussed by Patankar [37]. FLUENT allows the solution of elliptic partial differential equations of the form

$$\text{DIV}\ (\rho V\phi) = \text{DIV}\ (\Gamma_\phi\ \text{GRAD}\phi) + S_\phi\ , \qquad 4\text{-}4$$

where the first, second and third terms are the convection, diffusion and source terms respectively. In this problem ϕ, the flow parameter of interest, is u,w,k or ε, while Γ_ϕ is called the diffusivity constant and S_ϕ is the source term. It is possible to rewrite eq. 4-2 and 4-3 in the form of eq. 4-4. Table 7 summarizes the results.

Table 7. Diffusion and Source Terms

Equation	ϕ	Γ_ϕ	S_ϕ
Continuity	1	0	0
Navier-Stokes r:	u	μ_t	$\frac{\partial}{\partial z}\left(\mu_t \frac{\partial u}{\partial z}\right) + \frac{1}{r}\frac{\partial}{\partial r}\left(\mu_t r \frac{\partial u}{\partial r}\right) - \mu_t \frac{u}{r^2} - \frac{\partial p}{\partial r}$
Navier-Stokes z:	w	μ_t	$\frac{\partial}{\partial z}\left(\mu_t \frac{\partial w}{\partial z}\right) + \frac{1}{r}\frac{\partial}{\partial r}\left(\mu_t r \frac{\partial w}{\partial r}\right) - \frac{\partial p}{\partial z}$
TKE k:	k	$\frac{\mu_t}{\sigma_K}$	$P - \rho\varepsilon$
Dissipation Rate ε:	ε	$\frac{\mu_t}{\sigma_\varepsilon}$	$\frac{\varepsilon}{K}(C_1 P - C_2 \rho\varepsilon)$

Note: P and all the constants have been defined in Sect. 4.5.

Discretization results in a system of algebraic equations written in terms of the unknown properties ϕ_p, at a point p :

$$\phi_p \sum_i (A_i - S_p) = \sum_i A_i \phi_i - S_c ,$$

where the summation is over the neighboring computational cells, i = N,S,E,W,F,B. (i.e., North, South, East, West, Front and Back). The coefficients, A_i, contain terms from the convective and diffusive fluxes. The source terms, S_c and S_p are related to S_ϕ through

$$S_\phi = S_c + S_p \phi_p .$$

In order to interpolate between grid points, which are at the center of each cell, and to calculate the derivatives of the flow variables, a power law differencing scheme was utilized. The dependent variables (p,k,ε,ν_t) were calculated and stored at the center of the cells. Velocity components were calculated and stored on the cell boundaries, an arrangement known as a "staggered grid."

Boundary conditions for velocity require that the velocity be specified at all points on the boundary. Along the centerline the radial component of velocity is set to zero. At the other boundaries: 1) no-slip velocity at the tube wall and on the model; 2) axial velocity profile known or assumed at the inlet together with the zero-gradient condition; 3) at the outlet, the zero-gradient condition is applied.

Solution of the simultaneous set of algebraic equations

was accomplished using a semi-implicit iterative scheme, described in the next section.

Sect. 4.6.1 The Pressure-Correction Scheme

It is convenient to derive an equation that allows pressure to be calculated directly from the velocity field. The continuity equation is combined with the divergence of the momentum equation and is rewritten into a Poisson-type equation:

$$\frac{\partial^2 p}{\partial x_j \partial x_j} = -\rho \frac{\partial U_i}{\partial x_j} \frac{\partial U_j}{\partial x_i} . \qquad 4\text{-}5$$

Once eq. 4-5 is integrated over a control volume and subsequently discretized it is called the p′ equation or pressure correction equation. It is then possible to calculate p′ at a point P given the velocities at neighboring nodes. The FLUENT solution algorithm is as follows:

1. Guess a pressure field p^*.
2. Solve the Navier-Stokes equations to obtain guesses u^*, w^*.
3. Solve the p′ equation.
4. Update pressure, $p = p^* + p'$
5. Calculate velocity corrections, u′ and w′ from p′
6. Update velocity; $u = u^* + u'$, $w = w^* + w'$
7. Solve the k and ε equations with the updated velocities.
8. Directly calculate the ν_t field from the k and ε fields.
9. Let p become the new guess for pressure and start over.

Steps 2-9 are repeated until the pressure correction term

has decreased to a required value for each point on the grid. At this point local continuity has been satisfied. Global continuity is checked by integrating the velocity over the outlet boundary condition.

Sect. 4.7 Discussion of Computer Simulation

The author's experience with the computer algorithm indicates that the velocity field settles down to essentially the converged value after only 200-400 iterations, regardless of Reynolds number. The pressure field converges much slower, taking up to 8000 iterations in a number of cases, the number of iterations increasing with increasing Reynolds number.

Since the convergence and accuracy of the numerical simulation depend on grid size and the location of the inlet and outlet planes, these effects were studied during this investigation. Several grid layouts were used during the course of the study. The location of the inlet plane was varied with very little effect on the flow field or calculated drag force. It was also determined, by numerical experimentation, that drag force was relatively insensitive to the location of the outlet plane. Grid size was also varied. Table 8 presents results from the grid size and inlet and outlet locations and the effect on drag for the 875 model. The 875 body was selected since it had the smallest annular gap, causing the flow to distort a maximum amount to go from the tube into the annulus. In each case presented in

Table 8 it was assumed that the 875 model was traveling at a velocity of 75 ft/s in water, corresponding to $Re_d \approx 5.1E5$. Overall pressure drag is represented by D_p and total shear drag by D_τ, both given in pounds.

Table 8. Grid Size and Inlet/Outlet Location Effects on Drag

Case	Grid Size Axial X Radial	Inlet Location from the nose in.	Outlet Location from the tail in.	D_p, lb.	D_τ, lb.
1	80X70	1.0	12.5	50.88	2.173
2		15.0		50.99	2.172
3	80X70	12.5	1.0	50.87	2.173
4			5.0	50.97	2.175
5			15.0	50.99	2.172
6	100X100	15.0	15.0	50.95	2.169
7	80X70			50.99	2.172
8	70X50			51.29	2.194
8	58X50			51.37	2.200
9	40X35			53.54	2.362
10	30X26			63.53	2.509

Comparing cases 1 and 2 it is apparent that the inlet plane can be located anywhere from 1" to 15" from the nose with less than a 0.25% change in drag. Location of the outlet plane was studied under cases 3, 4 and 5, with the similar result that drag is insensitive to outlet plane location. The author suggests that the findings presented in cases 1 through 5 are an important result of this study. The conclusion that drag is independent of the location of inlet and outlet planes must be qualified by observing that this study was concerned only with highly streamlined bodies and

that a bluff body could not be expected to behave in a similar fashion.

Grid size was studied in cases 6 through 10. The inlet plane was located 15" ahead of the nose of the model. The outlet plane was placed 15" downstream from the extreme end of the tail to capture the wake. Originally, in order to establish a baseline, the finest grid allowed by FLUENT, figure 22 , having 100 divisions in the radial and 100 divisions in the axial direction, was run on the 875 model. The coarse 30X26 grid in case 10, over-predicts drag by about 24% compared to the finest 100X100 grid in case 6. Since case 8 deviated by only about 0.5% from case 6, with 65% fewer grid points and requiring less than 10% of the CPU time, it was decided to use the 70X50 grid for all the Reynolds numbers that were studied. The 70X50 grid required between 24 and 48 CPU hours to converge on the VAX 8600, depending on the Reynolds number. The larger the Reynolds number the slower the pressure field converges.

Sect. 4.8 Presentation and Discussion of Results

The 625 model was studied in the most detail primarily because the dimensionless groups $\Pi_2=\Lambda/D^3=1.64$ and $\Pi_5=\beta=D/d=1.6$, Sect. 3.7, were of the most immediate interest to the Navy. This case represented a prototype 21" diameter torpedo inside a 27" diameter torpedo tube, a realistic combination.

As discussed in Sect. 3.10, the 625 body also had the most interesting acceleration region, being the greatest in magnitude and over the longest time, of the three models. The 625 also had the highest terminal velocity, 56 in./s, and the highest gap Reynolds number, Re_g= 22200, using figure 12 :

$$Re_g = \frac{wD_e}{\nu}, \quad \text{where} \quad w = \frac{\beta^2}{\beta^2-1} V \quad \text{and} \quad D_e = D-d;$$

$$\text{then,} \quad Re_g = \frac{\beta^2}{\beta+1} Re_d . \qquad 4\text{-}6$$

For these reasons it was decided that the 625 would receive the most detailed study of the three configurations. The 750 and 875 were also studied for $1E10^5 \leq Re_g \leq 5E10^6$ in order to determine the functional dependence of C_d in terms of β and Re_g.

There was an assumption made in Sect. 2.10 that nose drag and tail drag are independent of the length of the annular region. The exact hypothesis in Sect. 2.10 was that total drag can be found by independently calculating nose drag, annular drag and tail drag and finally adding them together. Of course the question is whether the actual composite model behaves in this ideal independent fashion. To test this hypothesis a special case was run on FLUENT, called 625 Shorty. Shorty, figure 23 , was basically a nose and tail, with no annular region. Comparison of pressure coefficients over a wide range of Re_d, with the full 625 model revealed

that the hypothesis was valid.

A graph of C_p vs. axial position for various values of turbulent Re_d's on Shorty is presented in figure 24 . The two regions of interest, the nose and tail, are presented and discussed in the following.

Figure 25 shows a composite overlay of C_p on the nose. The inviscid prediction computed by finite differences is compared to FLUENT predictions for a wide range of turbulent Reynolds numbers. The overall prediction of nose drag compares very favorably, showing independence from Reynolds number and only about $\pm 4\%$ maximum variation between the inviscid and FLUENT at the back of the nose. In addition to corresponding well with the full 625 model, the nose drag on Shorty compares very well with the simple formula, eq. 2-9, where it was assumed that there was essentially no pressure drop over the nose due to friction. This important result conveniently allows use of eq. 2-9 with K_n=Nose loss coefficient=0, as in eq. 2-20, to compute the nose drag coefficient, C_n.

Figure 26 is a composite of various turbulent Reynolds numbers for C_p vs. axial position on the tail of Shorty. The tail curves from figure 24 have simply been shifted up or down by a constant in order to show that C_t from eq. 2-11, with K_t=Tail loss coefficient=1.0, as in eq. 2-20 accurately predicts the tail drag. This is another important result, and verifies that tail drag coefficient, C_t, may be found using

the constant-C_d model of eq. 2-20.

Figure 27 presents C_p vs. axial position for the full 625 model at various values of Re_d. For comparison the inviscid prediction was plotted with the FLUENT results. The nose is seen to behave inviscidly, as in Shorty. The straight section then opens up into a series of straight lines of differing slopes, and the tail curves look similar except that they are shifted by a constant. Each of the three regions of interest, nose, straight and tail are discussed next.

Figure 28 contains a composite overlay of C_p on the nose of the full 625 model for the inviscid and various turbulent Reynolds numbers. The inviscid prediction compares very favorably to the FLUENT results, as in figure 25 . There is especially excellent correlation at the back of the nose, resulting in about $\pm 1\%$ maximum deviation. This presents the final piece of evidence that eq. 2-20 can be used to compute the nose drag coefficient, C_n.

Figure 29 overlays C_p for the tail of the 625 body, showing that the tails are in fact shifted by a constant, as in the Shorty tail results of figure 26 . Comparing the tail results from Shorty in figure 26 to the tail results of the full 625 model in figure 29 shows that tail drag varies only about $\pm 2\%$ between the two. This is an extremely important result since it verifies the hypothesis that tail drag is essentially unaffected by the length of the

straight section.

Now that the nose and tail sections have been discussed and it has been shown that they both behave as hypothesized in Chap. 2, it is time to discuss straight section drag. Verification of Kotlow's [10] straight section model is obtained from figure 27 . Using Kotlow's formulas to compute C_s=Straight drag coefficient, eq. 2-17, the FLUENT results are predicted by ±5%, which is considered very good. Kotlow points out that neglect of the developing entrance region will produce about ±4% error in drag. Observe in figure 27 that there is essentially no discernible change in slope in the drag coefficient computed by FLUENT along the straight section. Kotlow's assertion that, for purposes of computation of drag, the entire straight region may be treated as fully developed is then verified by this study.

While it is apparent that the velocity profiles will be very different along the straight section, it is not apparent that the drag coefficient is essentially independent of axial position in the straight section. The next paragraphs discuss some FLUENT results for velocity profiles at various locations, called 'stations', in the flow field.

Recall that in a coordinate system fixed to the model, the 625 body has a zero velocity and the tube wall/inlet plane have a velocity of 4.67 ft/s, which corresponds to Re_d= 22200 at terminal velocity in a 1" tube filled with water. Figure 30 was run on FLUENT for the terminal velocity case on the

100X100 grid and shows velocity profiles just ahead of the nose (station 13), at the beginning of the straight annulus (station 25) and at the middle of the straight annulus (station 40). The flow is almost a slug flow as it enters the straight section and rapidly begins to form into a classic curved profile due to friction with the wall and model.

Figure 31 is an extension of figure 30 displaying velocity profiles at the end of the annulus (station 56), middle of the tail (station 62), just behind the model (station 74) and at the outlet plane positioned 15 inches downstream of the tail (station 100). The flow is seen to reach a nicely developed profile in the straight section and then expand out into the tail region. Back out in the tube, at station 100, the effects of the high gap velocity are fading but still noticeable.

A comparison of velocity profiles with the predictions of Kotlow [10] is also of interest. Figure 32 shows Kotlow's fully developed profile compared to the profile predicted by the differential model. The maximum difference is about $\pm 3.5\%$ between the two velocity profiles, which is considered quite good.

Figure 33 presents the ratio of profile drag to total drag for the three bodies. For the 625 body, the profile drag is seen to start at 80% for $Re_g = 10^5$ and increase to 85% for $Re_g = 5E10^6$. Figure 33 highlights the fact that drag is primarily caused by pressure forces.

Drag coefficients are plotted vs. gap Reynolds number in figure 13 . A curve fit in the range of interest, $1.14 \leq \beta \leq 1.6$ and $1E5 \leq Re_g \leq 5E6$, was developed to predict drag coefficient:

Define: $\lambda = \frac{\beta^2}{\beta^2-1} = \frac{A}{A-a}$ and $Re_g = \frac{\beta^2}{\beta+1} Re_d$.

Then: $C_d = \lambda^r \exp(55/\sqrt{Re_g})\ Re_g^{-b}$, 4-7

where $b = 0.01 + 0.014(\lambda-1)^{-0.6}$,

and $r = 2.92 - 0.853\beta$ (yields ±5% accuracy for C_d),

or $r = -0.6069\beta^2 + 0.7678\beta + 1.8652$ (±3% for C_d).

	625	750	875
β	1.600	1.333	1.143
λ	1.641	2.286	4.267
b	0.02828	0.02204	0.01688
r	1.54	1.81	1.95

It is of interest to note in figure 13 that if a power law relation is assumed,

$$C_d = k\ Re_g^{-n} \qquad \text{(k and n are constants)},$$

the best fit values in the range $10^5 \leq Re_g \leq 5E10^6$ are

	625	750	875
β	1.600	1.333	1.143
k	3.833	31.797	998.15
n	0.06475	0.1458	0.2791

It is clear from this table that C_d is a strong function of β, as discussed next.

When β is small, the gap clearance is small, with the result that C_d becomes large and highly sensitive to changes in body velocity. The reason is that the gap velocity is greatly magnified by the small clearance area compared to the tube area. Hence, for small values of β, C_d is very sensitive to changes in Re_d.

However, when β is large, the gap area becomes large compared to the tube area and the gap velocity is less sensitive to changes in body velocity. Hence, for large values of β, C_d is less sensitive to changes in Re_d.

Summary

This chapter has presented and discussed drag computed by finite differences to both the inviscid and viscous problem of a body falling through fluid in a closed-end tube. It has been shown that nose drag in an inviscid flow is the same as nose drag in viscous flow, i.e. the effect of shear on the nose is negligible. It has also been shown that nose drag and tail drag are independent of the length of the cylindrical section. This conclusion allows for convenient independent calculation of nose, straight and tail section drag, eq. 2-19. Total drag is then the sum of the independently computed components. It has been further shown that nose and tail drag for turbulent flow are independent of Reynolds number. Drag on the straight section does depend on Reynolds number in accordance with Kotlow's prediction, eq. 2-16 and 2-17. Finally drag coefficients have been plotted as a function of $\beta=D/d$ and Reynolds number using both the constant-C_d model of Chap. 2 and the numerical simulation of Chap. 4. A curve-fit has been proposed for the range of β and Reynolds numbers of interest to the Navy.

CONCLUSIONS AND RECOMMENDATIONS

Conclusions

1. This study has shown that nose drag and tail drag are independent of the length of the straight annular region. This conclusion is specific to a model having a hemispherical nose, parallel midsection and conical tail, moving concentrically in a fluid-filled tube. This conclusion was confirmed numerically for $1.14 \leq \beta \leq 1.6$ by comparison of drag from calculations on a body, called SHORTY, having essentially zero length in the cylindical section, with drag calculations on bodies of finite length.

2. Drag coefficients predicted by control volume methods, experimental drop tests, and numerical simulation were consistent (within $\pm 5\%$) for turbulent Reynolds numbers in the range $1E5 \leq Re_g \leq 5E6$. Estimates obtained in this study are consistent (within $\pm 5\%$) with those of previous investigators.

3. A curve-fit has been proposed to predict drag coefficients for bodies in the range $1.14 \leq \beta \leq 1.6$ with $1E5 \leq Re_g \leq 5E6$, which has $\pm 5\%$ accuracy. This is the range of most interest to the Navy for torpedo launching.

4. The variable-C_d analysis is only approximately correct. The physics of the accelerating flow around the model are not well understood. Differential analysis of the unsteady problem, where the vehicle accelerates from rest to the terminal velocity,, was not attempted in this study.

Recommendations

1. Future investigators may want to attempt a numerical solution of the unsteady case.

2. A companion problem to the one discussed in this study involves the investigation of a model in a finite length open-end tube. In this case the pressure drop developed across the model exactly equals the pressure drop across the tube. Flow is thereby induced in the tube in the far field. A numerical solution of the flow field and model drag may be attempted. The one dimensional constant-C_d analysis developed in this study could be generalized to handle this case.

3. The problem described in 2. above could be examined for the unsteady case also.

4. Another companion problem, of interest to the Navy, is the case of a favorable pressure gradient, i.e., from a pump, applied to the model in order to push it out of the tube.

REFERENCES

[1] Hoerner, S.F., Fluid Dynamic Drag, published by the author, 148 Busteed Drive, Midland Park, New Jersey, 07432, pp. 3 - 19.

[2] Gouse, S.W., and Nwude, J., "Aerodynamic Drag on Vehicles in Enclosed Guideways," M.I.T., Engineering Projects Laboratory Report No. DSR 76108-1, Mech. Engr. Dept., December 1966, NTIS No. PB 173 646.

[3] Goodman, T.R., "The Aerodynamic Characteristics of a Slender Body Traveling in a Tube," U.S. Dept. of Commerce Report, Contract No. C-265-66.

[4] Sutter, K., "Der Luftwiderstand auf Eisenbahnzuge in Tunneln," Munchen, 1930.

[5] Abramovich, G.N., "Calculation of Air Resistance of Trains when Moving in the Open and in Tunnels," Trudy Tsentr, Aerogedradinam, Inst. 400, 1939.

[6] Hara, Tomoshige, "Method of Measuring the Aerodynamic Drag of Trains," Bulletin of JSME, Vol. 8, No. 31, 1965.

[7] Gouse, S.W., et al., "Aerodynamic Drag on a Body Traveling in a Tube," U.S. Dept. of Transportation Report, Contract No. C-85-65, October 1967, NTIS No. PB 177 211.

[8] Davidson, J.V., "Aerodynamic Drag of Tube Vehicles," Master's Thesis, Duke University, Durham, N.C., 1974.

[9] Sud, I., and Chaddock, J.B., "Drag Calculations for Vehicles in Very Long Tubes from Turbulent Flow Theory," Journal of Fluids Engineering, Vol. 103, June 1981, pp. 361-366.

[10] Kotlow, D.A., "Aerodynamic Drag of Vehicles in Long Tubes," Master's Thesis, University of Rhode Island, Kingston, R.I., 1985.

[11] Hoppe, R.G., and Gouse, S.W., "Fluid Dynamic Drag on Vehicles Traveling Through Tubes," Carnegie-Mellon University Report No. 1-59076-1, August 1969, NTIS No. PB 188 451.

[12] Nayak, U.S.L., et al., "The Aerodynamic Drag of Tube Vehicles Traveling at Low Subsonic Speeds," BHRA Fluid Engineering Second International Symposium on Aerodynamics and Ventilation of Vehicle Tunnels, Paper E1, held at Churchill College, Cambridge, England, 23rd-25th March, 1976.

[13] Rodi, W.,"Turbulence Models and Their Application in Hydraulics - A State of the Art Review," International Association for Hydraulic Research, The Netherlands, June, 1980.

[14] Weismann, C.,"Die Kunsliche Luftung in Stollen und Tunnelbau," 1919.

[15] Tollmein, Walter,"Luftwiderstand und Druckverlauf bei der Fahrt von Zugen in einem Tunnel," Zeitschrift des Verines Deutscher Ingerieure, Vol. 71, No. 6, Feb 5, 1927, pp. 199-202.

[16] Langer, R.E.,"Versuche an einem Schnellbahnwagen," Ergebnisse der Aerodynamischen Versuchstalt zu Gottingen, 111, Lieferung, 1927.

[17] Kurtz, Donald W.,et al.,"Experimental Aerodynamic Characteristics of Vehicles in Confined Spaces," Caltech Technical Report No. UMTA-DC-06-0010-72-14, Contract No. DC-290, December 1972, NTIS No. PB 231 386.

[18] Quarmby, A.,"An Analysis of Turbulent Flow in Concentric Annuli," Applied Scientific Research, Vol. 19, July 1968, pp. 250-293.

[19] Wilson,N.W.,and Medwell, J.O.,"An Analysis of the Developing Turbulent Hydrodynamic and Thermal Boundary Layers in an Internally Heated Annulus," ASME Journal of Heat Transfer, Vol. 64, February 1971, pp. 25-32.

[20] Hammitt, Andrew G., The Aerodynamics of High Speed Ground Transportation, published by Western Periodicals Co., 13000 Raymer St., North Hollywood, California, 1973.

[21] Kawaguti, M.,"Effects of the Ground and a Tunnel on the Frictional Drag of High-Speed Trains," Quarterly Report of Railroad Technology Research Inst., Japanese National Railways, Vol. 2, No. 4, 1961, pp. 1-6.

[22] Miki, N.,"Research Report on the New Japanese National Railways, Tokaido Line,"Vol. 3, 1962, pp. 12.

[23] Hara, T.,"Aerodynamic Force on a High Speed Train at Tunnel Entrance," Bull. of JSME, Vol. 4, No. 15, 1961, pp. 547-553.

[24] Ono, Ito, Nishimura, and Kawamura, Memo. Railroad Technology Research Inst., No. 253, Japanese National Railways, 1959.

[25] Hara,T.,and Okushi, J.,"Model Tests on Aerodynamical Phenomena of a High Speed Train Entering a Tunnel," Quarterly Report of Railroad Technology Research Inst., Japanese National Railways, Vol. 3, No. 4, 1962, pp. 6-10.

[26] Hara, T.,Ohkushi,J.,and Nishimura, B.,"Aerodynamic Drag of Trains," Quarterly Report of Railroad Technology Research Inst., Japanese National Railways, Vol. 8, No. 4, 1967, pp. 226-229.

[27] Hara, T.,"Aerodynamic Drag of Trains in Tunnels," Quarterly Report of Railroad Technology Research Inst., Japanese National Railways, Vol. 8, No. 4, 1967, pp. 229-235.

[28] Tanaka,T.,et al.,"Research Report on the New Tokaido Line,"Vol. 4, 1963, p. 142.

[29] Fukuchi,G.,and Nischizawa, S.,"Estimate of Aerodynamic Drag of a Train in a Long Tunnel," Quarterly Report of Railroad Technology Research Inst., Japanese National Railways, Vol. 8, No. 1, 1967, pp. 30-33.

[30] Fukuchi, G.,"A Method of Aerodynamic Drag Abatement for High-Speed Train in Single-Tracked Tunnel," Railroad Technology Research Inst., Japanese National Railways, 1967.

[31] Nouvion, F.,"The Train Drag at High Speed," Paper presented at the International Conf. on Vehicle Mechanics Wayne State University, July 1968.

[32] Van Driest, E.R.,"On Turbulent Flow Near a Wall," Journal Aero. Science, vol. 23, 1956, pp. 1007-1012.

[33] Cromack, D.E.,"Experiments on the Propulsion of Vehicles in Tubes of Varying Porosities," R.P.I. Report TR PT 6803, to Office of High Speed Ground Transportation, U.S. Department of Transportation, June 1968.

[34] Gregorek,G.M.,and Engle, J.H.,"An Experimental Study of Aerodynamics of Vehicles Traveling at High Speeds Through Long Tubes," The Ohio State Univ., Columbus, Ohio. Presented at the International Conf. on Vehicle Mechanics at Wayne State Univ., July 1968.

[35] Hammitt, Andrew G.,"High Speed Ground Transportation System Engineering Program,"T.R.W. Rept. No. 06818-6026-R000, for the Office of High Speed Ground Transportation, U.S. Dept. of Transportation, April 15, 1968.

[36] Nixon, D., "A Report on a Workshop on Turbulence Research," prepared for Air Force Office of Scientific Research, Bolling Air Force Base, Washington D.C. 20332, dated March 28, 1986, covering the period, August 8, 1985 to April 12, 1986, NEAR TR-361.

[37] Patankar, S.V., Numerical Heat Transfer and Fluid Flow, Hemisphere Publishing Corp., McGraw-Hill Book Co., 1980.

[38] FLUENT release 2.81, Licensed by and the property of CREARE Inc., P.O. Box 71, Hanover, New Hampshire, 03755, phone (603) 643-3800.

[39] White, F.M., Fluid Mechanics, McGraw-Hill Inc., New York, 1979.

[40] White, F.M., Viscous Fluid Flow, McGraw-Hill Inc., New York, 1974.

[41] Ferziger, J.H., "Simulation of Incompressible Turbulent Flows," Journal of Computational Physics, Vol. 69, No. 1, March 1987, pp. 1-48.

[42] CRC Handbook of Chemistry and Physics, CRC Press, Inc., 2000 Corporate Blvd. N.W., Boca Raton, Florida, 33431, 1980.

[43] Mark's Standard Handbook for Mechanical Engineers, McGraw-Hill Book Co., New York, Eighth Edition, 1978.

[44] CRC Handbook of Tables for Applied Engineering Science, CRC Press, Inc., 2000 Corporate Blvd. N.W., Boca Raton, Florida, 33431, Second Edition, 1985.

[45] Barbin, A.R., and Jones, J.B., "Turbulent Flow in the Inlet Region of a Smooth Pipe," Journal of Basic Engineering, Trans. ASME, Vol. 85, Series D, Mar 1963, pp. 29-34.

[46] Bowlus, D.A., and Brighton, J.A., "Incompressible Turbulent Flow in the Inlet Region of a Pipe," Journal of Basic Engineering, Trans. ASME, Vol. 90, Series D, No. 3, Sept. 1968, pp. 431-433.

[47] Deissler, R.G., and Taylor, M.F., "Analysis of Fully Developed Turbulent Heat Transfer and Flow in an Annulus with Various Eccentricities," NACA TN 3451, 1951.

[48] Streeter, V.L., Handbook of Fluid Dynamics, McGraw-Hill Book Company, Inc., 1961, pp. 3-21.

[49] Skinner, J.H., "Tube-Vehicle Drag," General Electric Co., Research and Development Center, Schenectady, New York, 1969.

[50] Becker, E., "Stromungsvorgange In Ringformigen Splaten (Labyrinth-Dichugen)," Zeitschrift V.D.I., vol. 51, 1907, pp. 1133-1141.

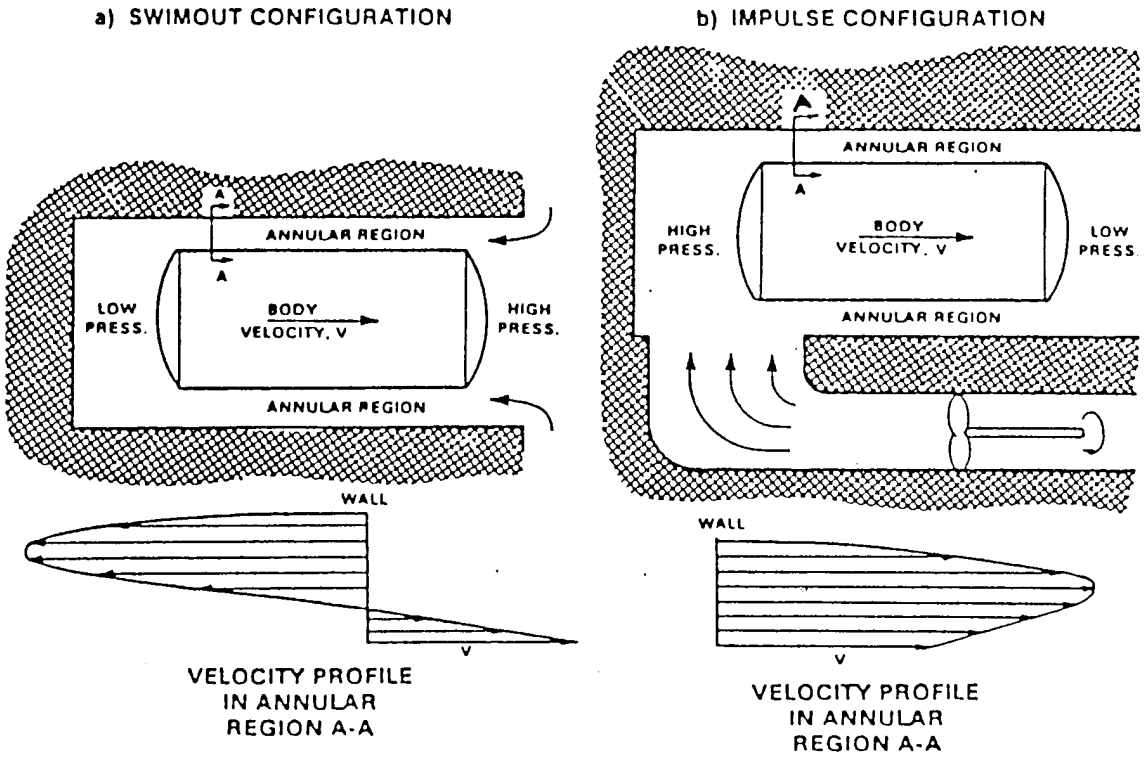

Figure 1. Basic Torpedo Launch Configurations

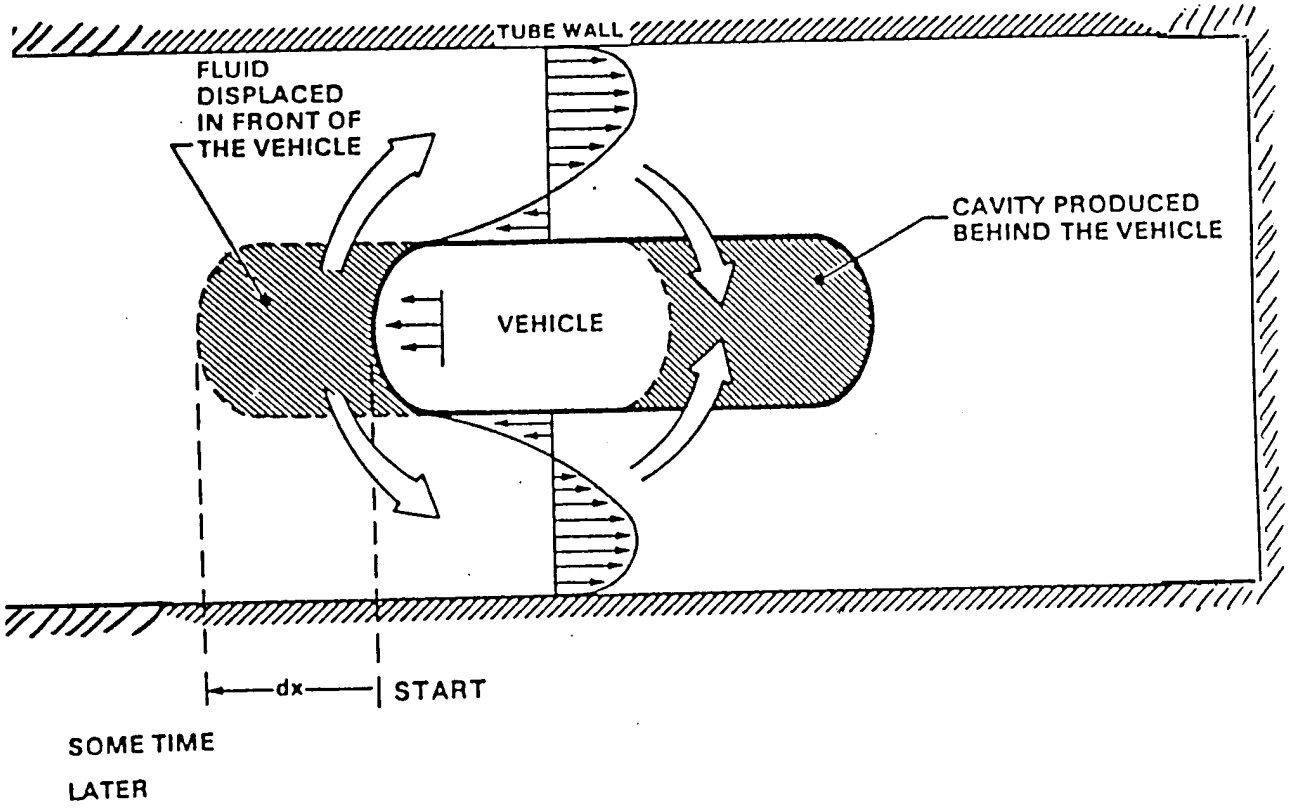

Figure 2. Simplified Swimout Model

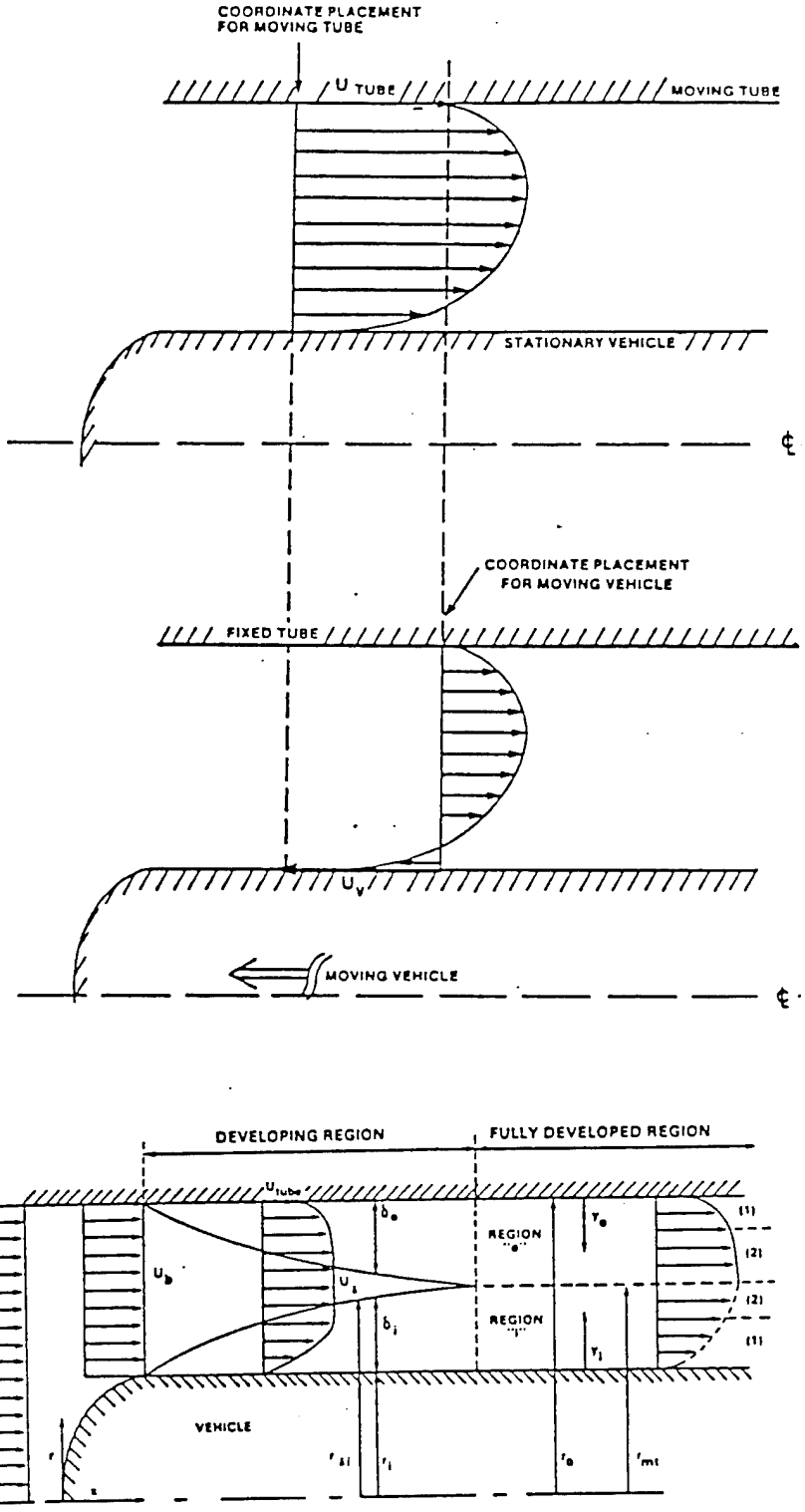

Figure 3. Velocity Profiles in the Annular Region, after Kotlow [10]

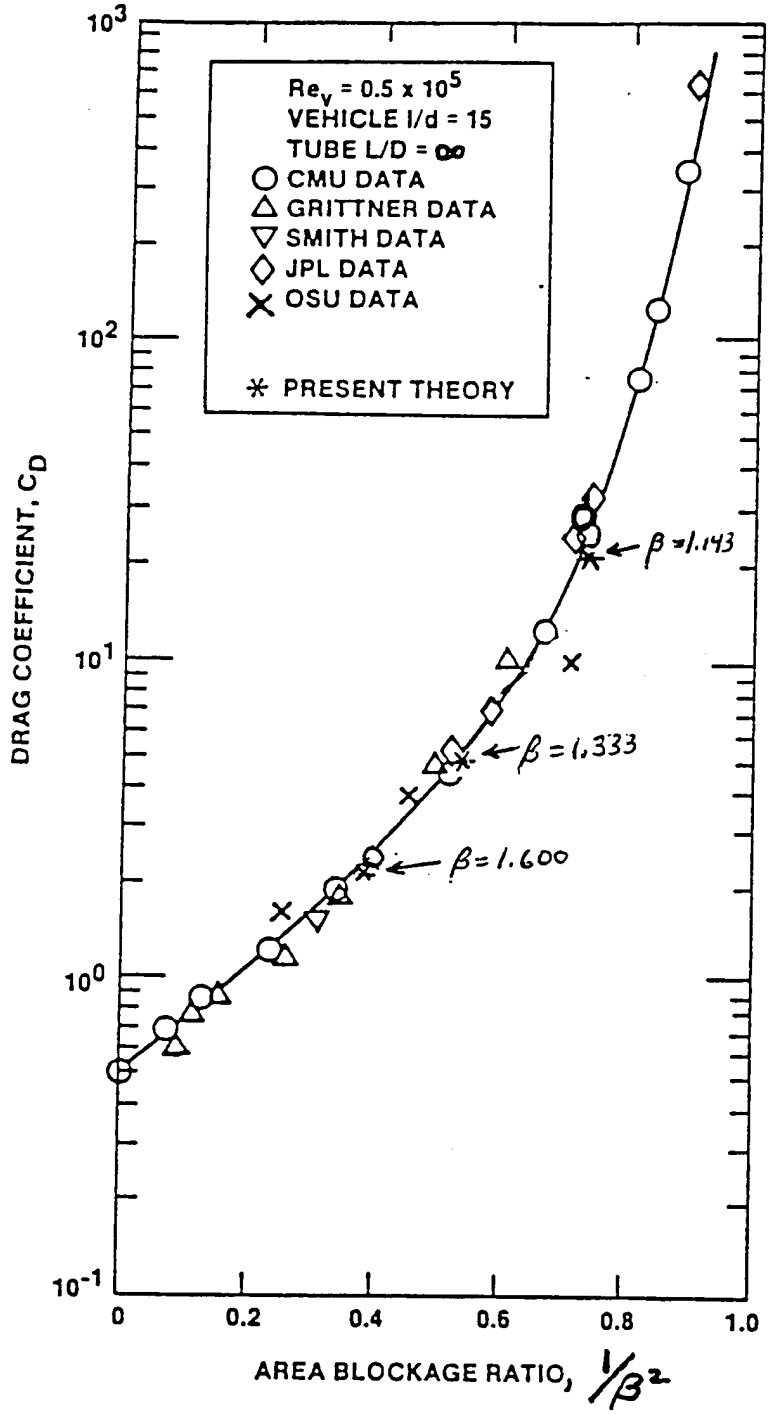

Figure 4. Comparison of Experimental Drag Coefficients from Previous Studies

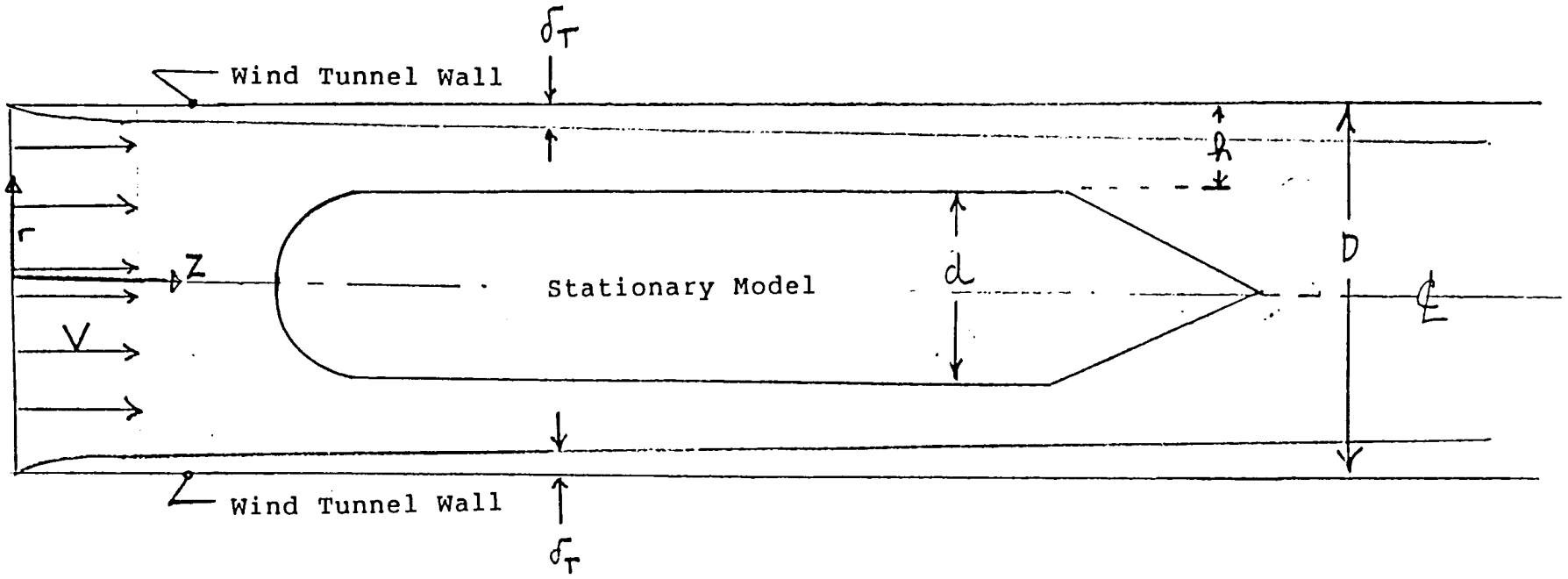

Figure 5. Boundary Layer on the Tube Wall in a Wind Tunnel

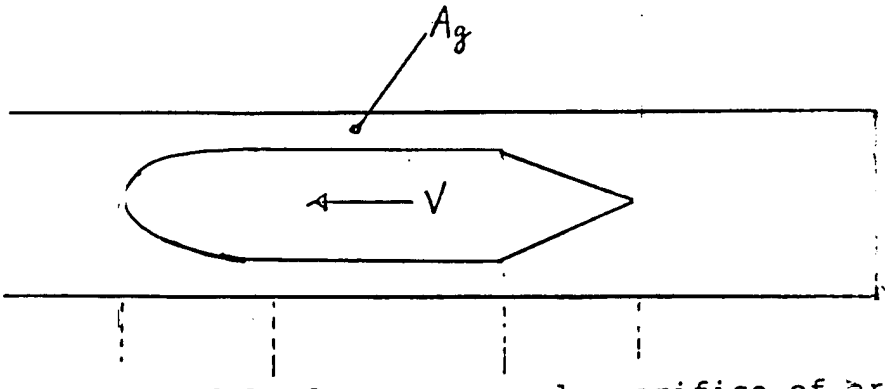

Figure 6a. Tube-Model, forms an annular orifice of area, A_g

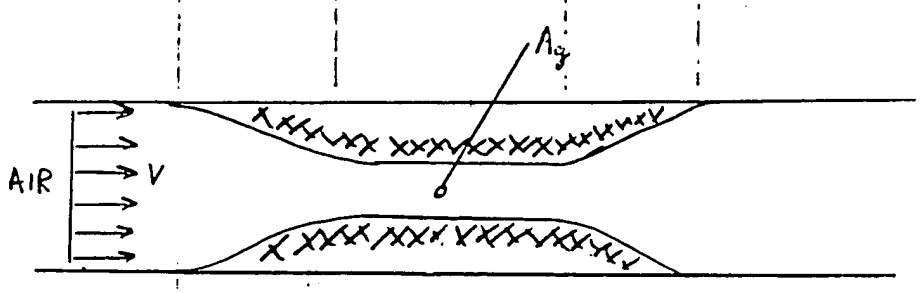

Figure 6b. Converging-Diverging Nozzle, of area A_g, used to model the tube-model flow in figure (6a)

Figure 6. Converging-Diverging Nozzle model of actual Tube-Model flow (used to model compressible effects, as discussed in Appendix A)

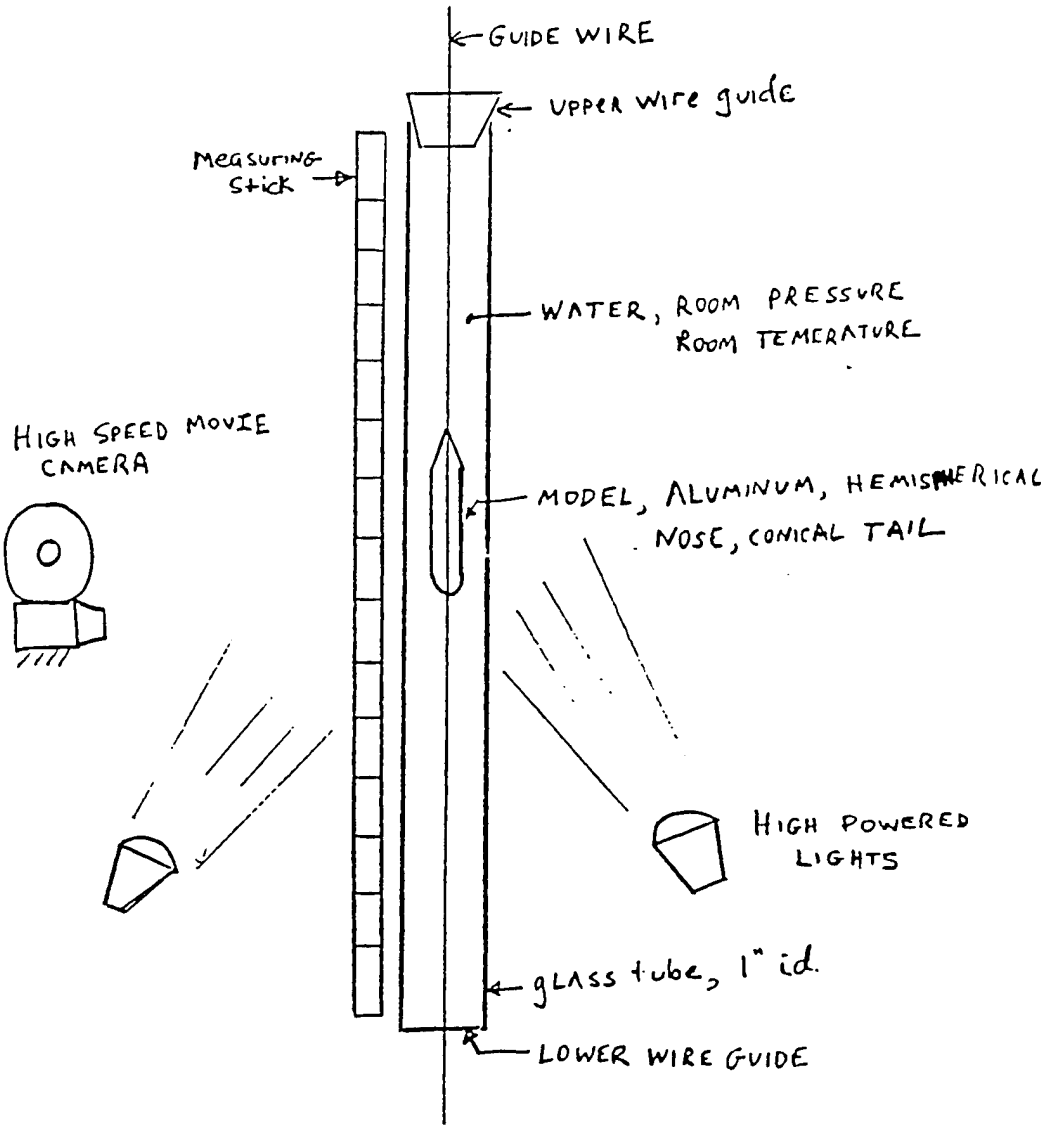

Figure 7. Drop Test Apparatus

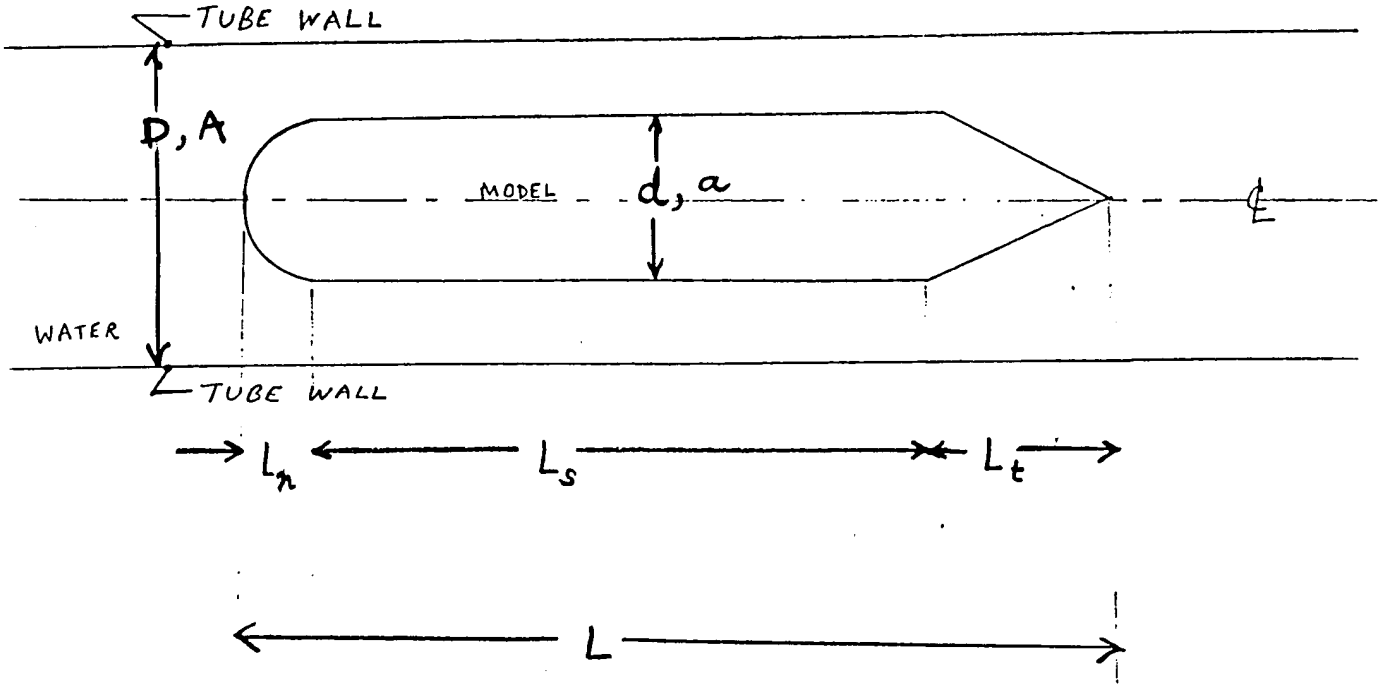

Figure 8. Model Geometry

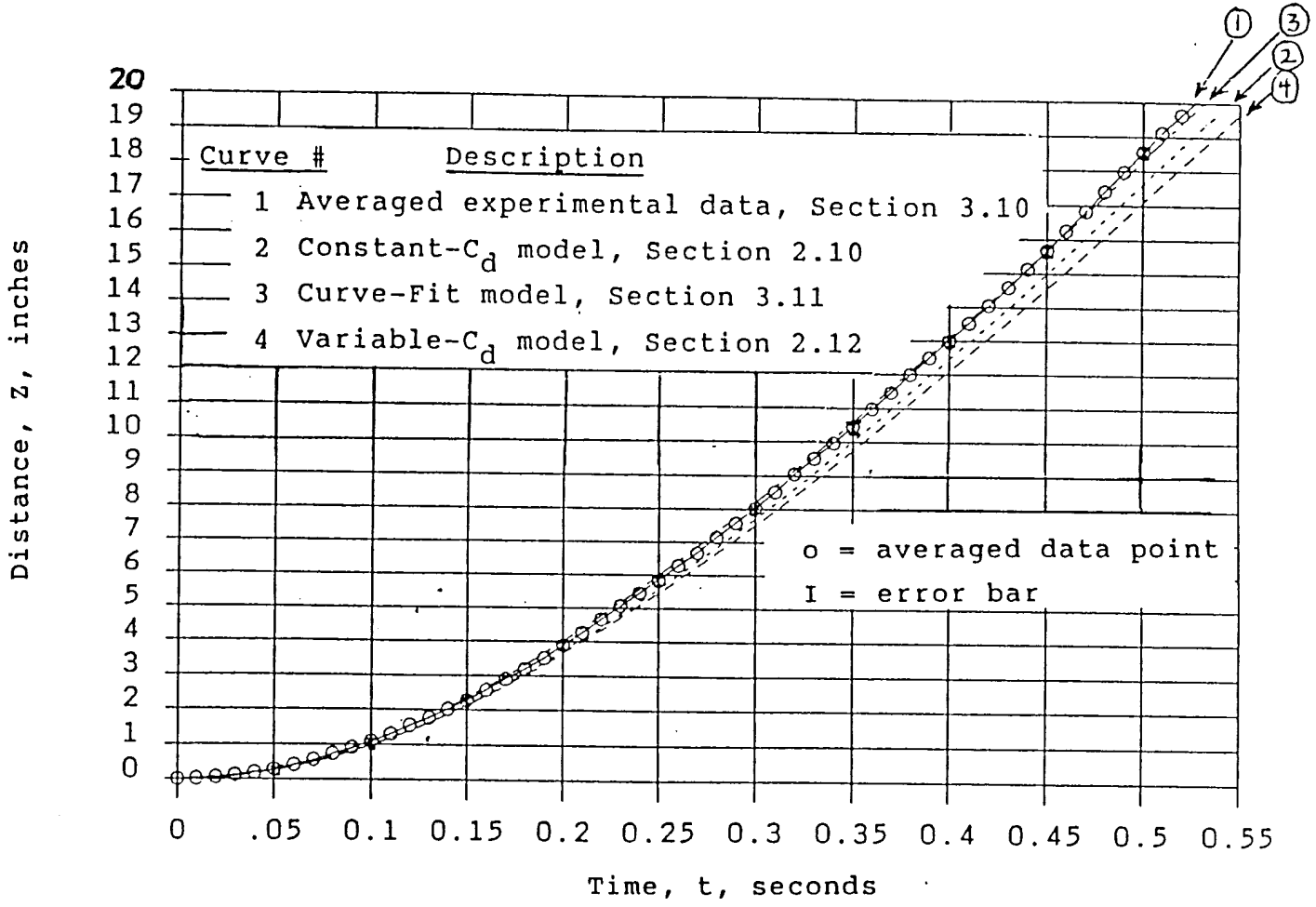

Figure 9. Dist., Z, vs. Time, t, for the 625 model, Averaged Experimental Data compared to Constant-C_d model, Variable-C_d model and Curve-Fit model

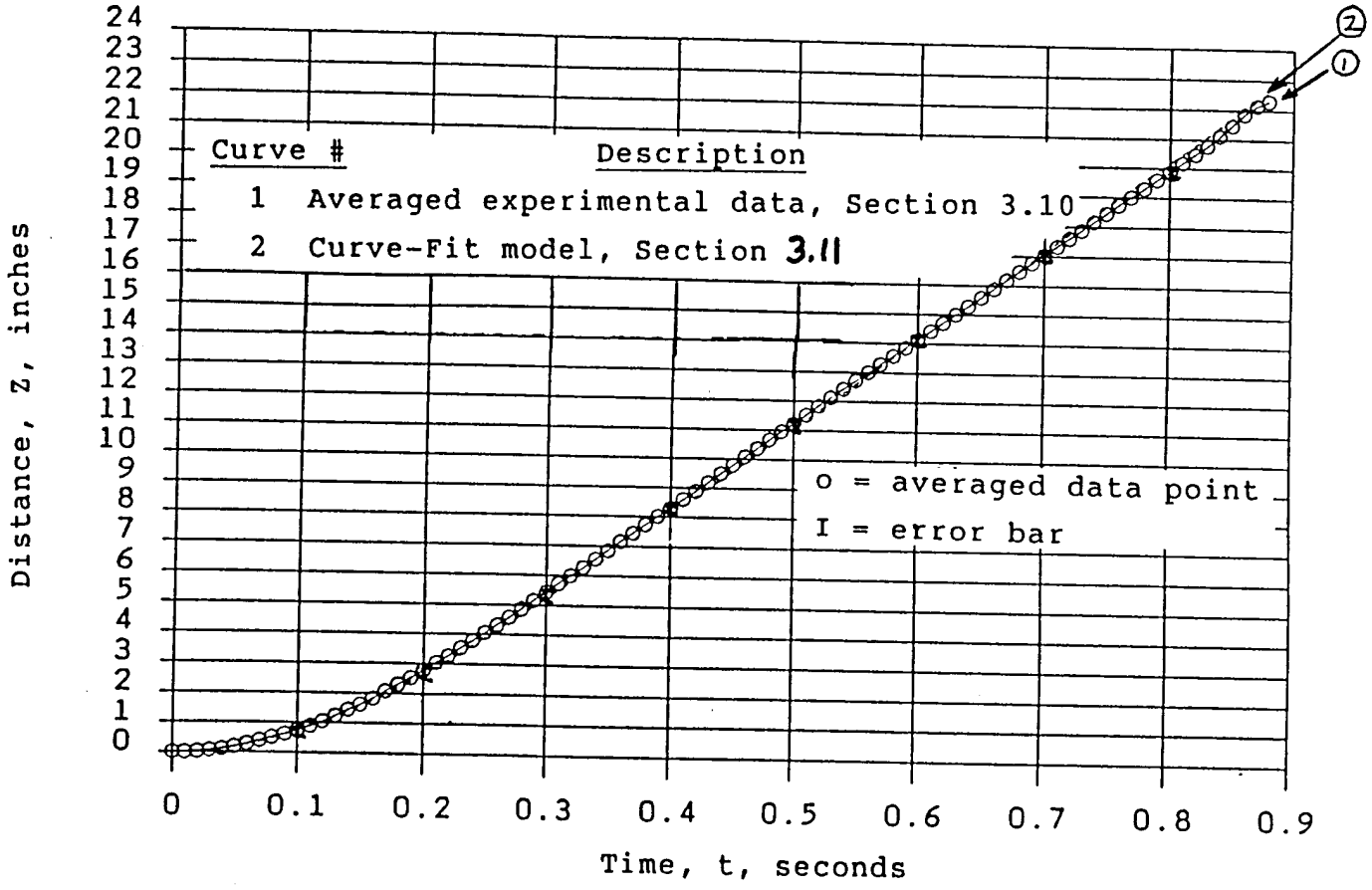

Figure 10. Distance, Z, vs. Time, t, for the 750 model

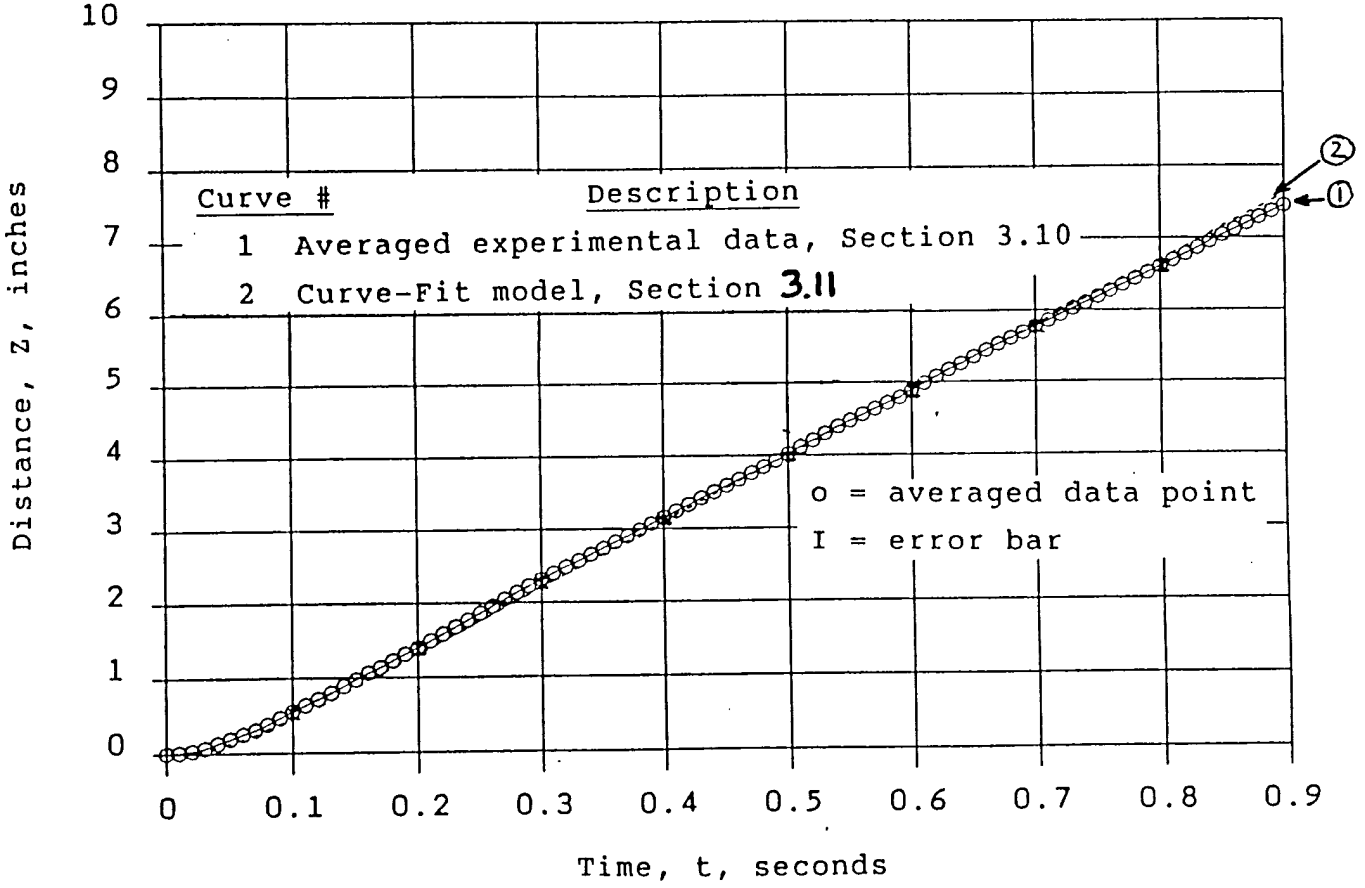

Figure 11. Distance, Z, vs. Time, t, for the 875 model

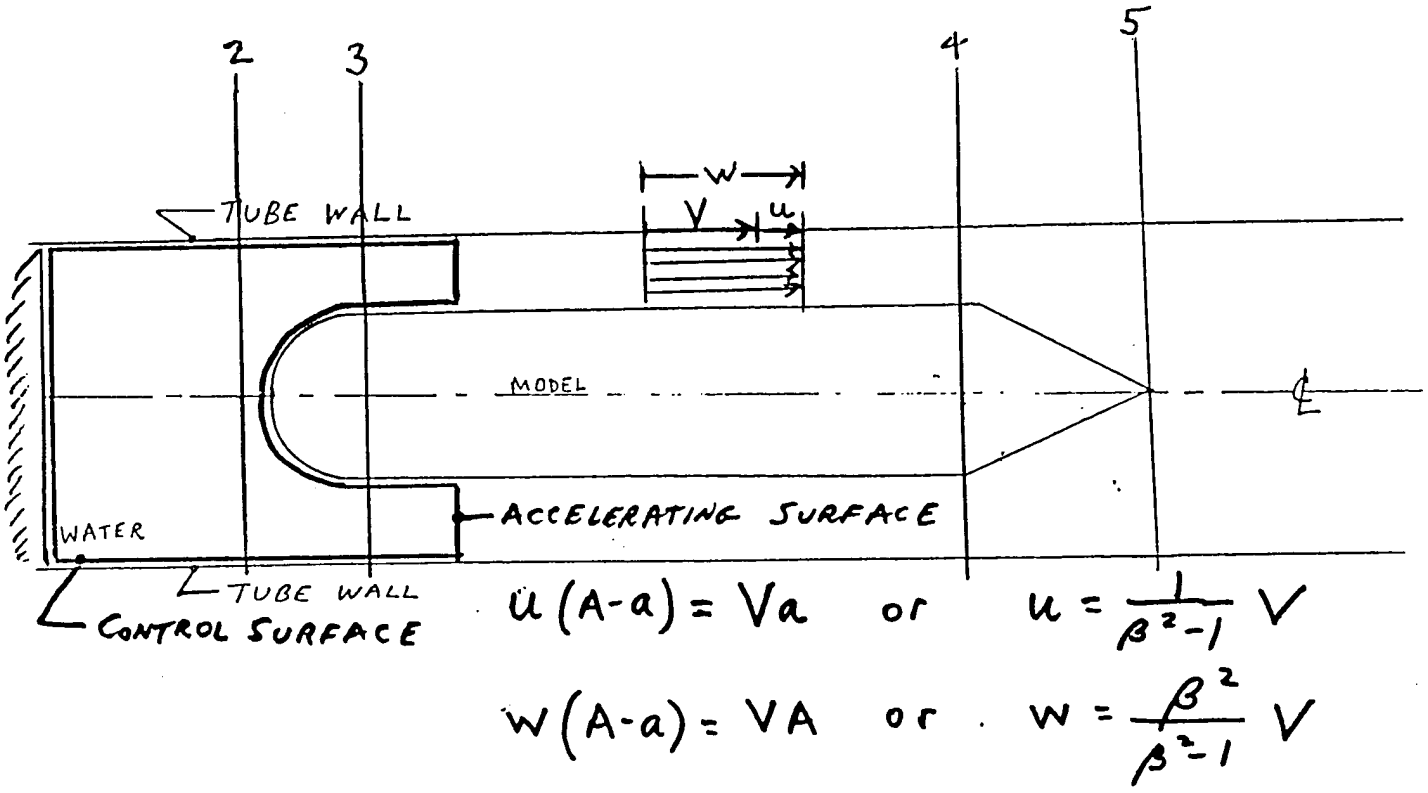

Figure 12. Control Volume with Accelerating Surface

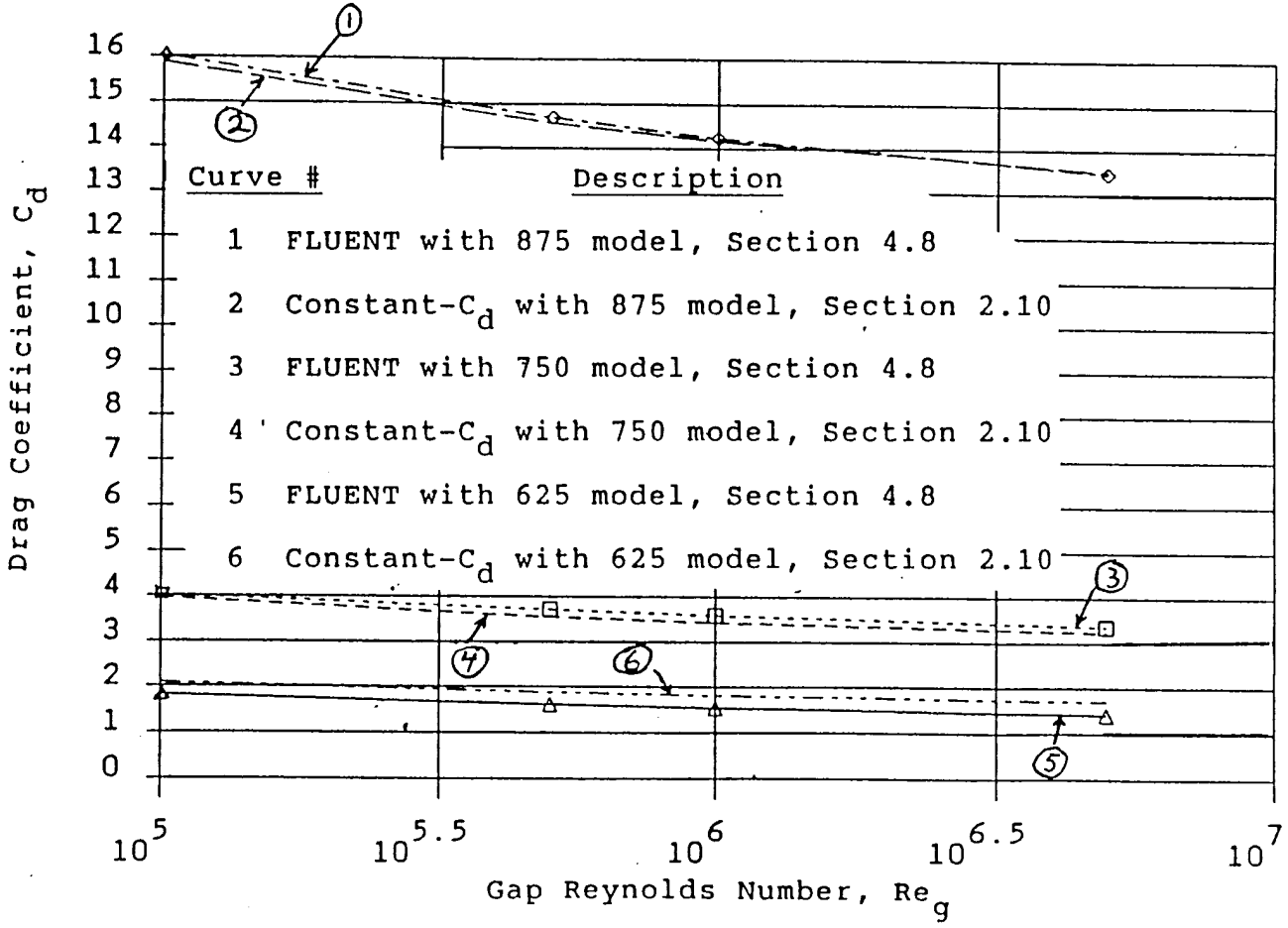

Figure 13. Computed Drag Coefficients, C_d vs. Gap Reynolds Number, Re_g

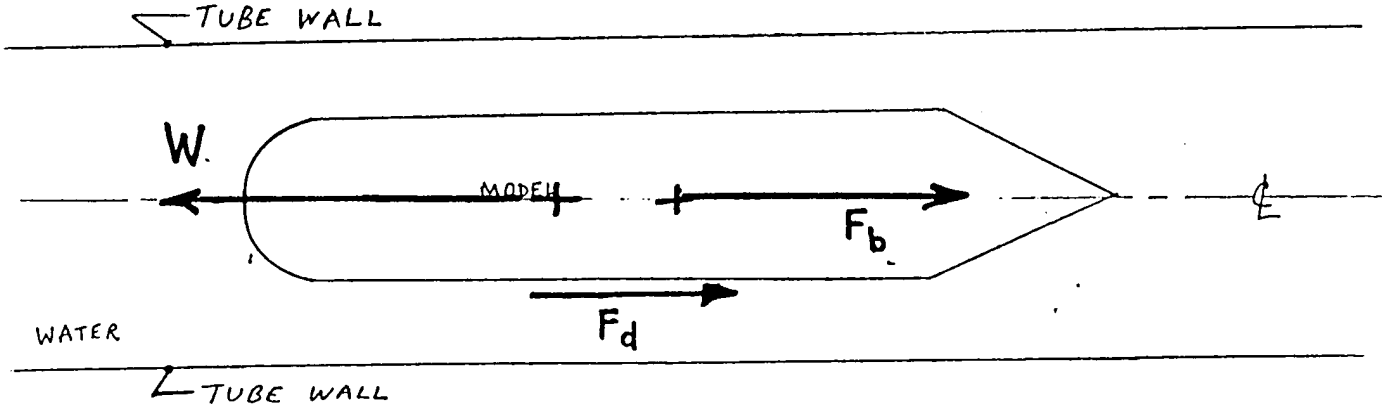

$$\overset{+}{\leftarrow} \quad W - F_b - F_d = (m + m_H)\frac{dV}{dt}$$

$$\text{or} \quad W_n - \frac{1}{2}\rho V^2 C_d a = (m + m_H)\frac{dV}{dt}$$

Figure 14. Free Body Diagram of the Model

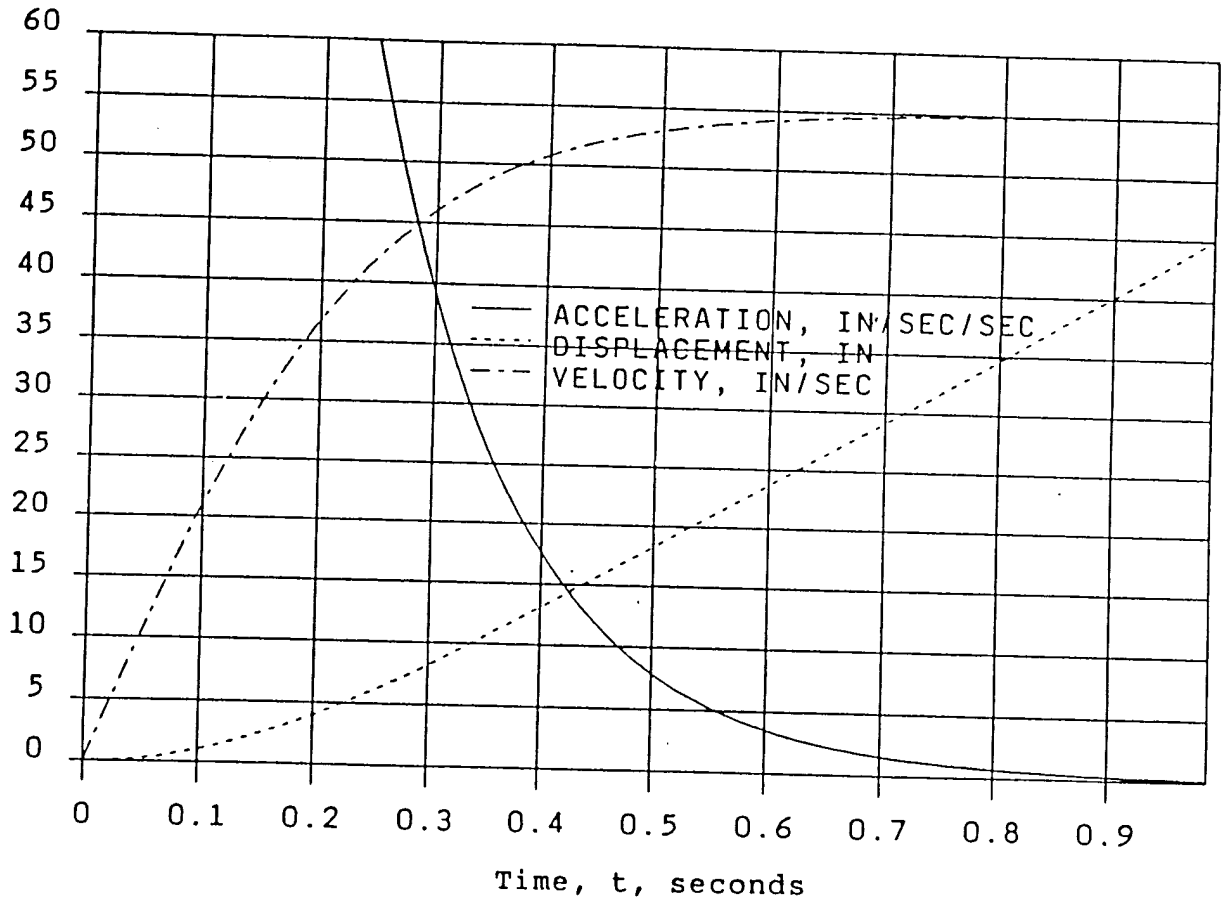

Figure 15. Displacement, Velocity and Acceleration vs. Time for the 625 model

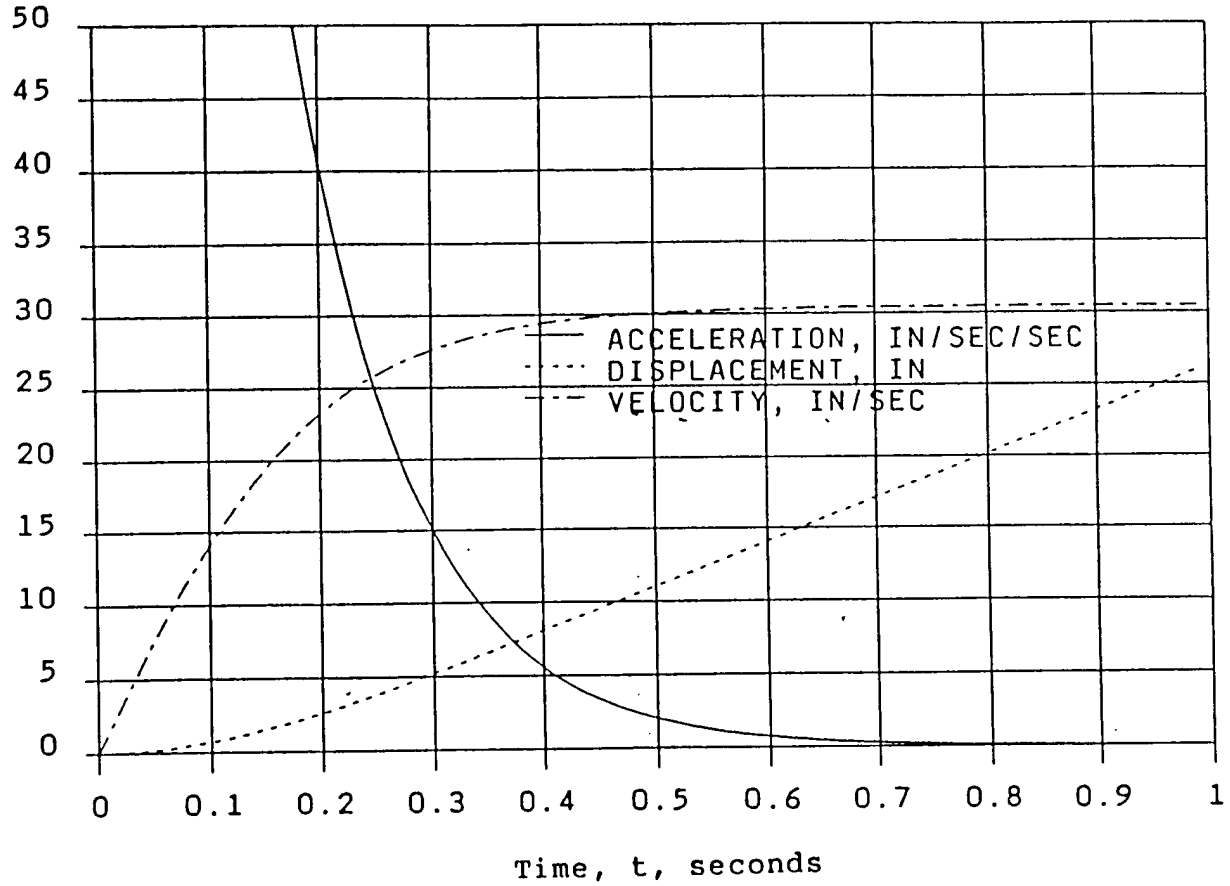

Figure 16. Displacement, Velocity and Acceleration vs. Time for the 750 model

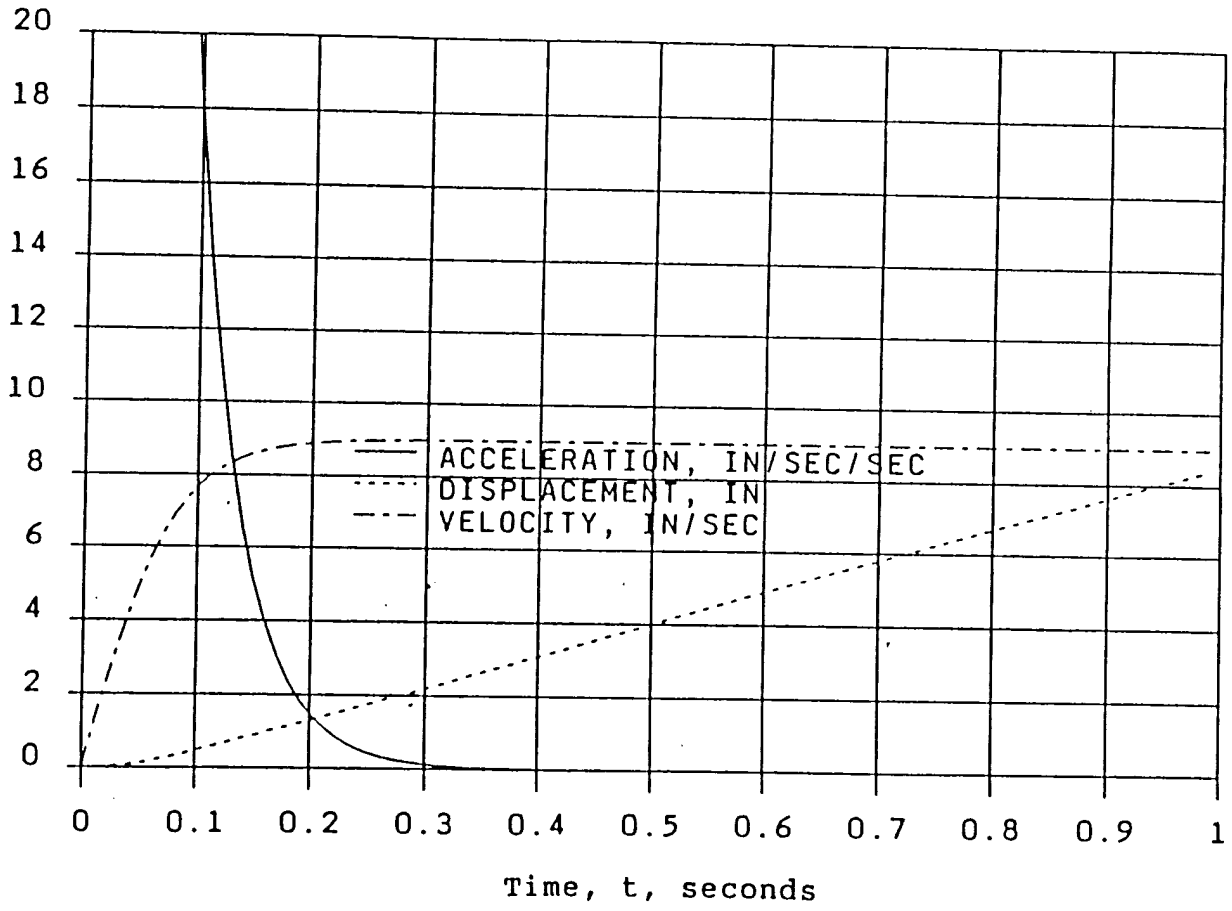

Figure 17. Displacement, Velocity and Acceleration vs. Time for the 875 model

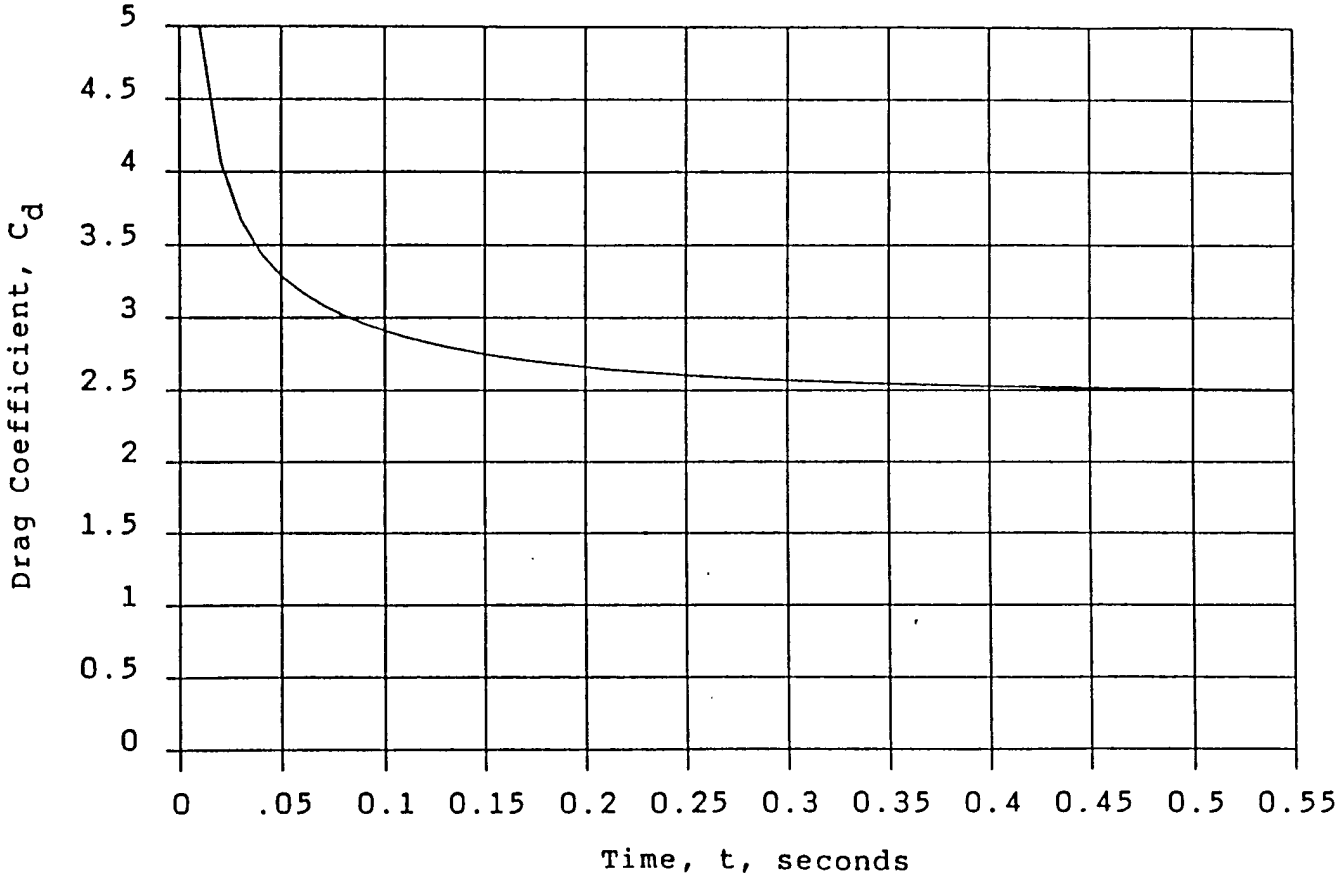

Figure 18. Drag Coefficient vs. Time, predicted by Variable-C_d model, Sect. 2.12

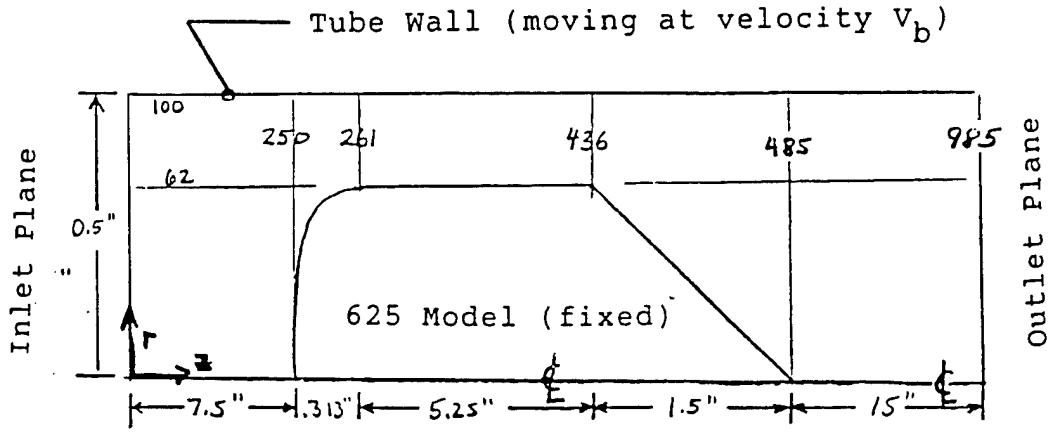

$\Delta z = 0.03"$ Uniform Grid

$\Delta r = 0.005"$ 625 model

Numbers inside the grid signify node numbers; for example, node 62 in the r direction is the outer radius of the model, corresponding to a physical distance of 62*0.005 = 0.031".

Figure 19. Inviscid Grid Layout for the 625 model

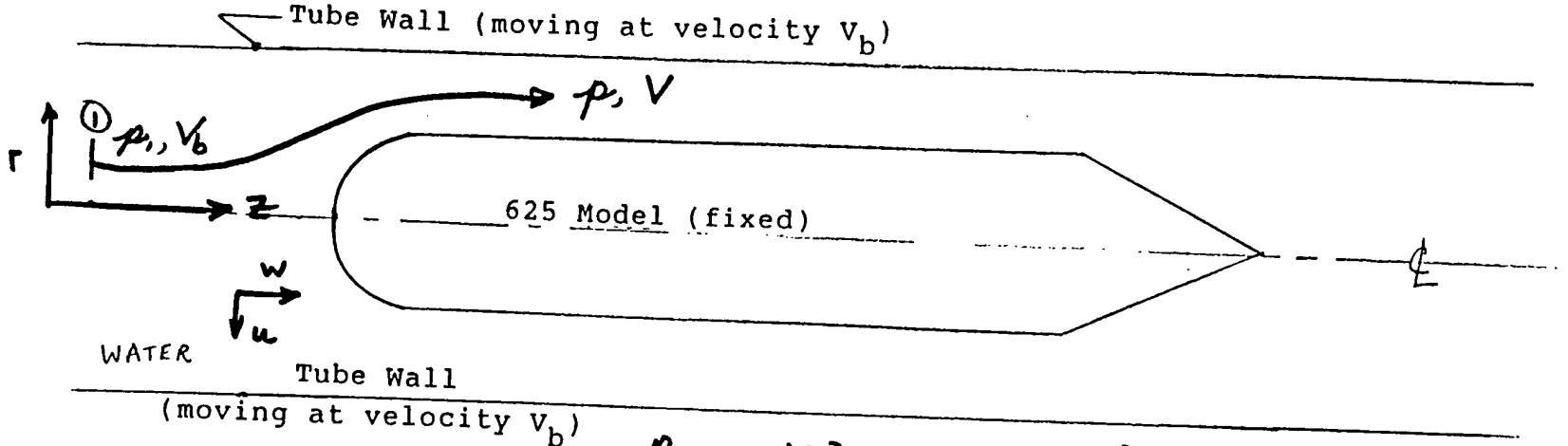

$$\frac{p_1}{\rho} + \frac{V_b^2}{2} = \frac{p}{\rho} + \frac{V^2}{2}$$

$u = v_r$

$v = 0 = v_\theta$

$w = v_z$

$V^2 = u^2 + w^2$

$$\therefore \Delta p = \frac{\rho V_b^2}{2}\left[1 - \frac{V^2}{V_b^2}\right]$$

Figure 20. Streamlines used to Compute Pressure Coefficients, for Inviscid Model

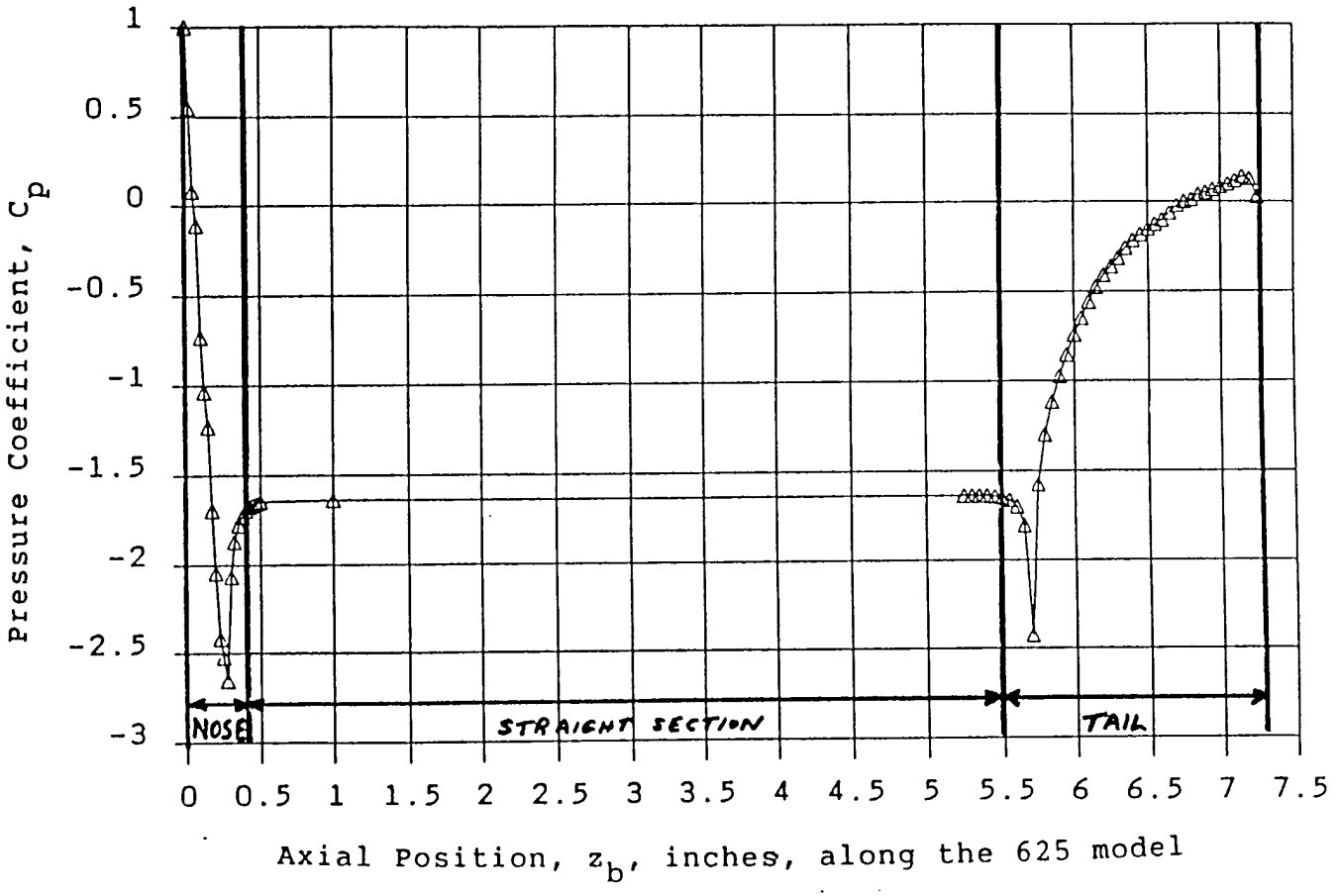

Figure 21. Inviscid Pressure Coefficient vs. Axial Position for the 625 model

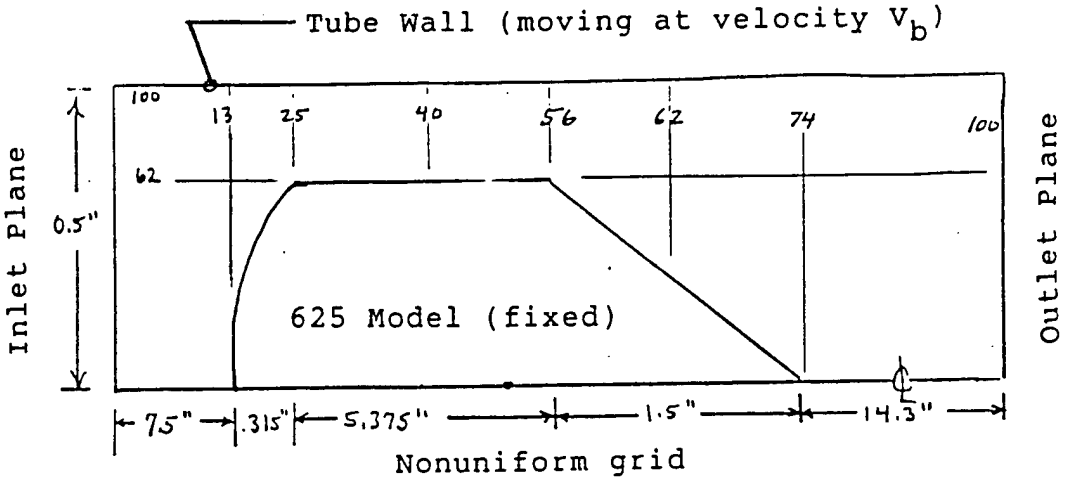

Figure 22. FLUENT grid layout for the 625 model

Numbers inside the grid signify node numbers

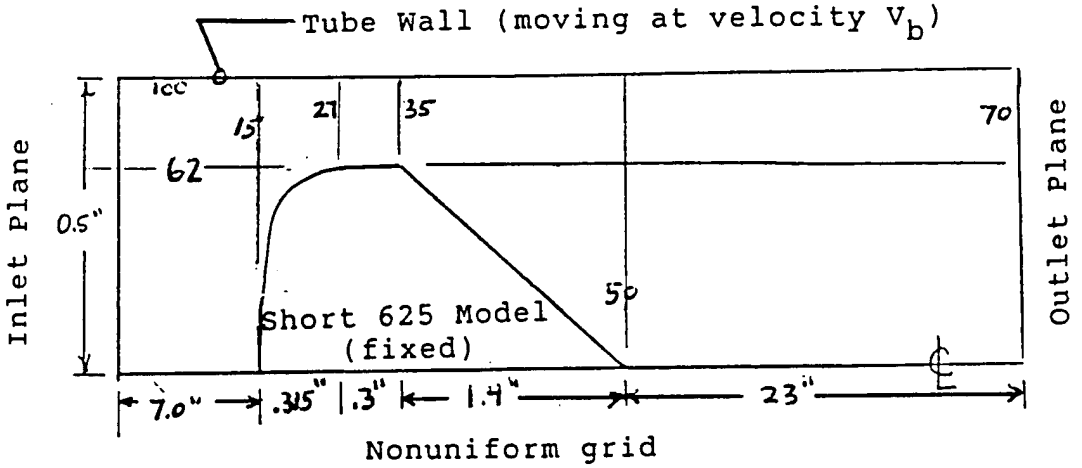

Figure 23. FLUENT grid layout for the Short 625 model

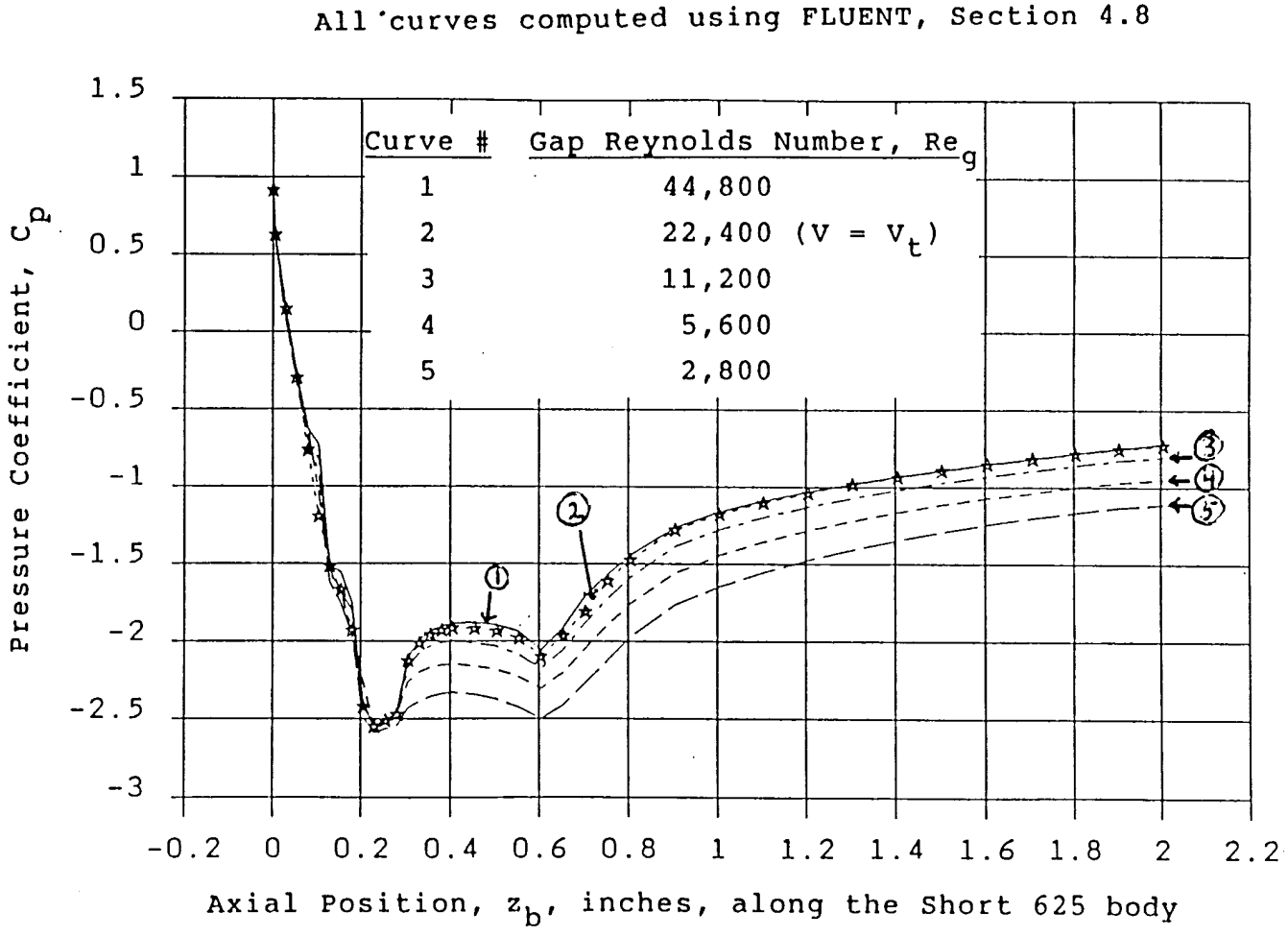

Figure 24. Pressure Coefficient vs. Axial Position for the Short 625 model

Curves #2 through #6 computed using FLUENT, Section 4.8

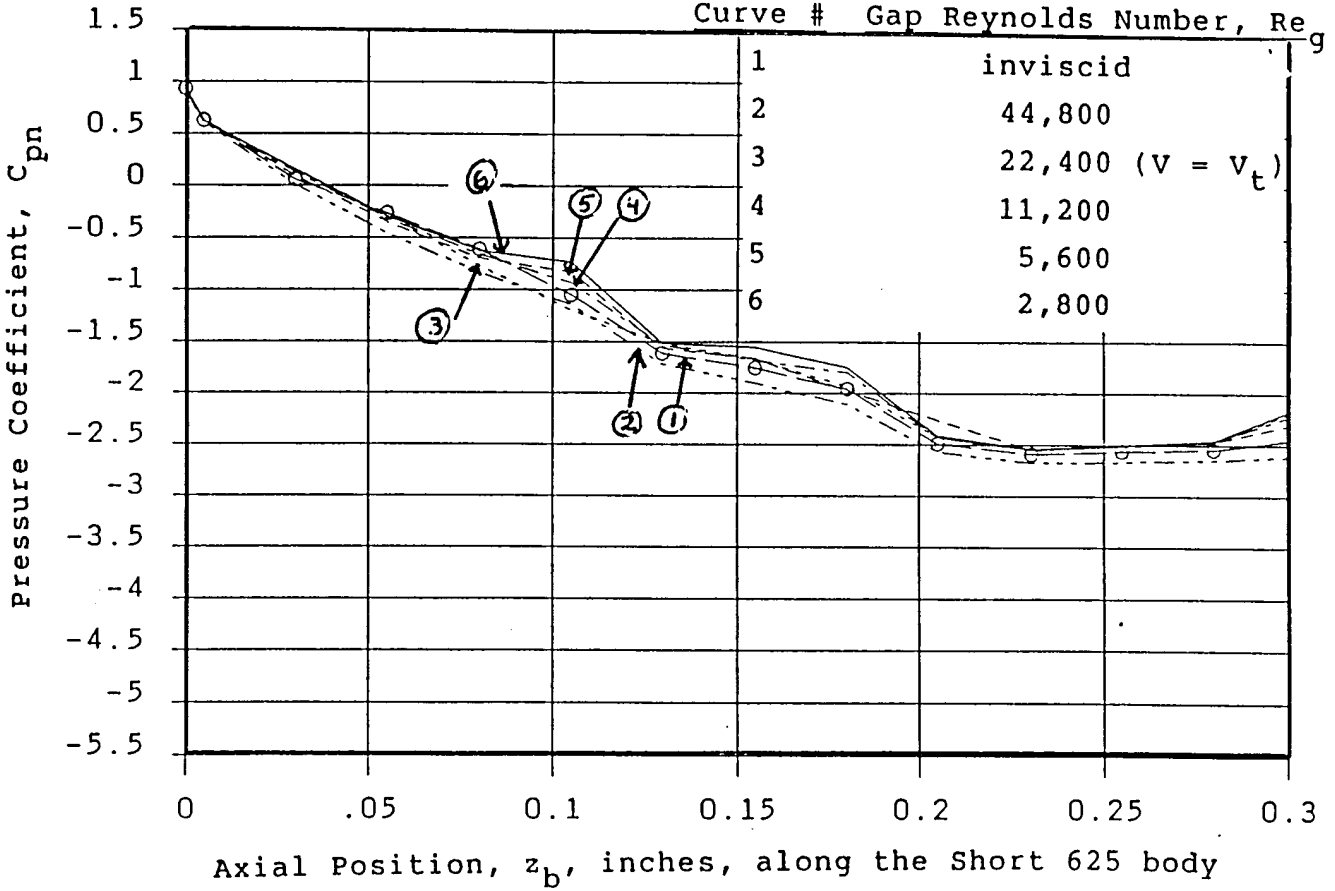

Figure 25. Nose Pressure Coefficient vs. Axial Position for the Short 625 model

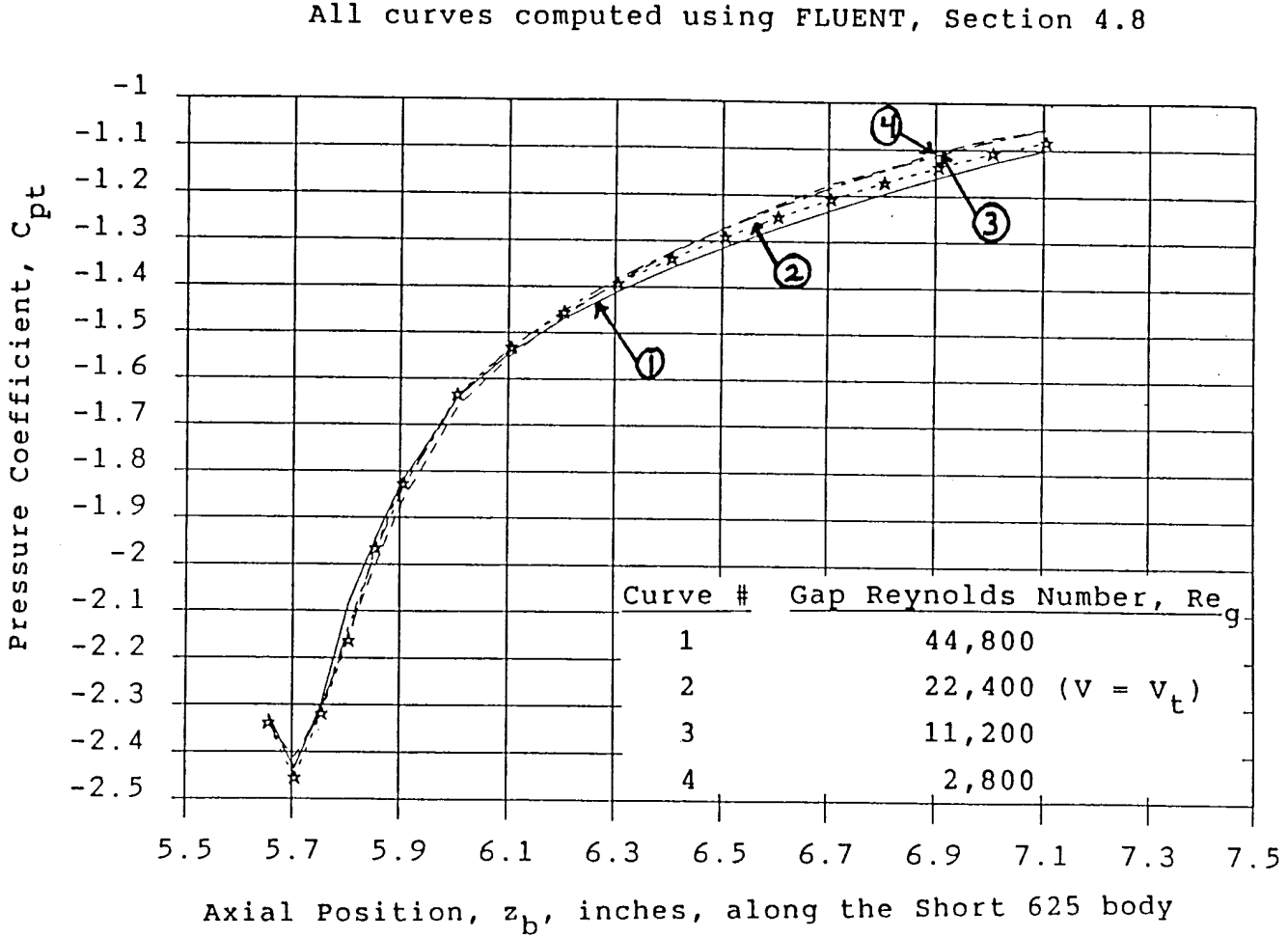

Figure 26. Tail Pressure Coefficient vs. Axial Position for the Short 625 model

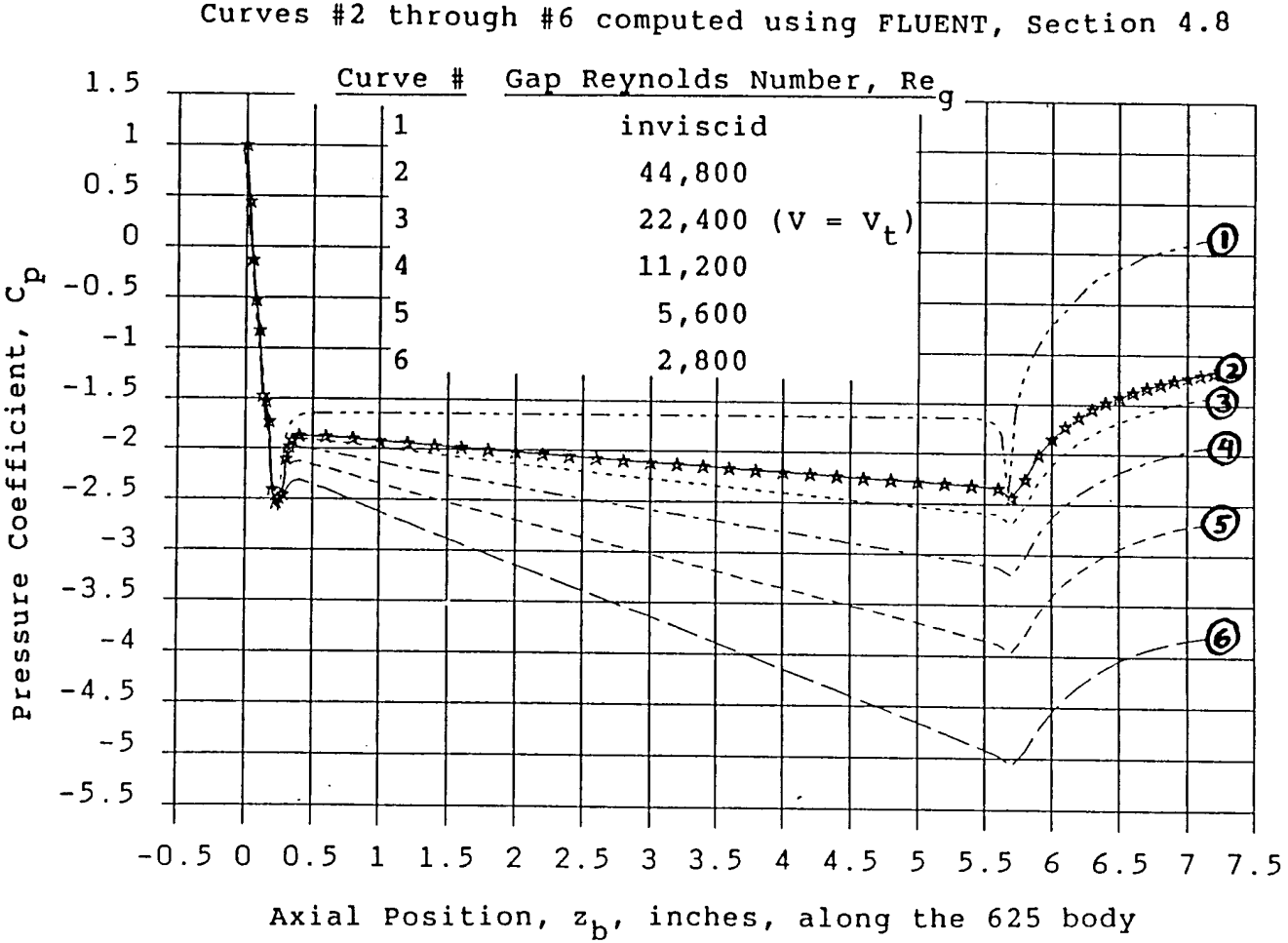

Figure 27. Pressure Coefficient vs. Axial Position for the 625 model

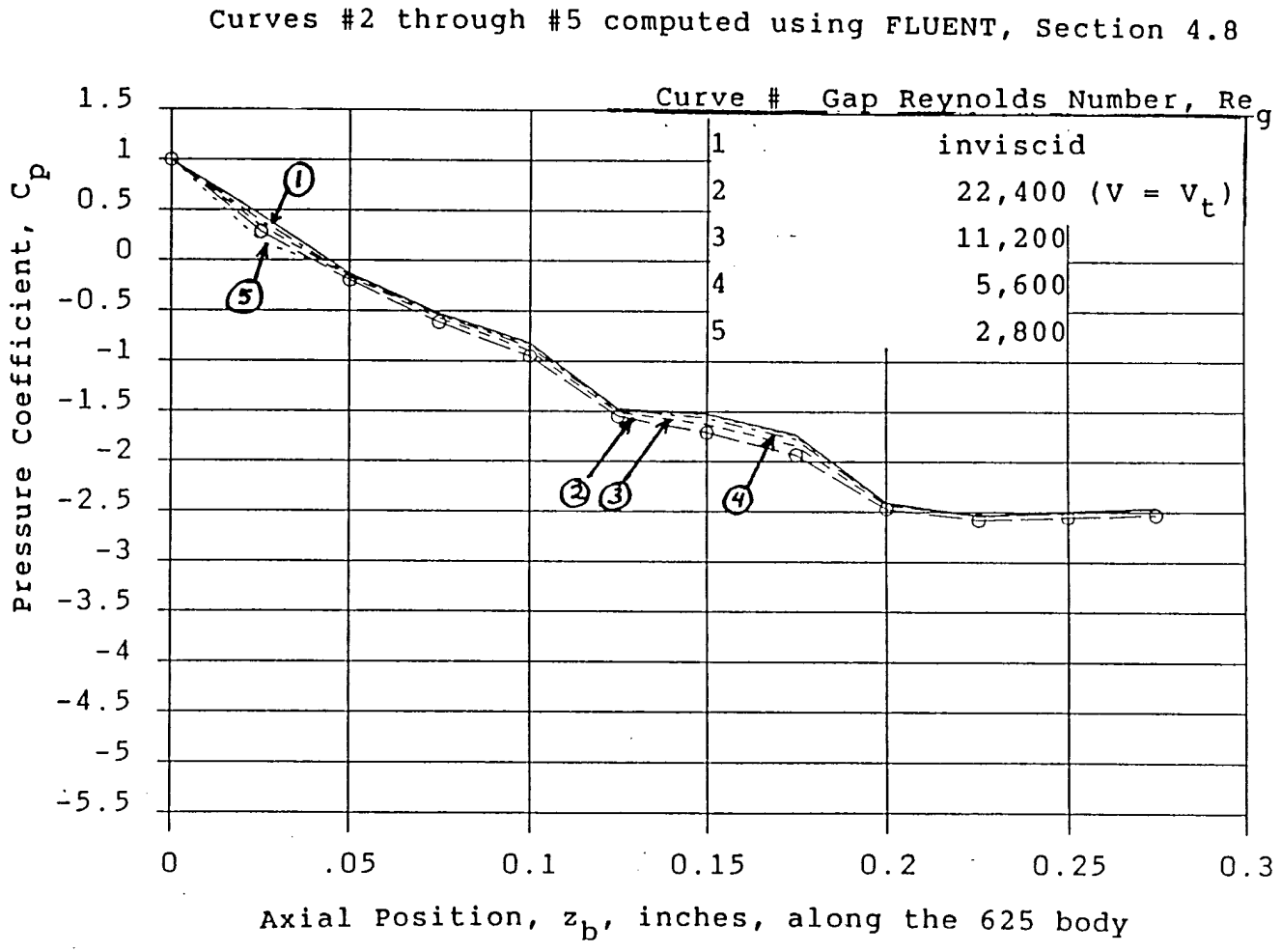

Figure 28. Nose Pressure Coefficient vs. Axial Position for the 625 model

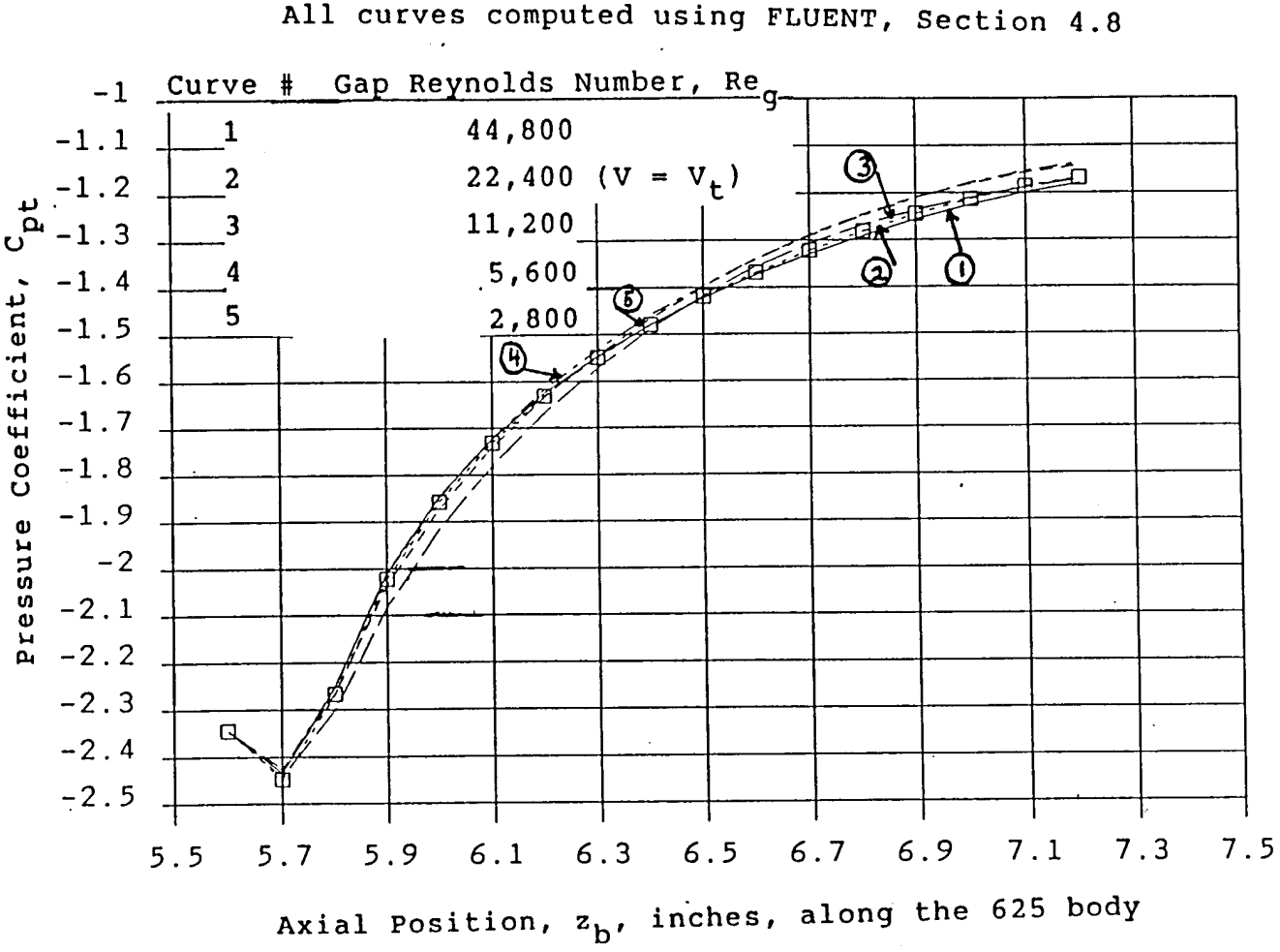

Figure 29. Tail Pressure Coefficient vs. Axial Position for the 625 model

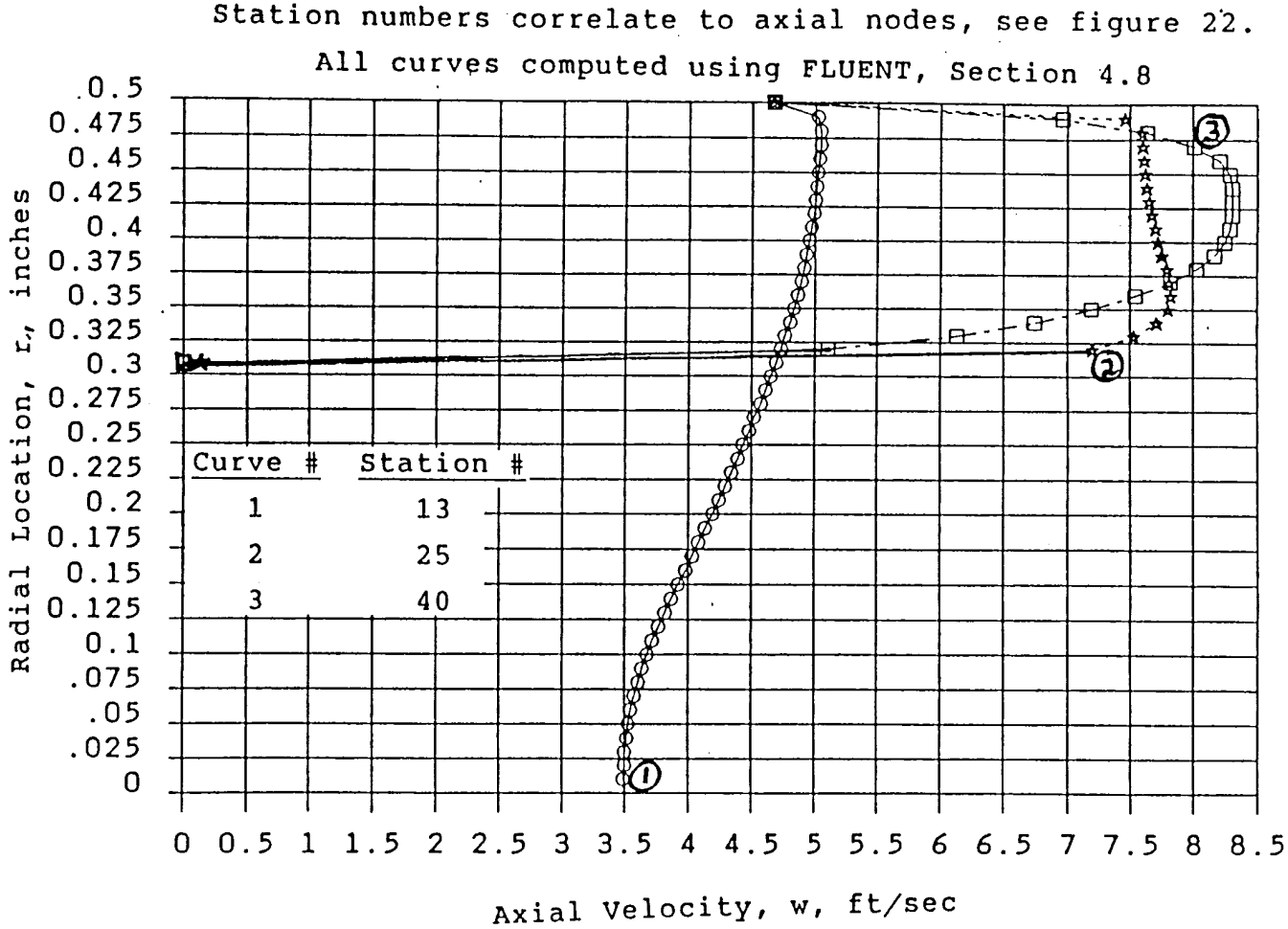

Figure 30. Velocity Profiles, Stations 13, 25 & 40, for the 625 model

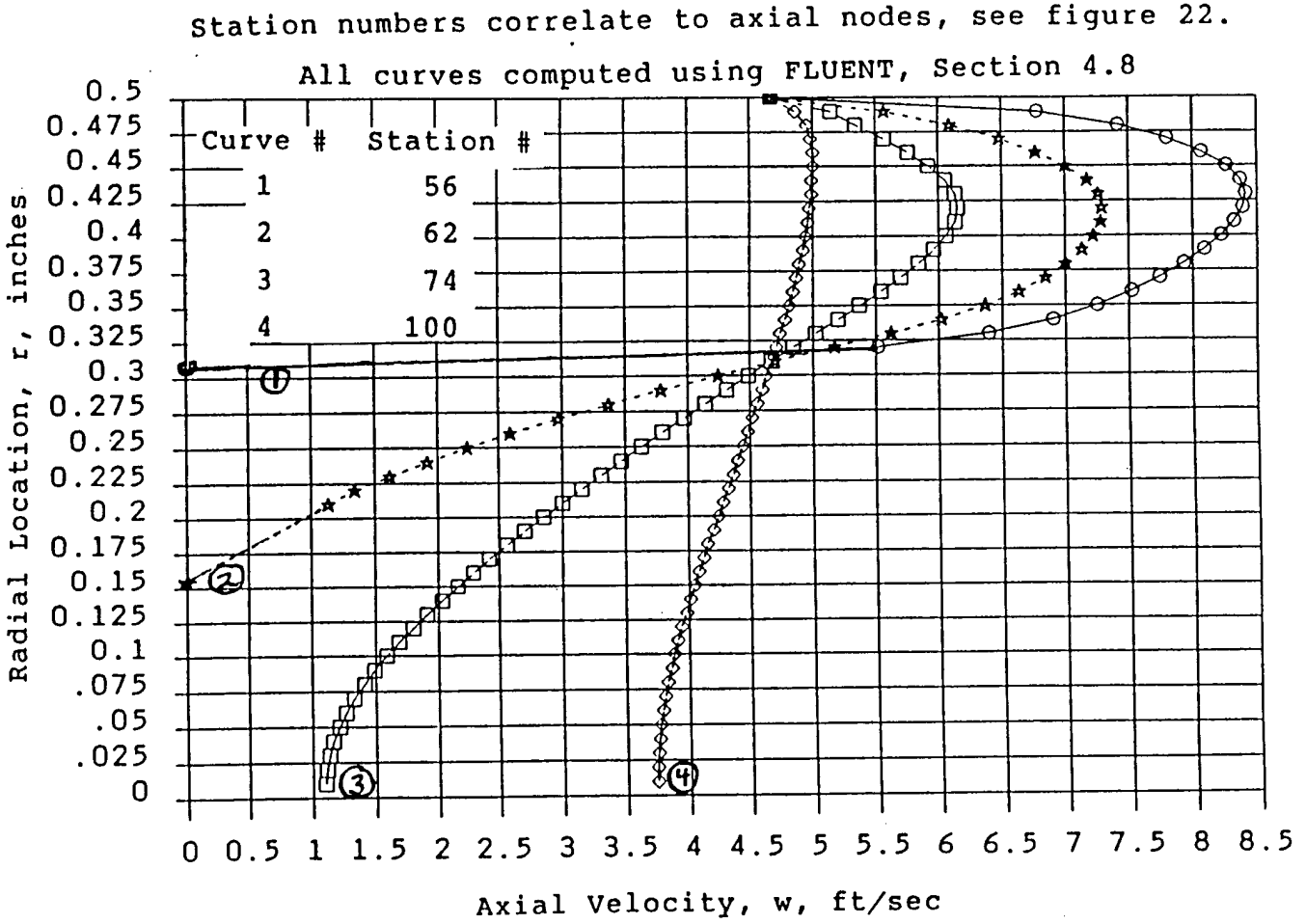

Figure 31. Velocity Profiles, Stations 56, 62, 74 & 100 for the 625 model

Station #56 correlates to axial node #56, see figure 22.

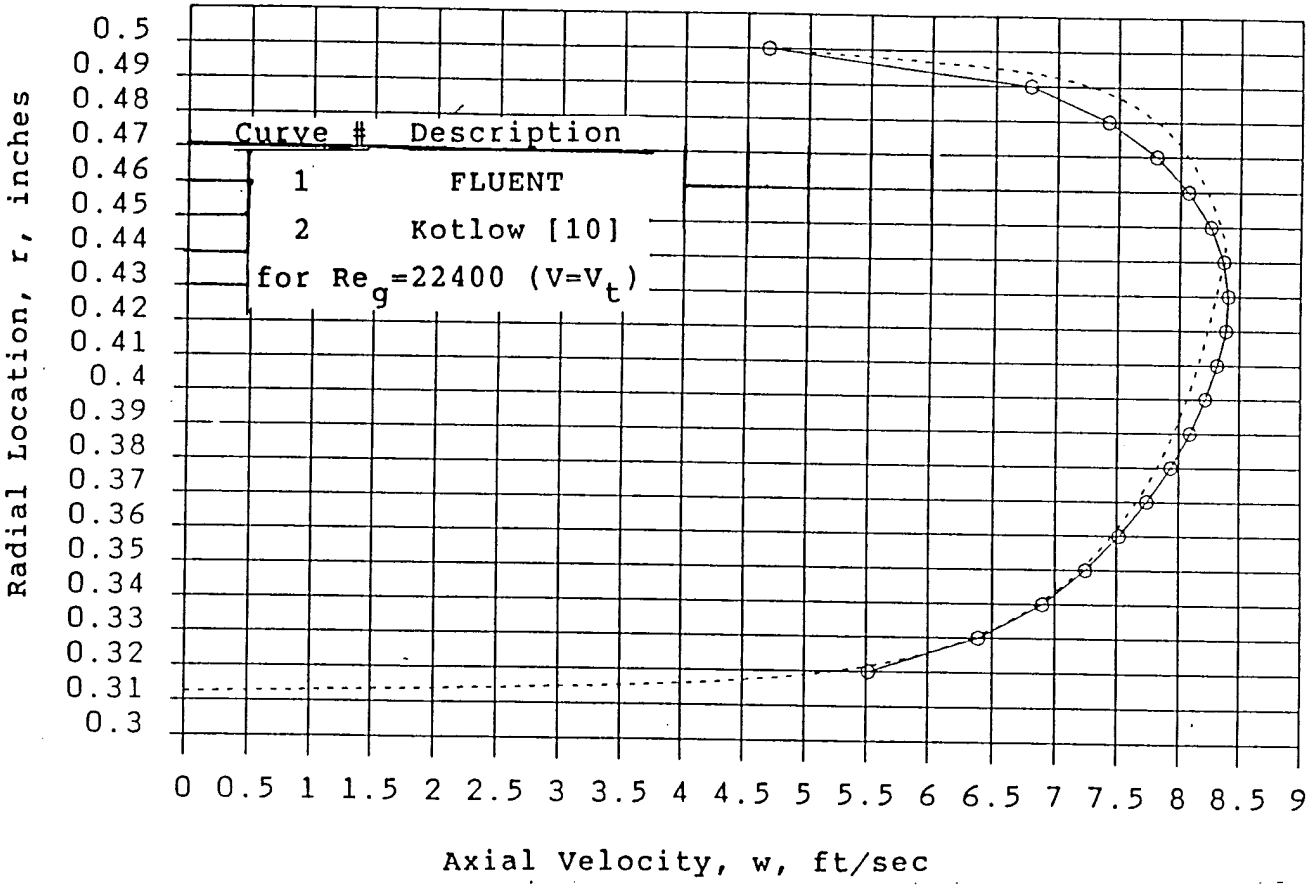

Figure 32. Velocity Profile, Station 56, for 625 model compared to Kotlow [10]

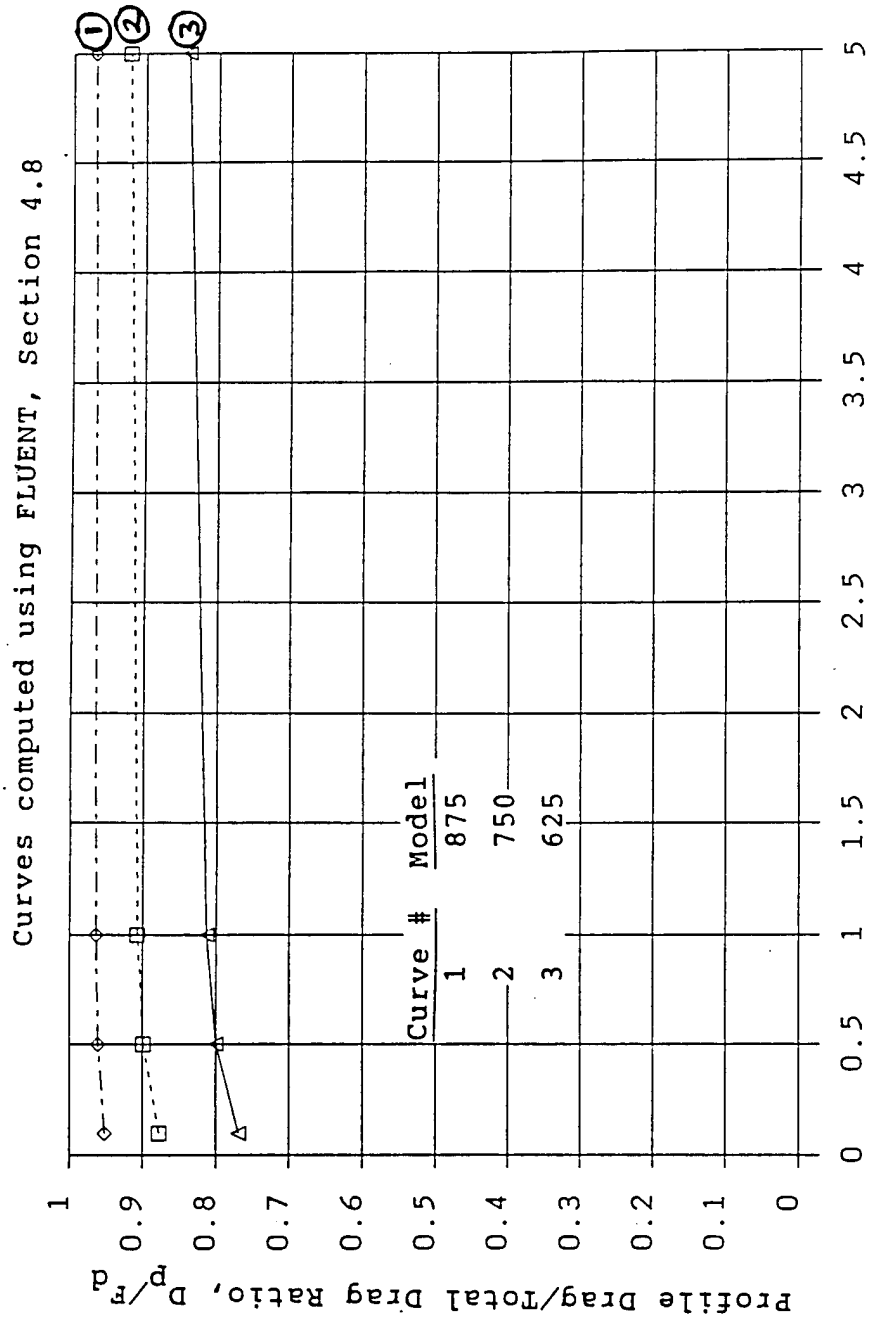

Figure 33. Profile Drag/Total Drag Ratio for the 625, 750 & 875 models

APPENDIX A

FLUID PROPERTIES AND EXPERIMENTAL CONSIDERATIONS

This appendix presents several tables of viscosities for various fluids and discusses experimental methods of achieving low viscosities. Several other experimental issues are briefly discussed including compressibility effects and cavitation.

Gaseous Medium

In order to maximize the Reynolds number, a fluid with very low kinematic viscosity is desirable. In this connection, it is instructive to examine a relation from kinetic theory, White [40] for kinematic viscosity of gas (there is no comparable formula for liquids):

$$\nu = \frac{1.442\text{E-}5\ T^{3/2}}{\sigma^2\ \Omega\ p\ M^{1/2}}\quad \frac{ft^2}{sec}\ ,$$

$$\Omega \simeq 1.147\left(\frac{T}{T_\varepsilon}\right)^{-0.145} + \left(\frac{T}{T_\varepsilon} + 0.5\right)^{-2.0}\ ,$$

where σ = collision diameter, Angstroms; M = molecular wt; T = absolute temperature, °R; T_ε = effective temperature, K; p = pressure, psi; Ω = collision integral, dimensionless. At standard conditions, p = 14.7 psi, T = 530 °R, we have:

(T = 294 K in Ω equation)

Table A-1. Kinematic Viscosities from Kinetic Theory

Gas	M	σ	T_ε	Ω	ν
Air	29	3.711	78.6	1.003	1.61E-4
Ar	39.9	3.542	93.3	1.046	1.44E-4
Cl_2	70.9	4.217	316.0	1.648	4.85E-5
CH_4	16	3.758	148.6	1.202	1.76E-4
CO_2	44	3.941	195.2	1.329	8.74E-5
CO	28	3.690	91.7	1.042	1.60E-4
H_2	2	2.827	59.7	0.944	1.13E-3
He	4	2.551	10.22	0.706	1.30E-3
N_2	28	3.798	71.4	0.981	2.26E-4
NO	30	3.492	116.7	1.113	1.61E-4
N_2O	44	3.828	232.4	1.430	8.61E-5
O_2	32	3.467	106.7	1.085	1.62E-4

Thus from the above table it is seen that chlorine offers the lowest viscosity. Indeed it is difficult to get below ν=2E-5 for any gas at standard pressure and temperature, given the range of σ and T_ε. Chlorine under 1000 atm pressure at room temperature (294 K) gives ν=5E-8. On the other hand it could be done with chlorine at 1 atm. pressure and liquid helium temperatures (3 K). From the formula, one should look for a gas with large collision diameter, σ, large collision integral, Ω, and a large molecular weight, M.

In the event that a gas is chosen as the fluid medium, one must attempt to match both the Reynolds and Mach numbers.

The point in the flow field that will experience the highest velocity (and therefore greatest Mach number) occurs at that cross-section of the body having the greatest diameter. This study was concerned with just the incompressible case, so velocity must be kept well below the speed of sound of the fluid. An approximate analysis can be performed to relate Reynolds number as a function of β and the physical constants of the gas. The tube-model interaction is similar, figure 6 to a one dimensional analysis of a converging-diverging nozzle with Mach number = 0.2 at the throat. To push the allowable Reynolds number even higher demands that a gas be found having a combination of the highest speed of sound, c, and lowest kinematic viscosity.

$$V_g = 0.2c = \frac{\beta^2}{\beta^2 - 1} V, \quad Re_d = \frac{Vd}{\nu}, \quad d = \frac{D}{\beta}, \quad R = \frac{49700}{M},$$

$$Re_{d,max} = \frac{3.716\ D\ (\beta^2-1)}{\beta^3\ \nu} \left(\frac{\gamma T}{M}\right)^{1/2},$$

where D=Tube diameter, inches; M=molecular weight; T=absolute temperature, °R; ν=kinematic viscosity, ft^2/s. Specifically, a gas should have a low molecular weight, low kinematic viscosity and a high specific heat ratio. A careful search was made [42], [43], [44] and the results for 37 different gases follow: (with T = 530°R, D = 1 in., β = 1.6)

Table A-2. Kinematic Viscosities and Limiting Reynolds Numbers for Various Gases

Gas	Formula	M	γ	$\nu * 10^6$		$Re * 10^3$
Acetylene	C_2H_2	26	1.24	100.		71
Air	...	29	1.40	163.		44
Ammonia	NH_3	17	1.29	155.		58
Argon	Ar	39.9	1.66	131.		51
n-Butane	C_4H_{10}	58.1	1.10	31.2		143
Carbon dioxide	CO_2	44	1.28	82.7		68
Carbon monoxide	CO	28	1.40	169.		43
Chlorine	Cl_2	70.9	1.33	51.9		87
Deuterium	D_2	4	1.40	1700.		16
Ethane	C_2H_6	30.1	1.19	78.9		82
Ethylene	C_2H_4	28.1	1.24	93.4		73
Fluorine	F_2	38	1.36	166.		37
R-11[1]	CCl_3F	137.4	1.14	170.	(1)	17
				16.5		180
R-12	CCl_2F_2	120.9	1.14	20.7	(107)	153
				30.5		104
R-22	$CHClF_2$	86.5	1.19	18.3	(22)	209
				41.5		92
R-113	CCl_2F-$CClF_2$	187.4	1.12	318.	(0)	8
				25.5		99

1. Two values are given for each R-XYZ. The first is for saturated vapor at -27°F with the approximate pressure shown in parentheses. The second value is for superheated vapor at 86°F and 1 atm pressure. All pressures ( ), psia.

Table A-2. continued

R-114	C_2Cl2F_4	170.9	1.09	78.7 (3)	33
				16.7	156
R-502	$CHClF_2CClF_2CF_3$	111.6	1.14	13.2 (31)	249
				24.5	134
R-717	NH_3	17	1.29	104. (16)	86
				140.	64
Helium	He	4	1.67	13100.	16
Hydrogen	H_2	2	1.41	1170.	23
Hydr. chloride	HCl	36.5	1.39	108.	59
Hydr. sulfide	H_2S	34.1	1.34	101.	64
Krypton	Kr	83.8	1.67	78.5	59
Methane	CH_4	16	1.30	179.	52
Methyl chloride	CH_3Cl	50.5	1.24	54.7	93
Neon	Ne	20.2	1.67	417.	22
Nitric oxide	NO	30	1.39	167.	42
Nitrogen	N_2	28	1.40	169.	43
Nitrous oxide	N_2O	44	1.27	89.9	62
Nonane	C_3H_{20}	128.3	1.15	20.	154
Oxygen	O_2	32	1.39	164.	42
Ozone	O_3	48	1.27	71.3	74
Propane	C_3H_8	44.1	1.13	47.2	110
Propylene	C_3H_6	42.1	1.15	531.	10
Sulfur dioxide	SO_2	64.1	1.39	53.4	90
Xenon	Xe	131.3	1.15	46.2	66

Looking at the preceding table, one concludes that it is very difficult to get a Reynolds number over 200,000 at

standard pressure and temperature without introducing compressible effects. This survey shows that only marginal improvements can be expected by varying the type of gas, certainly not the 3 orders of magnitude improvement that is required to match the prototype Reynolds number.

The previous arguments from kinetic theory can be invoked to achieve a combination of pressure and temperature that would get the low kinematic viscosity required. One interesting alternative would be to use room temperature Freon-11 at about 500 atm pressure.[2] This would cause the viscosity to come down to about 5E-8 and the density would simultaneously increase on the order of 500 times, causing the model to fall on the order of 10 ft/sec at terminal velocity. Thus one would match both the Reynolds and Mach numbers of the prototype precisely, and still have a reasonably short tube. However, the practical difficulties of performing such a test are impressive.

One is left to conclude that at standard pressure and temperature, assuming a drop test using any gas, there results a very long apparatus to achieve terminal velocity and that compressibility effects are unavoidable. Due to these concerns, the decision was made to use a liquid in the drop test apparatus.

---

2. It must be borne in mind that the critical point of F-11 is at 388.4°F, 635 psia, so that at 500 atm. the perfect gas law will not apply, so the formula for maximum Reynolds number should not be used since it was assumed that the speed of sound was equal to that of an ideal gas.

Liquid Medium

Once again, the goal of high Reynolds numbers motivated a thorough search [42], [43], [44] for liquids with low kinematic viscosities, the results for 52 liquids follow:

(Pressure = 1 atm)[3]

Table A-3. Kinematic Viscosities of Various Liquids

Liquid	Formula	Temperature °C	$\nu * 10^7$ ft*ft/s
Acetic Acid	$C_2H_4O_2$	25	119
Acetone	C_3H_6O	40	43.3
Alcohol, butyl	C_4H_9OH	30	306
Alcohol, ethyl	C_2H_5OH	30	150
Alcohol, methyl	CH_3OH	25	76.6
Alcohol, propyl	C_3H_8O	30	258
Ammonia (~171.)	NH_3	30	32.3
Benzene	C_6H_6	25	74
Bismuth	Bi	285	17.3
	Bi	600	10.7
Bromine	Br_2	20	34.9
Carbolic acid (phenol)	C_6H_6O	25	803
Carbon disulfide	CS_2	25	30.7
Carbon tetrachloride	CCl_4	25	61.8
Castor Oil	...	25	73200
Chloroform	$CHCl_3$	25	39

3. Pressures other than 1 atm. are shown in parenthesis and are in psia. ex. (~171.) means 'about 171 psi absolute'.

Table A-3. continued

Decane	$C_{10}H_{22}$	25	127
Dodecane	$C_{12}H_{26}$	25	196
Ether	$C_4H_{10}O$	25	33.7
Ethyl Acetate	$C_4Cl_3H_5O_2$	25	33.9
Ethyl Bromide	C_2H_5Br	30	26.2
Fuel oil no. 1[4]	...	38	151
Fuel oil no. 2	...	38	215
Fuel oil no. 4	...	38	624
Fuel oil no. 5 (light)	...	38	3443
Fuel oil n0. 5 (heavy)	...	38	8070
Gasoline	...	25	47
Glycerin	$C_3H_8O_3$	25	81200
Heptane	C_7H_{16}	25	62.7
Hexane	C_6H_4	25	48.8
Kerosene	...	25	240
Lead	Pb	350	26.1
	Pb	844	12.0
Linseed oil	...	25	3840
Mercury	Hg	25	12.1
Octane	C_8H_{18}	25	78.6
Pentane	C_5H_{12}	20	41.3
Propane	C_3H_8	-45	20.2
Propylene	C_3H_6	-50	15.9
Propylene glycol	$C_3H_8O_2$	25	4350

4. Fuel oils are taken at the minimum allowed for that grade.

Table A-3. continued

R-11[5] (1)	CCl_3F	-27°F	42.2
(18)		86°F	29.6
R-12 (14)	CCl_2F_2	-27°F	24.1
(107)		86°F	21.1
R-22 (22)	$CHClF_2$	-27°F	23.1
(171)		86°F	21.1
R-113 (0)	$CCl_2F-CClF_2$	-27°F	81.9
(5)		86°F	43.7
R-114 (3)	$C_2Cl_2F_4$	-27°F	41.0
(37)		86°F	26.6
R-500 (18)	$CCl_2F_2-CH_3-CHF_2$	-27°F	23.8
(139)		86°F	20.8
R-502 (31)	$CHClF_2-CClF_2CF_3$	-27°F	24.9
(191)		86°F	21.2
R-717 (16)	NH_3	-27°F	39.5
(171)		86°F	37.6
Sodium bromide	NaBr	780	43.0
Sulfuric acid	H_2SO_4	20	1491
Toluene	C_7H_8	25	68.7
Turpentine	$C_{10}H_{16}$	25	171
Water	H_2O	25	96.1
Zinc	Zn	280	27.9

Mercury looks best at ν=1.21E-6 ft^2/sec at 25°C (77°F), but mercury is opaque, highly reflective and impossible to

5. All the refrigerants, R-XYZ, are for saturated liquid. The first value is taken at -27°F, and the second value is at 86°F.

use since high speed photography is ineffective as are magnetic switches or other commonly used methods of vehicle monitoring. Other fluids are grouped around ~3.E-6 ft^2/sec at standard conditions; however, due primarily to their flammability and/or volatility they were eliminated. The practical choice was water at 1.07E-5 ft^2/sec at 70°F since the viscosity is reasonably low and filming could be easily accomplished. Using water also allows the use of aluminum models, which are easily produced on a lathe and have enough negative buoyancy to fall reasonably fast yet are light enough to reach terminal velocity in a 5 foot tube.

There are two primary concerns when using water or any other liquid. The first is cavitation and the second is model stability. Cavitation is undesirable because it creates a low pressure zone (concern is primarily at the tail region) that will produce a high profile drag. Cavitation can be reduced or eliminated by avoiding flow separation at the rear of the model. In this connection, it is helpful to keep model speed down and simultaneously place a conical tail on the model. If higher model speeds or blunt tail cones are desired, the problem can be eliminated by pressurizing the system so that at no point in the flow field does the fluid experience less than the vapor pressure. The approach taken in this study was to keep model speed low (terminal velocity less than 5 ft/sec) and to have an integral conical tail with a slope of 1:3. The high speed film was then closely examined for

tell-tale vapor bubbles at the rear of the falling model; thus, it was decided that cavitation was not a factor. Model stability was provided by a central guidewire as discussed in Chap. 3.

A presentation of experimental data of distance vs. time, i.e., Z vs. t, from the drop tests is given in the following three tables. Table A-4 presents five representative runs of the 625 body falling through a water filled tube of 1" inside diameter (d=0.625", D=1.0"). Table A-5 gives five runs for the 750 body (d=0.75", D=1"). Table A-6 presents five runs for the 875 body (d=0.875", D=1.0").

Table A-4. Model 625 Drop Test Data

TIME sec.	Z(1) in.	Z(2) in.	Z(3) in.	Z(4) in.	Z(5) in.	Z_{avg} in.
0.00	0.00	0.00	0.00	0.00	0.00	0.00
0.01	0.03	0.01	0.04	0.00	0.04	0.02
0.02	0.08	0.04	0.09	0.01	0.09	0.06
0.03	0.14	0.07	0.17	0.06	0.15	0.12
0.04	0.20	0.12	0.29	0.16	0.21	0.19
0.05	0.26	0.19	0.40	0.30	0.29	0.29
0.06	0.35	0.32	0.55	0.44	0.38	0.41
0.07	0.50	0.48	0.67	0.59	0.56	0.56
0.08	0.69	0.67	0.80	0.77	0.75	0.74
0.09	0.89	0.85	0.97	0.91	0.91	0.91
0.10	1.14	1.01	1.15	1.09	1.05	1.09
0.11	1.34	1.24	1.34	1.32	1.27	1.30
0.12	1.54	1.47	1.61	1.58	1.58	1.55
0.13	1.74	1.70	1.85	1.79	1.76	1.77
0.14	1.96	1.93	2.16	2.10	2.00	2.03
0.15	2.22	2.23	2.42	2.33	2.22	2.29
0.16	2.50	2.51	2.75	2.59	2.59	2.59
0.17	2.80	2.88	3.05	2.89	2.89	2.90
0.18	3.13	3.18	3.32	3.17	3.18	3.19
0.19	3.40	3.51	3.68	3.48	3.54	3.52
0.20	3.86	3.87	4.00	3.84	3.95	3.90
0.21	4.28	4.13	4.37	4.26	4.31	4.27
0.22	4.66	4.54	4.77	4.70	4.67	4.67
0.23	5.05	4.96	5.19	5.13	5.01	5.07
0.24	5.48	5.31	5.62	5.54	5.38	5.47
0.25	5.91	5.67	6.03	5.92	5.82	5.87
0.26	6.30	6.09	6.47	6.28	6.33	6.29
0.27	6.63	6.44	6.83	6.72	6.80	6.68
0.28	7.11	6.86	7.33	7.21	7.22	7.14
0.29	7.52	7.42	7.68	7.62	7.67	7.58
0.30	7.99	7.87	8.09	8.08	8.13	8.03

Table A-4. continued

TIME sec.	Z(1) in.	Z(2) in.	Z(3) in.	Z(4) in.	Z(5) in.	Z_{avg} in.
0.31	8.51	8.32	8.65	8.59	8.54	8.52
0.32	9.01	8.95	9.08	9.10	9.09	9.05
0.33	9.46	9.45	9.50	9.57	9.56	9.51
0.34	9.94	9.91	9.93	10.06	10.04	9.97
0.35	10.48	10.34	10.38	10.57	10.61	10.48
0.36	10.99	10.82	10.86	11.13	11.11	10.98
0.37	11.49	11.31	11.35	11.58	11.62	11.47
0.38	12.00	11.80	11.89	12.07	12.20	11.99
0.39	12.55	12.32	12.43	12.53	12.62	12.49
0.40	13.10	12.82	12.96	13.03	13.13	13.01
0.41	13.65	13.32	13.50	13.54	13.63	13.53
0.42	14.19	13.82	14.04	14.10	14.14	14.06
0.43	14.74	14.32	14.58	14.67	14.65	14.59
0.44	15.30	14.82	15.12	15.25	15.17	15.13
0.45	15.85	15.33	15.67	15.82	15.76	15.69
0.46	16.40	15.89	16.23	16.40	16.35	16.25
0.47	16.95	16.45	16.80	16.98	16.94	16.82
0.48	17.51	17.01	17.36	17.56	17.53	17.40
0.49	18.08	17.56	17.92	18.15	18.12	17.97
0.50	18.65	18.14	18.49	18.74	18.69	18.54
0.51	19.22	18.73	19.03	19.32	19.27	19.11
0.52	19.78	19.33	19.57	***	19.84	19.63
		#### steady state ####				
0.53	***	19.92	20.11	***	20.42	20.15
0.54	***	20.52	20.65	***	***	20.58

Table A-5. Model 750 Drop Test Data

TIME sec.	Z(1) in.	Z(2) in.	Z(3) in.	Z(4) in.	Z(5) in.	Z_{avg} in.
0.00	0.00	0.00	0.00	0.00	0.00	0.00
0.01	0.00	0.00	0.00	0.03	0.02	0.01
0.02	0.00	0.02	0.01	0.08	0.06	0.03
0.03	0.00	0.06	0.04	0.09	0.11	0.06
0.04	0.03	0.13	0.08	0.14	0.17	0.11
0.05	0.10	0.23	0.15	0.23	0.22	0.19
0.06	0.20	0.33	0.26	0.34	0.33	0.29
0.07	0.30	0.40	0.39	0.44	0.45	0.39
0.08	0.44	0.50	0.53	0.54	0.53	0.51
0.09	0.57	0.59	0.66	0.65	0.62	0.62
0.10	0.71	0.70	0.76	0.80	0.76	0.74
0.11	0.84	0.86	0.89	0.95	0.91	0.89
0.12	0.99	1.07	1.04	1.11	1.07	1.06
0.13	1.21	1.27	1.22	1.31	1.26	1.25
0.14	1.48	1.42	1.42	1.47	1.46	1.45
0.15	1.66	1.60	1.63	1.62	1.63	1.63
0.16	1.83	1.79	1.84	1.82	1.86	1.83
0.17	2.03	2.11	2.06	2.07	2.14	2.08
0.18	2.27	2.33	2.32	2.29	2.32	2.31
0.19	2.50	2.53	2.58	2.51	2.52	2.53
0.20	2.75	2.80	2.84	2.77	2.76	2.78
0.21	3.02	3.06	3.08	3.03	3.05	3.05
0.22	3.26	3.28	3.33	3.23	3.28	3.28
0.23	3.48	3.61	3.58	3.49	3.59	3.55
0.24	3.79	3.80	3.84	3.70	3.79	3.78
0.25	4.09	4.16	4.10	3.96	4.03	4.07
0.26	4.35	4.44	4.36	4.21	4.29	4.33
0.27	4.58	4.70	4.61	4.47	4.57	4.59
0.28	4.91	4.96	4.87	4.73	4.84	4.86
0.29	5.20	5.26	5.14	5.01	5.15	5.15
0.30	5.46	5.57	5.43	5.28	5.45	5.44

Table A-5. continued

TIME sec.	Z(1) in.	Z(2) in.	Z(3) in.	Z(4) in.	Z(5) in.	Z_{avg} in.
0.31	5.77	5.83	5.70	5.61	5.73	5.73
0.32	6.11	6.09	5.96	5.86	6.00	6.00
0.33	6.37	6.37	6.21	6.12	6.27	6.27
0.34	6.67	6.68	6.53	6.39	6.55	6.56
0.35	7.02	6.96	6.84	6.67	6.83	6.86
0.36	7.32	7.25	7.13	6.95	7.12	7.15
0.37	7.58	7.54	7.43	7.23	7.41	7.44
0.38	7.89	7.82	7.72	7.51	7.70	7.73
0.39	8.20	8.12	8.01	7.78	7.99	8.02
0.40	8.47	8.42	8.30	8.07	8.28	8.31
0.41	8.76	8.68	8.58	8.38	8.59	8.60
0.42	9.06	8.94	8.87	8.70	8.90	8.89
0.43	9.37	9.19	9.15	9.01	9.20	9.19
0.44	9.72	9.51	9.44	9.32	9.51	9.50
0.45	10.01	9.81	9.73	9.61	9.81	9.79
0.46	10.27	10.13	10.03	9.88	10.11	10.08
0.47	10.54	10.46	10.32	10.15	10.40	10.37
0.48	10.86	10.74	10.62	10.41	10.70	10.67
		#### steady state ####				
0.49	11.15	11.02	10.91	10.68	10.99	10.95
0.50	11.42	11.29	11.19	10.99	11.29	11.23
0.51	11.68	11.63	11.46	11.30	11.58	11.53
0.52	11.95	11.99	11.74	11.62	11.88	11.83
0.53	12.23	12.28	12.02	11.94	12.17	12.13
0.54	12.52	12.57	12.29	12.26	12.47	12.42
0.55	12.81	12.86	12.57	12.53	12.76	12.71
0.56	13.10	13.16	12.86	12.80	13.05	12.99
0.57	13.38	13.45	13.15	13.07	13.33	13.28
0.58	13.67	13.74	13.43	13.34	13.62	13.56
0.59	13.95	14.03	13.72	13.62	13.91	13.84
0.60	14.23	14.32	14.00	13.90	14.19	14.13

Table A-5. continued

TIME sec.	Z(1) in.	Z(2) in.	Z(3) in.	Z(4) in.	Z(5) in.	Z_{avg} in.
0.61	14.50	14.62	14.29	14.22	14.47	14.42
0.62	14.78	14.91	14.57	14.54	14.74	14.71
0.63	15.06	15.20	14.86	14.86	15.01	15.00
0.64	15.36	15.49	15.15	15.19	15.29	15.29
0.65	15.67	15.78	15.45	15.48	15.57	15.59
0.66	15.98	16.07	15.75	15.78	15.87	15.89
0.67	16.29	16.35	16.05	16.07	16.16	16.19
0.68	16.60	16.62	16.35	16.37	16.46	16.48
0.69	16.89	16.90	16.63	16.66	16.75	16.77
0.70	17.19	17.17	16.90	16.93	17.04	17.05
0.71	17.48	17.44	17.17	17.20	17.33	17.33
0.72	17.78	17.72	17.44	17.47	17.62	17.60
0.73	18.07	18.00	17.71	17.74	17.91	17.89
0.74	18.36	18.28	17.99	18.01	18.20	18.17
0.75	18.64	18.57	18.27	18.30	18.47	18.45
0.76	18.92	18.85	18.56	18.59	18.74	18.73
0.77	19.20	19.14	18.85	18.89	19.01	19.02
0.78	19.48	19.45	19.14	19.18	19.28	19.30
0.79	19.78	19.75	19.43	19.48	19.54	19.60
0.80	20.08	20.06	19.72	19.77	19.83	19.89
0.81	20.38	20.37	20.01	20.06	20.12	20.18
0.82	20.68	20.67	20.30	20.34	20.41	20.48
0.83	20.98	20.98	20.58	20.63	20.70	20.78
0.84	21.27	21.30	***	20.92	20.99	21.12
0.85	21.53	21.61	***	***	21.28	21.47
0.86	21.79	21.92	***	***	***	21.85
0.87	22.05	22.23	***	***	***	22.14
0.88	22.31	***	***	***	***	22.31

Table A-6. Model 875 Drop Test Data

TIME sec.	Z(1) in.	Z(2) in.	Z(3) in.	Z(4) in.	Z(5) in.	Z_{avg} in.
0.00	0.00	0.00	0.00	0.00	0.00	0.00
0.01	0.01	0.02	0.01	0.01	0.01	0.01
0.02	0.03	0.04	0.03	0.03	0.03	0.03
0.03	0.06	0.09	0.05	0.08	0.07	0.07
0.04	0.11	0.14	0.09	0.18	0.15	0.13
0.05	0.15	0.19	0.14	0.26	0.20	0.19
0.06	0.20	0.24	0.24	0.32	0.25	0.25
0.07	0.25	0.29	0.28	0.42	0.30	0.31
0.08	0.34	0.37	0.34	0.50	0.35	0.38
0.09	0.44	0.47	0.44	0.57	0.41	0.46
0.10	0.53	0.57	0.53	0.66	0.50	0.56
0.11	0.62	0.63	0.62	0.73	0.59	0.64
0.12	0.70	0.70	0.71	0.81	0.66	0.72
0.13	0.75	0.80	0.80	0.90	0.76	0.80
0.14	0.84	0.89	0.84	1.00	0.86	0.89
0.15	0.94	0.98	0.90	1.09	0.96	0.97
0.16	1.03	1.07	0.99	1.17	1.05	1.06
0.17	1.07	1.14	1.09	1.25	1.15	1.14
0.18	1.17	1.21	1.17	1.33	1.24	1.23
0.19	1.26	1.31	1.24	1.42	1.33	1.31
0.20	1.35	1.40	1.34	1.50	1.41	1.40
0.21	1.45	1.49	1.44	1.60	1.50	1.50
0.22	1.53	1.58	1.54	1.70	1.58	1.59
0.23	1.62	1.68	1.64	1.79	1.66	1.68
0.24	1.71	1.77	1.74	1.89	1.75	1.77
0.25	1.80	1.86	1.85	1.99	1.84	1.87
0.26	1.89	1.96	1.95	2.08	1.93	1.96
0.27	1.97	2.05	2.03	2.18	2.02	2.05
		#### steady state ####				
0.28	2.06	2.14	2.11	2.28	2.11	2.14
0.29	2.14	2.23	2.20	2.38	2.21	2.23
0.30	2.23	2.32	2.28	2.47	2.29	2.32

Table A-6. continued

TIME sec.	Z(1) in.	Z(2) in.	Z(3) in.	Z(4) in.	Z(5) in.	Z_{avg} in.
0.31	2.31	2.40	2.37	2.54	2.38	2.40
0.32	2.40	2.49	2.46	2.62	2.47	2.49
0.33	2.48	2.57	2.55	2.70	2.56	2.57
0.34	2.55	2.65	2.64	2.78	2.65	2.66
0.35	2.63	2.73	2.73	2.86	2.74	2.74
0.36	2.71	2.80	2.83	2.95	2.83	2.82
0.37	2.80	2.88	2.90	3.04	2.91	2.91
0.38	2.89	2.95	2.98	3.13	3.00	2.99
0.39	2.99	3.03	3.05	3.22	3.09	3.08
0.40	3.08	3.12	3.13	3.30	3.18	3.16
0.41	3.18	3.21	3.21	3.38	3.26	3.25
0.42	3.27	3.30	3.29	3.46	3.35	3.33
0.43	3.35	3.40	3.37	3.54	3.44	3.42
0.44	3.44	3.49	3.46	3.62	3.52	3.51
0.45	3.53	3.58	3.55	3.70	3.60	3.59
0.46	3.62	3.66	3.63	3.79	3.68	3.68
0.47	3.70	3.75	3.72	3.87	3.76	3.76
0.48	3.79	3.83	3.81	3.96	3.83	3.84
0.49	3.88	3.91	3.90	4.04	3.91	3.93
0.50	3.97	4.01	3.98	4.13	4.01	4.02
0.51	4.06	4.12	4.07	4.23	4.10	4.12
0.52	4.15	4.22	4.15	4.32	4.20	4.21
0.53	4.24	4.32	4.24	4.42	4.30	4.30
0.54	4.33	4.43	4.32	4.51	4.39	4.40
0.55	4.42	4.49	4.41	4.61	4.47	4.48
0.56	4.51	4.55	4.49	4.70	4.55	4.56
0.57	4.59	4.61	4.57	4.79	4.63	4.64
0.58	4.68	4.67	4.64	4.88	4.71	4.72
0.59	4.76	4.72	4.72	4.98	4.79	4.79
0.60	4.85	4.79	4.79	**	**	4.81

APPENDIX B

DEFORMING AND ACCELERATING CONTROL VOLUME ANALYSIS

A control volume analysis proceeding from an inertial coordinate system requires proper development of the integral form of the momentum equation with a deforming and accelerating boundary, figure 12 . The moving boundary is assumed to be attached to the nose of the body and the stationary boundary is fixed to the plugged end of the tube. The fixed tube wall provides the remaining boundary. Begin the analysis with Newton's Second Law of Motion:

$$\Sigma \vec{F} = m \vec{a} = m (\vec{a}_0 + \vec{a}_{rel}),$$

where $\vec{a}_0$ = acceleration of non-inertial coordinate system (xy) wrt the fixed inertial system (XY),

$\vec{a}_{rel}$ = acceleration of a particle wrt the non-inertial system (xy).

Apply Reynolds Transport Theorem (RTT) to, $m \vec{a}_0$:[1]

$$m \vec{a}_0 = \frac{d}{dt} \int_{cv} \vec{V}_0 \, \rho \, d\Lambda + \int_{cs} \rho \vec{V}_0 (\vec{V}_r \cdot \vec{n}) \, dA ,$$

where $\vec{V}_0$ = instantaneous velocity of xy system wrt XY system. Note that $\vec{V}_0$ is not a function of either the volume or the shape of the c.v.,

$\vec{V}_r$ = velocity of particles wrt the c.s. velocity.

---

1. notation: c.v.=cv=control volume, c.s.=cs=control surface, Λ = volume, A = area

$$m\,\vec{a}_0 = \frac{d}{dt}\left(\vec{V}_0 \int_{cv} \rho\, d\Lambda\right) + \vec{V}_0 \int_{cs} \rho\,(\vec{V}_r \cdot \vec{n})\, dA\,.$$

Now use Law of Conservation of Mass:

$$0 = \frac{d}{dt}\int_{cv} \rho\, d\Lambda + \int_{cs} \rho\,(\vec{V}_r \cdot \vec{n})\, dA\,,$$

or $$\int_{cs} \rho\,(\vec{V}_r \cdot \vec{n})\, dA = -\frac{d}{dt}\int_{cv} \rho\, d\Lambda\,.$$

Expanding:

$$m\,\vec{a}_0 = \vec{V}_0 \frac{d}{dt}\int_{cv} \rho\, d\Lambda + \frac{d\vec{V}_0}{dt}\int_{cv} \rho\, d\Lambda - \vec{V}_0 \frac{d}{dt}\int_{cv} \rho\, d\Lambda\,,$$

$$\therefore \quad m\,\vec{a}_0 = \frac{d\vec{V}_0}{dt}\int_{cv} \rho\, d\Lambda\,.$$

Now, apply Reynolds Transport Theorem to the quantity, $m\,a_{rel}$:

$$m\,\vec{a}_{rel} = \frac{d}{dt}\int_{cv} \vec{V}_{rel}\,\rho\, d\Lambda + \int_{cs} \rho\vec{V}_{rel}\,(\vec{V}_r \cdot \vec{n})\, dA,$$

where $\vec{V}_{rel}$ = instantaneous particle velocity in xy.

$$\therefore\ \Sigma\,\vec{F} = \frac{d\vec{V}_0}{dt}\int_{cv} \rho\, d\Lambda + \frac{d}{dt}\int_{cv} \vec{V}_{rel}\,\rho\, d\Lambda + \int_{cs} \rho\vec{V}_{rel}\,(\vec{V}_r \cdot \vec{n})\, dA,$$

which is the law of conservation of momentum for a deforming, accelerating control volume. The form presented here is easily seen to reduce to the familiar form commonly used in fixed control volume analysis.

APPENDIX C

EXPERIMENTAL ACCURACY

This appendix obtains quantitative estimates of experimental accuracy for the measured variables. In cases where quantitative information is unavailable, qualitative estimates are made concerning relative error.

Measured Displacement[1]

Model displacement, S (or Z), was calculated from

$$S = \frac{s_m L}{L_m},$$

where s_m = measured distance, L = actual model length, L_m = measured model length. Note: L/L_m = conversion scale. The relative error is then

$$\frac{\Delta S}{S} = \frac{\Delta s_m}{s_m} + \frac{\Delta L}{L} + \frac{\Delta L_m}{L_m}.$$

$\frac{\Delta s_m}{s_m}$ & $\frac{\Delta L_m}{L_m}$: Both terms are errors introduced by reading the ruler. The ruler was marked in .01 increments. At times the image of the model would become slightly blurred or out of focus when projected on the screen. To help minimize errors the measurements were taken twice, by two different people, then averaged. The maximum Δ was $\pm.03$ inches. Since s_m and L_m were both in a range from 3 to 4 inches, the pessimistic

---

1. subscript: m = measured

estimate of relative error will be taken as $\pm .03/3 = \pm 1\%$.

$\frac{\Delta L}{L}$: This term comes from errors measuring the actual length of the model using a micrometer. The micrometer is accurate to at least $\pm .001$ inch. A skilled machinist read the measurements. The value for L ranged from 3.5 to 7.125 inches. The relative error is then $\pm .001/3.5 \simeq .03\%$, which is negligible.

The relative error is then

$$\frac{\Delta S}{S} = \frac{\Delta s_m}{s_m} + \frac{\Delta L}{L} + \frac{\Delta L_m}{L_m} .$$

S rms error: $(.01^2 + .0003^2 + .01^2)^{0.5} = 1.4\%$.

Velocity Error

The terminal velocity was calculated using the slope of the displacement vs. time curve. The equation for velocity is

$$V = \frac{\delta S}{\delta t} .$$

Relative error is

$$\frac{\Delta V}{V} = \frac{\Delta \delta S}{\delta S} + \frac{\Delta \delta t}{\delta t} .$$

$\frac{\Delta \delta S}{\delta S}$: This term may be described as "the error reading δS divided by δS." The maximum error reading δS is $2*\pm .02$, so $\Delta \delta S = \pm .04$. At a terminal velocity of 9 in./sec for the slowest model, $\delta S \simeq 0.1$ inch from frame to frame. But care was

taken to use a minimum of 2 inches for δS when determining terminal velocity. The result is a relative error of $\pm 2\%$.

$\frac{\Delta\delta t}{\delta t}$: Similar to the preceding term, this term can be thought of as "the error in reading δt." Time was accurately measured with a stroboscope mounted internally to the camera. The strobe was checked against a laboratory quality stroboscope accurate to $\pm .0001$ sec, and found to have essentially perfect synchronization. The internal strobe placed timing marks on the film at $\delta t = .01$ sec. At the highest terminal velocity measured, 56 in./sec, care was taken to use at least 2 inches of travel, which takes $\delta t = .036$ sec or 3.6 timing marks. The most pessimistic approach is to assume an error of 1/10 of the interval between two timing marks. The result is a relative error of $\pm .001/.036 = 2.8\%$. The maximum relative error for terminal velocity is

$$\frac{\Delta V}{V} = \frac{\Delta\delta S}{\delta S} + \frac{\Delta\delta t}{\delta t} .$$

V rms error: $(.02^2 + .028^2)^{0.5} = 3.4\%$.

Drag Coefficient

At terminal velocity, total drag equals the net weight of the model. Drag coefficient is calculated from the relation

$$C_d = \frac{2\, W_n}{\rho\, V^2\, a} .$$

Relative error is then

$$\frac{\Delta C_d}{C_d} = \frac{\Delta W_n}{W_n} + \frac{\Delta \rho}{\rho} + 2\frac{\Delta V}{V} + \frac{\Delta a}{a},$$

where $$\frac{\Delta W_n}{W_n} = \frac{\Delta W}{W} + \frac{\Delta \rho}{\rho} + \frac{\Delta \Lambda}{\Lambda},$$

and $$\frac{\Delta a}{a} = 2\frac{\Delta d}{d}.$$

$\frac{\Delta d}{d}$: The diameter of the model was measured using a micrometer. The maximum relative error is $\pm .001/.625 = \pm .2\%$.

$\frac{\Delta D}{D}$: The tube was measured internally to obtain a diameter at several places on both ends. It was found that the variation in internal diameter was no more than $\pm .005$ inches. Relative error is then $\pm .005/1.0 = .5\%$.

So: $$\frac{\Delta \beta}{\beta} = \frac{\Delta d}{d} + \frac{\Delta D}{D}.$$

β rms error: $(.002^2 + .005^2)^{0.5} = 0.54\%$.

$\frac{\Delta W}{W}$: The models were weighed on a laboratory quality balance scale that was calibrated immediately beforehand. The scale is taken to be accurate to within at least $\pm .5$ gm. The lightest model had a mass of 62.47 gm. The relative error is then $\pm .5/62.5$ or $\pm 0.8\%$.

$\frac{\Delta\rho}{\rho}$: The temperature of the water was measured at the top of tube before each test series. The accuracy of the temperature is $\pm.5°F$. Density was then found from ref [42] to within ± 5 kg/m**3. The relative error is then $\pm 5/1000. = .5\%$.

$\frac{\Delta\nu}{\nu}$: Kinematic viscosity was found from ref [42] to within a relative error of $\pm.5\%$ using the temperature of the water.

So: $$\frac{\Delta Re_d}{Re_d} = \frac{\Delta V}{V} + \frac{\Delta d}{d} + \frac{\Delta \nu}{\nu} .$$

Re_d rms error: $(.034^2 + .002^2 + .005^2)^{0.5} = 3.4\%$.

$\frac{\Delta\Lambda}{\Lambda}$: Volume of the models was found by displacing water in a large graduated cylinder. The readings were repeated a number of times by two different people. The readings were consistent to within $\pm.5$ ml. The model with the smallest volume had 22.4 ml. Relative error is $\pm.5/22.4 = \pm 2.2\%$. The relative error is then

$$\frac{\Delta C_d}{C_d} = \frac{\Delta W_n}{W_n} + \frac{\Delta \rho}{\rho} + 2\frac{\Delta V}{V} + \frac{\Delta a}{a} .$$

C_d rms error: $(.024^2 + .005^2 + .068^2 + .004^2)^{0.5} = 7.2\%$,

where $$\frac{\Delta W_n}{W_n} = \frac{\Delta W}{W} + \frac{\Delta \rho}{\rho} + \frac{\Delta \Lambda}{\Lambda} .$$

W_n rms error: $(.008^2 + .005^2 + .022^2)^{0.5} = 2.4\%$,

and $\frac{\Delta a}{a} = 2(\pm .4\%) = \pm .8\%$

$\frac{\Delta a_{oe}}{a_{oe}} \simeq 25\%$ estimated from the stiffness of eq. 2-4a.

$\frac{\Delta b_{oe}}{b_{oe}} \simeq 25\%$ estimated from the stiffness of eq. 2-4b.

Relative error: $\frac{\Delta m}{m} = \frac{\Delta W}{W}$.

m rms error = W rms error = 0.8% .

Relative error: $\frac{\Delta m_h}{m_h} = \frac{\Delta \rho}{\rho} + \frac{\Delta \Lambda}{\Lambda} + 2\frac{\Delta \beta}{\beta}$.

m_h rms error = $(.005^2 + .022^2 + .01^2)^{.5} = 2.5\%$.

Relative error: $\frac{\Delta a_o}{a_o} = \frac{\Delta m}{m} + \frac{\Delta m_h}{m_h} + \frac{\Delta \rho}{\rho} + \frac{\Delta C_{dt}}{C_{dt}} + \frac{\Delta a}{a}$.

a_o rms error = $(.008^2+.025^2+.005^2+.072^2+.004^2)^{.5} = 8.6\%$.

Relative error: $\frac{\Delta b_o}{b_o} = \frac{\Delta V_t}{V_t} + \frac{\Delta a_o}{a_o}$.

b_o rms error = $(.072^2 + .086^2) = 11.2\%$.

Relative error: $\frac{\Delta m_{he}}{m_{he}} = \frac{\Delta W_n}{W_n} + \frac{\Delta V_t}{V_t} + \frac{\Delta b_{oe}}{b_{oe}} + \frac{\Delta W}{W}$.

m_{he} rms error = $(.024^2+.034^2+.25^2+.008^2)^{.5} = 25.4\%$.

APPENDIX D

INVISCID ANALYSIS

This appendix presents the development of the inviscid finite difference formulation of a cylindrical body falling through fluid in a closed-end tube.

Problem Formulation

Assuming an incompressible fluid with constant transport properties the general governing partial differential equations are, figure 12 :

Continuity (Law of Conservation of Mass, LCM):

$$\vec{\nabla} \cdot \vec{V} = 0.$$

Navier-Stokes:

$$\rho\vec{g} - \vec{\nabla}p + \vec{\nabla} \cdot \vec{\tau}_{ij} = \rho \frac{D\vec{V}}{Dt}.$$

The cylindrical coordinates (r,θ,z) are related to the Cartesian (x,y,z) by

$$x = r\cos\theta, \qquad y = r\sin\theta, \qquad z = z.$$

Let $$\vec{V} = v_r\vec{i} + v_\theta\vec{j} + v_z\vec{k} = u\vec{i} + v\vec{j} + w\vec{k},$$

where $v_r = u$ = velocity in r direction,

$v_\theta = v$ = velocity in θ direction,

$v_z = w$ = velocity in z direction.

It is convenient to list some useful relationships for

cylindrical coordinates:

$$\frac{D}{Dt} = \frac{\partial}{\partial t} + u\frac{\partial}{\partial r} + \frac{v}{r}\frac{\partial}{\partial \theta} + w\frac{\partial}{\partial z},$$

$$\vec{\nabla}p = \frac{\partial p}{\partial r}\vec{i} + \frac{1}{r}\frac{\partial p}{\partial \theta}\vec{j} + \frac{\partial p}{\partial z}\vec{k},$$

$$\vec{\nabla}\cdot\vec{V} = \frac{1}{r}\frac{\partial}{\partial r}(ru) + \frac{1}{r}\frac{\partial v}{\partial \theta} + \frac{\partial w}{\partial z},$$

$$\vec{V}\cdot\vec{\nabla} = u\frac{\partial}{\partial r} + \frac{1}{r}v\frac{\partial}{\partial \theta} + w\frac{\partial}{\partial z},$$

$$\nabla^2 = \frac{\partial^2}{\partial r^2} + \frac{1}{r}\frac{\partial}{\partial r} + \frac{1}{r^2}\frac{\partial^2}{\partial \theta^2} + \frac{\partial^2}{\partial z^2}.$$

Assuming steady axisymmetric flow, all θ and t dependence is ignored. The additional inviscid assumption gives $\vec{\tau}_{ij} = 0$. These assumptions allow one to write:

Continuity :

$$\frac{1}{r}\frac{\partial}{\partial r}(ru) + \frac{\partial w}{\partial z} = 0.$$

Navier-Stokes (ignoring all body forces,i.e.,gravity):

r: $$u\frac{\partial u}{\partial r} + w\frac{\partial u}{\partial z} = -\frac{1}{\rho}\frac{\partial p}{\partial r}.$$

θ: $0 = 0$

z: $$u\frac{\partial w}{\partial r} + w\frac{\partial w}{\partial z} = -\frac{1}{\rho}\frac{\partial p}{\partial z}.$$

Rewriting continuity:

$$\frac{\partial}{\partial r}(ru) + \frac{\partial}{\partial z}(rw) = 0.$$

Introducing the Stokes stream function ψ with units of $\frac{in.^3}{sec}$

$$\frac{\partial}{\partial r}\left[-\frac{\partial \psi}{\partial z}\right] + \frac{\partial}{\partial z}\left[\frac{\partial \psi}{\partial r}\right] = 0.$$

Comparing the last two equations it is seen that

$$ru = -\frac{\partial \psi}{\partial z} \qquad \text{and} \qquad u = -\frac{1}{r}\frac{\partial \psi}{\partial z},$$

$$rw = \frac{\partial \psi}{\partial r} \qquad \text{and} \qquad w = \frac{1}{r}\frac{\partial \psi}{\partial r}.$$

The irrotational assumption is made: $\vec{\omega} = \vec{\nabla} \times \vec{V} = \vec{0}$.

$$\vec{\omega} = \vec{\nabla} \times \vec{V} = \begin{vmatrix} \frac{1}{r}\vec{i} & \vec{j} & \frac{1}{r}\vec{k} \\ \frac{\partial}{\partial r} & \frac{\partial}{\partial \theta} & \frac{\partial}{\partial z} \\ u & rv & w \end{vmatrix} = \omega_r \vec{i} + \omega_\theta \vec{j} + \omega_z \vec{k} = \vec{0},$$

which reduces to

$$\omega_\theta = \left[\frac{\partial u}{\partial z} - \frac{\partial w}{\partial r}\right] = 0.$$

Substituting for u and w in terms of $\psi(r,z)$:[1]

---

1. It is of interest to note that for axi-symmetric flow the Laplace equation $\nabla^2 \psi \neq 0$, although $\nabla^2 \phi = 0$. Further the Cauchy-Riemann relations from plane flow do not hold. Plane flow: ψ = Lagrange stream function, in^2/sec
ϕ = Potential function, in^2/sec

Cauchy-Riemann: $u = \frac{\partial \phi}{\partial x} : \frac{\partial \phi}{\partial x} = \frac{\partial \psi}{\partial y}$ and $v = \frac{\partial \phi}{\partial y} : \frac{\partial \phi}{\partial y} - \frac{\partial \psi}{\partial x}$

Axi-symmetric flow: ψ = Stokes stream function, in^3/sec

ϕ = Potential function, in^2/sec

$$D^2\psi = \frac{\partial^2\psi}{\partial r^2} - \frac{1}{r}\frac{\partial\psi}{\partial r} + \frac{\partial^2\psi}{\partial z^2} = 0 \quad \text{for} \quad \begin{matrix} 0 \le r \le r_o \\ 0 \le z \le c \end{matrix},$$

with the body defined in figure 8 : $(0 \le z_b \le L)$ by:

$$r_b = \sqrt{(r_i^2 - (r_i - z_b)^2)} \qquad \text{from } 0 \le z_b \le r_i$$

$$r_b = r_i \qquad \text{from } r_i \le z_b \le (L - L_3)$$

$$r_b = r_i(L - L_3)/L_3 \qquad \text{from } (L - L_3) \le z_b \le L,$$

subject to the following (mixed) boundary conditions:

a.) Dirichlet: $\psi = 0$ axis of symmetry (AOS) and on the body.[2]

b.) Neumann: $v_z = w$ = specified at inlet.

c.) Dirichlet: ψ = constant ($\neq 0$) on the tube wall.[3]

d.) Neumann: $v_z = w$ = specified at outlet.

Each of these boundary conditions are now discussed:

Let V_b = body velocity, in./sec.

a.) $\psi(0,z) = 0$ and $\psi(r_b,z_b) = 0$.

b.) Assuming the inlet velocity is parallel to the AOS:[4]

$$\psi(r,0) = \frac{V_b}{2} r^2 \quad \text{for} \quad (0 \le r \le r_o).$$

(Footnote 1 continued from previous page)

$$v_r = u = \frac{\partial\phi}{\partial r} : \frac{\partial\phi}{\partial r} = -\frac{1}{r}\frac{\partial\psi}{\partial z} \quad \text{and} \quad v_z = w = \frac{\partial\phi}{\partial z} : \frac{\partial\phi}{\partial z} = \frac{1}{r}\frac{\partial\psi}{\partial r}$$

Lines of constant ψ are orthogonal to lines of constant ϕ in plane and axi-symmetric flow.

2. Mathematics requires that ψ = constant on a streamline. It is simply convenient to choose the constant to be zero since the axis of symmetry and the body itself form what turns out as a streamline.

3. ψ must equal a constant along the tube wall because the tube is a streamline. However ψ must be different from zero or else there would be no flow in the region of interest.

4. To specify that $v_r = u = 0$ makes $\psi(r,z) = f(r)$ only.

c.) $\psi(r_o,z) = \frac{V_b}{2} r_o^2$ for $(0 \leq z \leq c)$.

d.) Assuming the outlet velocity is parallel to the AOS:

$$\psi(r,c) = \frac{V_b}{2} r^2 \quad \text{for} \quad (0 \leq r \leq r_o).$$

In the event that the outlet is chosen to be at some point on the body where $u = 0$, say in the middle of the horizontal section, at $z = d$:

$$\psi(r,d) = \frac{V_b}{2} r_o^2 \frac{r^2 - r_i^2}{r_o^2 - r_i^2} \quad \text{for} \quad (r_i \leq r \leq r_o).$$

The result is a transformation from the original mixed boundary value problem to a Dirichlet, or first, boundary value problem.

The next section will discuss the discretization and methods used to solve the inviscid relations just derived.

Discretization Method

For convenience the differential equation is repeated here:

$$D^2\psi = \frac{\partial^2\psi}{\partial r^2} - \frac{1}{r}\frac{\partial\psi}{\partial r} + \frac{\partial^2\psi}{\partial z^2} = 0 \quad \text{for} \quad \begin{matrix} 0 \le r \le r_o \\ 0 \le z \le c \end{matrix} .$$

The terms of which may be expressed in a direct analogous finite difference form [5] (refer to figure 19):

$$\frac{\partial^2\psi}{\partial r^2} \simeq \frac{\psi_{i,j+1} - 2\psi_{i,j} + \psi_{i,j-1}}{\Delta r^2} ,$$

$$\frac{\partial^2\psi}{\partial z^2} \simeq \frac{\psi_{i+1,j} - 2\psi_{i,j} + \psi_{i-1,j}}{\Delta z^2} ,$$

$$\frac{1}{r}\frac{\partial\psi}{\partial r} \simeq \frac{\psi_{i,j+1} - \psi_{i,j-1}}{2r_{i,j}\Delta r} .$$

After substituting into $D^2\psi = 0$ and rearranging, a working formula is found:

$$\psi_{i,j} = A\,(\psi_{i+1,j} + \psi_{i-1,j}) + B\,\psi_{i,j+1} + C\,\psi_{i,j-1} ,$$

where $A = \dfrac{\Delta r^2}{2(\Delta r^2 + \Delta z^2)}$, $B = \dfrac{(2r_{i,j} - \Delta r)\Delta z^2}{4r_{i,j}(\Delta r^2 + \Delta z^2)}$,

and $C = \dfrac{(2r_{i,j} + \Delta r)\Delta z^2}{4r_{i,j}(\Delta r^2 + \Delta z^2)} .$

Residual: $R_{i,j} = R - \dfrac{1}{2j}(\psi_{i+1,j} - \psi_{i-1,j}) - 4\psi_{i,j} ,$

where $R = \psi_{i,j+1} + \psi_{i,j-1} + \psi_{i+1,j} + \psi_{i-1,j} .$

---

5. i = column = 1,2,3, ... , MMAX
   j = row = 0,1,2,3, ... , NMAX
   Δr = uniform grid size in r direction, inches
   Δz = uniform grid size in z direction, inches
   $r_{i,j} = j*\Delta r$ = radial distance of mesh point from AOS

Implementation of the boundary conditions in the discretized form is obvious and will not be discussed. The reader is referred to Appendix E.2, showing the FORTRAN implementation of the Gauss-Seidel iterative solution, in program PSI.FOR. The overall flow chart used in PSI.FOR is shown below.

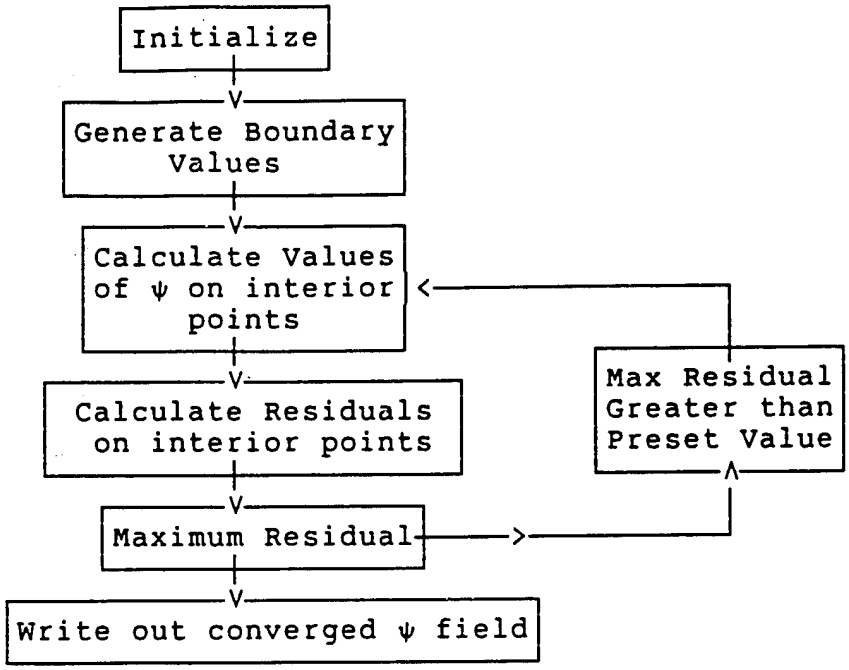

An alternative solution may be achieved by use of the TDMA or Tri-Diagonal-Matrix Algorithm from [37]. The first step is to write the equation to be solved in the proper format:[6]

z direction: $a_i \psi_{i,j} = b_i \psi_{i+1,j} + c_i \psi_{i-1,j} + d_i$,

or simply : (j=constant) $a_i \psi_i = b_i \psi_{i+1} + c_i \psi_{i-1} + d_i$,

where it is given that $\psi_1 = \frac{V_b}{2} r^2$, on the inlet, is known

and $\psi_{MMAX} = \frac{V_b}{2} r^2$, on the outlet, is known.

6. Subscripting done as in previous discussion.

Then, $\psi_i = P_i \psi_{i+1} + Q_i$,

where $P_i = \dfrac{b_i}{a_i - c_i P_{i-1}}$ and $Q_i = \dfrac{d_i + c_i Q_{i-1}}{a_i - c_i P_{i-1}}$.

The method is to forward calculate P_i, Q_i and then back calculate ψ_i along a horizontal line. Because d_i contains contributions from above and below this line, it is wise to repeat the process in the r direction where contributions from the right and left of each node come in through d_i. Convergence is speeded up by this alternate sweeping technique. An additional aid to fast convergence is the introduction of a relaxation parameter, α.[7]

$$\psi^*_{i,j} = \psi_{i,j} - \frac{\alpha}{4} R_{i,j}, \quad \text{where the } ^* \text{ denotes the update.}$$

The author found that TDMA with over-relaxation ($\alpha = 1.2$) converged 3 times faster than the point by point Gauss-Seidel method. So as not to burden the reader with the tedious algebraic details associated with TDMA a copy of the TDMA subroutine, called TDMA.SUB, written in FORTRAN, is included in Appendix E.3. Should the reader wish to use TDMA.SUB, it is simply necessary to replace CALL PSI with CALL TDMA on line # 132 in program PSI.FOR. TDMA is carried out in an alternate sweeping pattern. An extra pass through the annular region aids convergence by carrying information to the center of the flow region as quickly as possible. The overall flow

---

7. A change of 4 units in the residual produces a change of -1 units in the value of ψ; i.e., $\delta R_{i,j} = -4\delta\psi_{i,j}$

chart for TDMA is the same as for Gauss-Seidel, which was previously given.

Hydrodynamic Mass

Once the ψ field is converged it is routine matter to determine the velocity and pressure fields. The actual computations were carried out in program RESULTS.FOR in Appendix E.4. Hydrodynamic mass, m_h, is defined for constant acceleration in an inviscid fluid, by [8]

$$\frac{1}{2} m_h V_b^2 = \sum_{\substack{\text{all} \\ \text{fluid} \\ \text{elements}}} \frac{1}{2} \rho \left[(w^2 - V_b^2) + u^2 \right] \delta\Lambda ,$$

where $\delta\Lambda = 2\pi\, r\, \Delta r\, \Delta z$, Λ = volume.

An elementary assumption of constant acceleration in the inviscid fluid happens to give a good estimate of m_h.

$$m_g \simeq \rho\, (A-a)\, L_e , \quad \text{where} \quad L_e \simeq \frac{\Lambda_b}{a} .$$

Continuity: $(A-a)\, V_g = a\, V_b$.

Then, $$m_h \simeq m_g \left(\frac{a}{A-a} \right)^2 = m_g \left(\frac{d^2}{D^2 - d^2} \right)^2 = m_g \frac{1}{(\beta^2 - 1)^2} .$$

Example: $\beta = 1.6$, $L_g = 5.33$ in., $A = .7854$ in^2, $a = .3068$ in.^{2}.

Then, $m_g = 0.00286$ slugs, $\rho = 0.001123 \frac{\text{slugs}}{\text{in}^3}$,

$m_h = 0.00118$ slugs (elementary formula),

8. Subscripts: g = gap (between body and tube), b = body

m_h = 0.00121 slugs (Σ formula from program RESULTS). Thus, the elementary formula is only about 2.5% low.

Determination of C_p

The preceding sections have described the process utilized to determine the ψ field. Then, the velocity field was found using the definitions of u and w in terms of ψ. Hydrodynamic mass was calculated next, using u and w. The only remaining flow field to be determined is pressure, which can be done through the steady state Bernoulli equation. Start with a streamline drawn from the inlet to some point downstream, figure 20; neglect potential energy changes:

$$C_p = \frac{\Delta p}{0.5 \rho V_b^2}$$ by definition (V_b = abs. vel. of body)

and $$\frac{p_1}{\rho} + \frac{V_b^2}{2} = \frac{p}{\rho} + \frac{V^2}{2}$$ where $V^2 = u^2 + w^2$.

Then, $$C_p = \left(1 - \frac{V^2}{V_b^2} \right).$$

The flow field surrounding body 625 was analyzed in program PSI.FOR, Appendix E.2, and program RESULTS.FOR, Appendix E.4, was used to produce the velocity field. It is then possible to calculate C_p from the above relation. Figure 21 is a plot C_p for body 625, which is independent of V_b and hence Reynolds number.

APPENDIX E

COMPUTER PROGRAMS

E.1 UNSTEADY FORTRAN PROGRAM

```
      IMPLICIT REAL (A-H,J-Z)
      INTEGER M,NUM,K
      DIMENSION F(2),Y(2)
      CHARACTER*80 CHOICE
      OPEN(1,NAME='T.DAT',TYPE='NEW')
      OPEN(2,NAME='D.DAT',TYPE='NEW')
      OPEN(3,NAME='CD.DAT',TYPE='NEW')
      M = 0
      TIME = 0.0
      TIMEMAX = 1.0
      STEP = 0.01
      NUM = 2
      IPRINT = 1
      ISTOP = 0
      G = 32.2          !FT/SEC/SEC
      RHO = 1.94        !SLUGS/FT**3
      NU = 1.07E-05     !FT**2/SEC
C FOR 625 MODEL:
      DRYWT = 0.1640    !LBF
      FNET = 0.105      !LBF
      DM = 0.625        !INCHES
      L = 5.0           !INCHES
      D = 1.0           !INCHES
      HYMASS = 0.00118          !SLUGS
      MASS = DRYWT/G            !SLUGS
      TOTMASS = MASS + HYMASS
      DM = DM/12.
      L = L/12.
      D = D/12.
      B = D/DM
      DE = D - DM
      A = .7854*DM*DM
      GAM = (B*B - 1.)/B/B
      FUN1 = ((B*B+1)/2/(B*B-1))**2
C  Y(1) IS THE INITIAL VELOCITY FT/SEC, AT TIME=0.
C  Y(2) IS THE INITIAL POSTIION FT, AT TIME=0.
      Y(1) = 0.001      !0.0 CAUSES PROBLEMS
      Y(2) = 0.0
C  BEGIN THE MAIN LOOP
  8   IF(POS*12. .GE. 20.0)THEN
        ISTOP = 1
        GOTO 21
      END IF
  6   CALL RUNGE(NUM,Y,F,TIME,STEP,M,K)
      GOTO(10,20),K
  10  CONTINUE
      V = Y(1)
      POS = Y(2)
      Q = .5*RHO*V*V
      RED = V*DM/NU
      REW = B*B*RED/(B+1)
      FUN2 = .001 + 2.8*(ALOG10(REW))**-3.1
      FUNS = FUN1*FUN2
      CHI = 1.477 + .2195*ALOG10(RED)
      ZETA = 1.005*B**CHI
      TOS = FUNS*(B+1)/4/(B+ZETA)
      TIS = ZETA*TOS
      TI = TIS*Q
      DP = FUNS*Q/DE
      FOR = 3.14159*DM*L*TI + A*L*DP
```

```
      CS = FOR/A/Q
      CD = (GAM*GAM+(1-GAM)**2)/GAM/GAM + CS
      DRAG = A*CD*Q
      ACC = (FNET - DRAG)/TOTMASS
      F(1) = ACC
      F(2) = V
      IF(TIME.EQ.0.0)THEN
C  SET UP OUTPUT TABLE HEADINGS
        TYPE *,' TIME(SEC)',' VELOCITY   POSTION    CD'
        WRITE(5,23)TIME,V*12.,POS*12.,CD,ACC
        WRITE(1,27)TIME
        WRITE(2,27)POS*12.
        WRITE(3,27)CD
      END IF
      GOTO 6
C  END MAIN LOOP
C  THIS IS THE OUTPUT SECTION
 20   ICOUNT = ICOUNT+1
      IF(INT(ICOUNT/IPRINT)*IPRINT .EQ. ICOUNT)THEN
 21     WRITE(5,23)TIME,V*12.,POS*12.,CD,ACC
        WRITE(1,27)TIME
        WRITE(2,27)POS*12.
        WRITE(3,27)CD
 23     FORMAT(1X,5(F9.3,1X),2(F13.1,1X))
 27     FORMAT(1X,E12.6,'&')
      END IF
      IF(ISTOP .EQ. 1)STOP
C  GO BACK TO THE TOP OF THE MAIN LOOP
      GOTO 8
      END
C  ***************************************************************************
      SUBROUTINE RUNGE(N,Y,F,X,H,M,K)
C  THIS ROUTINE PERFORMS RUNGE-KUTTA CALCULATIONS
C  BY GILLS METHOD (FROM PROF. FRANK WHITE'S "VISCOUS
C  FLUID FLOW" BOOK).
      DIMENSION Y(10), F(10), Q(10)
      M = M+1
      GO TO (1,4,5,3,7),M
  1   DO 2 I = 1,N
  2   Q(I) = 0.
      A = .5
      GO TO 9
  3   A = 1.70710678
  4   X = X+.5*H
  5   DO 6 I = 1,N
      Y(I) = Y(I)+A*(F(I)*H-Q(I))
  6   Q(I) = 2.*A*H*F(I)+(1.-3*A)*Q(I)
      A = .2928932188
      GO TO 9
  7   DO 8 I = 1,N
  8   Y(I) = Y(I)+H*F(I)/6.-Q(I)/3.
      M = 0
      K = 2
      GO TO 10
  9   K = 1
 10   RETURN
      END
```

E.2 INVISCID FORTRAN PROGRAM

Fortran Program PSI.FOR

```
      C  SOLVE AXISYMMETRIC POTENTIAL FLOW AROUND MODEL IN A TUBE
      C  I=COLUMN J=ROW P(I,J)=VALUE OF PSI e.g. STOKES STREAM FUNCTION,
      C  Written by: Richard F. Hubbell (July 1987) at Univ. of R.I.
      C  For partial completion of PhD Mechanical Engineering
      C  Major Prof: Dr. Frank M. White
           LOGICAL FLOW
           CHARACTER*20 VIEW,VIEWRES
           DIMENSION IBODY(101),IBODY2(101)
           COMMON /GRID/JBOD,NMAX,MMAX
           COMMON /RESIDUAL/RES,IMAX,JMAX,RESMAX,DELMAX,IDELMAX,JDELMAX,RELAX
           COMMON /GENERAL/DR,DR2,DZ,DZ2,I,J,VIN,VGAP,RA,RB
           COMMON /MATRIX/A(101),B(101),C(101),R(101),P(1250,101),FLOW(1250,101)

           DATA ISTAG1,ISTAG2,NMAX,MMAX/401,684,101,1250/
           DATA DR,DZ/0.005,0.025/
           DATA VIN/400.0/
           DATA P,A,B,C/126250*0.,101*0.,101*0.,101*0./

           OPEN(1,TYPE='NEW',NAME='RES.OUT')
           TYPE *,'READ IN PSI FROM A FILE? Y OR N'
           ACCEPT 60,VIEW
           IF(VIEW .EQ. 'Y')THEN
            OPEN(2,TYPE='OLD',NAME='TDMA.PSI')
            READ(2,*)ICOUNT,ICOUNTRESMAX,IMAX,JMAX,RESMAX
            READ(2,83)((P(I,J),I=1,MMAX),J=1,NMAX)
       83   FORMAT(12625(10(F11.8,1X),/))
           TYPE *,' INPUT FROM TDMA.PSI'
      C    TYPE 65,((P(ISTAG1+K,4+L), K=-3,3), L=3,-3,-1)
      C    TYPE 65,((P(ISTAG2+K,4+L), K=-3,3), L=3,-3,-1)
           TYPE *,' 389,399'
           TYPE 9,((P(K,L),K=389,399),L=4,2,-1)
           TYPE *,' 400,410'
           TYPE 9,((P(K,L),K=400,410),L=4,2,-1)
           TYPE *,' 680,690'
           TYPE 9,((P(K,L),K=680,690),L=4,2,-1)
           TYPE *,' 691,701'
           TYPE 9,((P(K,L),K=691,701),L=4,2,-1)
         9 FORMAT(3(1X,11F7.4,/))
           ELSE
           VIEW = 'N'
           ENDIF

           RA = .625/2      !RA = BODY RADIUS INCHES
           DR2 = DR*DR
           DZ2 = DZ*DZ
           RB = (NMAX-1)*DR
           JBOD = INT(RA/DR) + 1
           RA = JBOD*DR
           RB2 = RB*RB
           RA2 = RA*RA
           ZSTAG1 = ISTAG1*DZ
           ZTAIL = 1.500    !TAIL IS 1.5 INCHES LONG
           ZSTAG2 = ISTAG2*DZ
           VGAP = VIN*RB2/(RB2-RA2)

           DO 52 J = 1,NMAX
           DO 52 I = 1,MMAX
        52 FLOW(I,J) = .TRUE.

      C FIRST DEFINE THE NOSE FOR IBODY( ) THEN DEFINE THE TAIL FOR IBODY2( )

           DO 50 J = JBOD,2,-1
           ZNOSE = SQRT(RA*RA - ((J-1)*DR)**2)
```

```
64            IBODY(J) = INT((ZSTAG1 + RA - ZNOSE)/DZ)
65            ZSLOPE = (J-1)*DR*ZTAIL/RA
66          50 IBODY2(J) = INT((ZSTAG2 - ZSLOPE)/DZ)
67
68            DO 53 J = 2,JBOD
69            DO 53 I = IBODY(J),IBODY2(J)
70          53 FLOW(I,J) = .FALSE.
71
72          C PERFORM ITERATIVE SOLUTION
73            R(1) = 0.
74            DO 4 J = 2,NMAX
75            R(J) = (J-1)*DR
76            TOPB = (2.*R(J) - DR)*DZ2
77            TOPC = (2.*R(J) + DR)*DZ2
78            DEN = 4.*R(J)*(DZ2 + DR2)
79            A(J) = DR2/2./(DZ2+DR2)
80            B(J) = TOPB/DEN
81            C(J) = TOPC/DEN
82          4 CONTINUE
83
84            IF(VIEW .EQ. 'N')THEN
85          C INITIAL AND BOUNDARY CONDITIONS
86            DO 1 I = 1,NMAX
87            P(I,NMAX) = 0.5*VIN*RB2
88          1 P(I,1) = 0.0
89            DO 2 J = JBOD+1,NMAX-1  !R(J)=(J-1)*DR ; RA=JBOD*DR ; SO ADD 1 TO JBOD
90            DO 2 I = IBODY(JBOD),IBODY2(JBOD)
91          2 P(I,J) = 0.5*VIN*(R(J)*R(J) - RA2)/(RB2-RA2)    !VIN HELPS IT CONVERGE
92            DO 3 J = 1,NMAX
93            P(1,J) = 0.5*VIN*R(J)*R(J)
94          3 P(NMAX,J) = P(1,J)
95            ICOUNT = 0
96            ICOUNTRESMAX = 0
97            ENDIF
98
99            TYPE *,'INPUT IRES (CONTROLS FREQUENCY OF OUTPUT)'
100           ACCEPT *,IRES
101         70 CONTINUE
102           TYPE *,'WHAT RELAXATION FACTOR (0 TO 3)?'
103           ACCEPT *,RELAX
104           IF(RELAX .LT. 0. .OR. RELAX .GT. 3.)GOTO 70
105           TYPE *,'HOW MANY (MORE) ITERATIONS?'
106           ACCEPT *,ITERMAX
107           IF(ITERMAX .LT. 1)THEN
108           TYPE *,' OUTPUT TO PSI.PSI'
109     C     TYPE 65,((P(ISTAG1+K,4+L), K=-3,3), L=3,-3,-1)
110     C     TYPE 65,((P(ISTAG2+K,4+L), K=-3,3), L=3,-3,-1)
111           TYPE *,' 389,399'
112           TYPE 9,((P(K,L),K=389,399),L=4,2,-1)
113           TYPE *,' 400,410'
114           TYPE 9,((P(K,L),K=400,410),L=4,2,-1)
115           TYPE *,' 680,690'
116           TYPE 9,((P(K,L),K=680,690),L=4,2,-1)
117           TYPE *,' 691,701'
118           TYPE 9,((P(K,L),K=691,701),L=4,2,-1)
119            TYPE *,'OUTPUT TO A FILE? Y OR N'
120            ACCEPT 60,VIEW
121           IF(VIEW .EQ. 'Y')THEN
122            OPEN(3,TYPE='NEW',NAME='PSI.PSI')
123            WRITE(3,*)ICOUNT,ICOUNTRESMAX,IMAX,JMAX,RESMAX
124            WRITE(3,81)((P(I,J),I=1,NMAX),J=1,NMAX)
125         81  FORMAT(1X,12625(10(F11.8,1X),/))
126           ENDIF
```

```
127             STOP 'END OF RUN'
128            ENDIF
129
130            DO 7 ITER = 1,ITERMAX
131            DELMAX = 0.0
132            CALL PSI
133        C   TYPE 65,((P(ISTAG1+K,4+L), K=-5,1), L=3,-3,-1)
134        C   TYPE 65,((P(ISTAG2+K,4+L), K=-5,1), L=3,-3,-1)
135         65 FORMAT(7(1X,7F11.9,/))
136
137            ICOUNT = ICOUNT + 1
138            TYPE 62,ICOUNT,ITER,ITERMAX,ICOUNTRESMAX,RESMAX,IMAX,JMAX
139            TYPE 63,DELMAX,IDELMAX,JDELMAX,RELAX
140            IF(INT(ICOUNT/IRES)*IRES .EQ. ICOUNT)THEN
141             RESMAX = 0
142             CALL RESIDUALS
143             ICOUNTRESMAX = ICOUNT
144             TYPE 62,ICOUNT,ITER,ITERMAX,ICOUNTRESMAX,RESMAX,IMAX,JMAX
145             WRITE(1,62)ICOUNT,ITER,ITERMAX,ICOUNTRESMAX,RESMAX,IMAX,JMAX
146             WRITE(1,63)DELMAX,IDELMAX,JDELMAX
147         62  FORMAT(1X,4(I4,3X),F12.4,3X,2(I4,3X))
148         63  FORMAT(1X,E12.5,3X,2(I4,3X),F5.3)
149            ENDIF
150
151            IF(ICOUNT .EQ. 1)THEN
152             TYPE *,'SPOT CHECK BOUNDARY CONDITIONS? Y OR N'
153             ACCEPT 50,VIEW
154            ENDIF
155            VIEW = 'N'
156            IF(VIEW .EQ. 'Y')THEN
157             TYPE *,'INPUT IVIEW,JVIEW'
158             ACCEPT *,IVIEW,JVIEW
159            ENDIF
160
161            IF(VIEW .EQ. 'Y')THEN
162            DO 31 I = 1,MMAX
163            IF(INT(I/IVIEW)*IVIEW.EQ.I)THEN
164             TYPE *,(I,(P(I,L), L=1,3))
165             TYPE *,(I,(P(I,L), L=NMAX-2,NMAX))
166             TYPE *,' '
167            ENDIF
168         31 CONTINUE
169            TYPE 103
170        103         FORMAT(///)
171
172            DO 32 J = 1,NMAX
173            IF(INT(J/JVIEW)*JVIEW.EQ.J)THEN
174             TYPE *,(J,(P(L,J), L=1,3))
175             TYPE *,(J,(P(L,J), L=MMAX-2,MMAX))
176            ENDIF
177         32 CONTINUE
178            ENDIF
179
180         7  CONTINUE
181
182         50 FORMAT(A10)
183
184            TYPE 62,ICOUNT,ITER,ITERMAX,ICOUNTRESMAX,RESMAX,IMAX,JMAX
185            WRITE(1,62)ICOUNT,ITER,ITERMAX,ICOUNTRESMAX,RESMAX,IMAX,JMAX
186            WRITE(1,63)DELMAX,IDELMAX,JDELMAX,RELAX
187            CALL VELOCITY
188
189            GOTO 70
```

```
190
191           END
192
193           SUBROUTINE RESIDUALS
194           LOGICAL FLOW
195           COMMON /GENERAL/DR,DR2,DZ,DZ2,I,J,VIN,VGAP,RA,RB
196           COMMON /GRID/JBOD,NMAX,MMAX
197           COMMON /RESIDUAL/RES,IMAX,JMAX,RESMAX,DELMAX,IDELMAX,JDELMAX,RELAX
198           COMMON /MATRIX/A(101),B(101),C(101),R(101),P(1250,101),FLOW(1250,101)
199
200           DO 1 I = 2,MMAX-1
201           DO 1 J = 2,NMAX-1
202           IF(FLOW(I,J))THEN
203           DELSQR = (P(I,J+1) - 2.*P(I,J) + P(I,J-1))/DR2
204           DELSQZ = (P(I+1,J) - 2.*P(I,J) + P(I-1,J))/DZ2
205           REMDER = (P(I,J+1) - P(I,J-1))/2./R(J)/DR
206           RES = DELSQR + DELSQZ - REMDER
207            IF(ABS(RES) .GT. ABS(RESMAX))THEN
208             IMAX = I
209             JMAX = J
210             RESMAX = RES
211            ENDIF
212           ENDIF
213         1 CONTINUE
214           TYPE 65,((P(IMAX+K,JMAX+L), K=-3,3), L=3,-3,-1)
215           WRITE(1,65)((P(IMAX+K,JMAX+L), K=-3,3), L=3,-3,-1)
216        65 FORMAT(1X,7(7(F8.5,2X),/))
217           RETURN
218           END
219
220           SUBROUTINE VELOCITY
221           LOGICAL FLOW
222           COMMON /GENERAL/DR,DR2,DZ,DZ2,I,J,VIN,VGAP,RA,RB
223           COMMON /GRID/JBOD,NMAX,MMAX
224           COMMON /RESIDUAL/RES,IMAX,JMAX,RESMAX,DELMAX,IDELMAX,JDELMAX,RELAX
225           COMMON /MATRIX/A(101),B(101),C(101),R(101),P(1250,101),FLOW(1250,101)
226           BIGKE = 0.0
227           ROW = 62.4/32.174/20736.          !WATER DENSITY LBM-SEC**2/IN**4
228           DO 1 J = 2,NMAX-1
229           DO 1 I = 2,MMAX-1
230           IF(FLOW(I,J))THEN
231            VZ = (P(I,J+1) - P(I,J-1))/2./R(J)/DR
232            VZABS = VZ - VIN
233            VR = - (P(I+1,J) - P(I-1,J))/2./R(J)/DZ
234            SMALLKE = 2.*3.14159*R(J)*DR*DZ*ROW*(VZABS*VZABS + VR*VR)
235            BIGKE = BIGKE + SMALLKE
236           ENDIF
237         1 CONTINUE
238           BODYMASS = 0.105/386.1
239           BYMASS = BIGKE/VIN/VIN
240           TYPE 10,BIGKE,BYMASS,BODYMASS
241           WRITE(1,10)BIGKE,BYMASS,BODYMASS
242        10 FORMAT(1X,'BIGKE=',F12.4,3X,'BYMASS=',F12.6,3X,'BODYMASS=',F12.6)
243           RETURN
244           END
245
246           SUBROUTINE PSI
247           LOGICAL FLOW
248           COMMON /GENERAL/DR,DR2,DZ,DZ2,I,J,VIN,VGAP,RA,RB
249           COMMON /GRID/JBOD,NMAX,MMAX
250           COMMON /MATRIX/A(101),B(101),C(101),R(101),P(1250,101),FLOW(1250,101)
251           COMMON /RESIDUAL/RES,IMAX,JMAX,RESMAX,DELMAX,IDELMAX,JDELMAX,RELAX
252           DO 1 J = 2,NMAX-1                 !OVERALL ITERATION
253           DO 1 I = 2,MMAX-1                 !DON'T ITERATE THE BOUNDARIES
254           IF(FLOW(I,J))THEN
255            DEL =A(J)*(P(I+1,J)+P(I-1,J))+B(J)*P(I,J+1)+C(J)*P(I,J-1) - P(I,J)
256            IF(ABS(DEL) .GT. ABS(DELMAX))THEN
257             DELMAX = DEL
258             IDELMAX = I
259             JDELMAX = J
260            ENDIF
261            P(I,J) = P(I,J) + RELAX*DEL
262           ENDIF
263         1 CONTINUE
264           RETURN
265           END
```

E.3 TRI-DIAGONAL MATRIX ALGORITHM FORTRAN PROGRAM

```
      C  Written by Richard F. Hubbell (July 1987) Univ. of R.I.
         SUBROUTINE TDMA
         LOGICAL FLOW
      C PERFORM TDMA IN Z DIRECTION (BUT ONLY IN THE ANNULUS)
         COMMON /GRID/JBOD,NMAX,MMAX
         COMMON /GENERAL/DR,DR2,DZ,DZ2,I,J,VIN,VGAP,RA,RB
         COMMON /MATRIX/A(101),B(101),C(101),R(101),P(1250,101),FLOW(1250,101)
         COMMON /RESIDUAL/RES,IMAX,JMAX,RESMAX,DELMAX,IDELMAX,JDELMAX,RELAX
         DIMENSION PZ(1250),QZ(1250)

      C BEGIN VERTICAL TDMA (DO IT ONCE)
         DO 40 L = 1,1
         DO 40 I = 2,MMAX-1
         PZ(1) = 0.0
         QZ(1) = P(I,1)
         DO 37 J = 2,NMAX-1
         IF(.NOT.FLOW(I,J))THEN
          ADUM = 1.E-15
          BDUM = 1.E-15
          CDUM = 1.E-15
          ELSE
           ADUM = A(J)
           BDUM = B(J)
           CDUM = C(J)
         ENDIF
         DENOM = 1. - CDUM*PZ(J-1)
         PZ(J) = BDUM/(1. - CDUM*PZ(J-1))
         QZNUM = ADUM*(P(I+1,J) + P(I-1,J))
      37 QZ(J) = (QZNUM + CDUM*QZ(J-1))/DENOM
         DO 38 J = NMAX-1,2,-1
         DEL = PZ(J)*P(I,J+1) + QZ(J) - P(I,J)
         IF(ABS(DEL) .GT. ABS(DELMAX))THEN
          DELMAX = DEL
          IDELMAX = I
          JDELMAX = J
         ENDIF
      38 P(I,J) = P(I,J) + RELAX*DEL
      40 CONTINUE

         DO 10 J = 2,NMAX-1                !BEGIN HORIZONTAL TDMA (DO IT ONCE)
         PZ(1) = 0.0
         QZ(1) = P(1,J)
         DO 7 I = 2,MMAX-1
         IF(.NOT.FLOW(I,J))THEN
          ADUM = 1.E-15
          BDUM = 1.E-15
          CDUM = 1.E-15
          ELSE
           ADUM = A(J)
           BDUM = B(J)
           CDUM = C(J)
         ENDIF
         DENOM = 1. - ADUM*PZ(I-1)
         PZ(I) = ADUM/(1. - ADUM*PZ(I-1))
         QZNUM = BDUM*P(I,J+1) + CDUM*P(I,J-1)
       7 QZ(I) = (QZNUM + ADUM*QZ(I-1))/DENOM
         DO 8 I = MMAX-1,2,-1              !BEGIN BACKWARDS SUBSTITION
         DEL = PZ(I)*P(I+1,J) + QZ(I) - P(I,J)
         IF(ABS(DEL) .GT. ABS(DELMAX))THEN
          DELMAX = DEL
          IDELMAX = I
          JDELMAX = J
         ENDIF

       8 P(I,J) = P(I,J) + RELAX*DEL
      10 CONTINUE
         RETURN
         END
```

E.4 PRESSURE COEFFICIENT FORTRAN PROGRAM

Fortran Program RESULTS.FOR

```
0           Written by Richard F. Hubbell (July 1987) Univ. of R.I.
1           DIMENSION R(101)
2           COMMON /FIELD/P(1250,101),VR(1250,101),VZ(1250,101),PRESS(1250,101)
3           DATA PRESS,P,VR,VZ,R/126250*0.,126250*0.,126250*0.,126250*0.,101*0./
4           DATA NMAX,MMAX,DR,DZ,VIN/101,1250,0.005,0.025,400./
5           OPEN(1,TYPE='OLD',NAME='TDMA.PSI')
6           READ(1,*)ICOUNT,ICOUNTRESMAX,IMAX,JMAX,RESMAX
7           READ(1,8)((P(I,J),I=1,MMAX),J=1,NMAX)
8        8  FORMAT(12625(10(F11.8,1X),/))
9           TYPE *,' 389,399'
10          TYPE 9,((P(K,L),K=389,399),L=4,2,-1)
11          TYPE *,' 400,410'
12          TYPE 9,((P(K,L),K=400,410),L=4,2,-1)
13          TYPE *,' 680,690'
14          TYPE 9,((P(K,L),K=680,690),L=4,2,-1)
15          TYPE *,' 691,701'
16          TYPE 9,((P(K,L),K=691,701),L=4,2,-1)
17       9  FORMAT(3(1X,11F7.4,/))
18
19          BODYMASS = 0.105/386.1          !LBM-SEC**2/IN
20          BIGKE = 0.0
21          ROW = 62.4/32.174/20736.        !WATER DENSITY LBM-SEC**2/IN**4
22
23          TYPE *,'WHAT IS THE BODY VELOCITY? INCHES/SEC'
24          ACCEPT *,VBOD
25          DO 3 J = 1,NMAX
26          DO 3 I = 1,MMAX
27       3  P(I,J) = P(I,J)*VBOD/VIN
28
29          DO 1 J = 2,NMAX-1
30          R(J) = (J-1)*DR
31          DO 1 I = 2,MMAX-1
32          IF(P(I,J) .GT. 1.E-05)THEN
33           VZ(I,J) = (P(I,J+1) - P(I,J-1))/2./R(J)/DR
34           VZABS = VZ(I,J) - VBOD
35           VR(I,J) = - (P(I+1,J) - P(I-1,J))/2./R(J)/DZ
36           VELSQ = VZ(I,J)*VZ(I,J) + VR(I,J)*VR(I,J)
37           PRESS(I,J) = 0.5*ROW*(VBOD**2 - VELSQ)
38           SMALLKE = 2.*3.14159*R(J)*DR*DZ*ROW*(VR(I,J)**2 + VZABS**2)
39           BIGKE = BIGKE + SMALLKE
40          ENDIF
41       1  CONTINUE
42
43          HYMASS = BIGKE/VBOD/VBOD
44          TYPE 20,HYMASS,BODYMASS
45          TYPE *,' GOING TO OUTPUT :'
46          TYPE *,' 389,399'
47          TYPE 9,((P(K,L),K=389,399),L=4,2,-1)
48          TYPE *,' 400,410'
49          TYPE 9,((P(K,L),K=400,410),L=4,2,-1)
50          TYPE *,' 680,690'
51          TYPE 9,((P(K,L),K=680,690),L=4,2,-1)
52          TYPE *,' 691,701'
53          TYPE 9,((P(K,L),K=691,701),L=4,2,-1)
54
55          OPEN(2,TYPE='NEW',NAME='RESULTS.OUT')
56          DO 2 I = 300,380,20
57       2  CALL OUTPUT(I,5,NMAX)    !PRINT OUT EVERY FIFTH J i.e. J = 2,7,9 etc
58          DO 4 I = 390,419,1
59       4  CALL OUTPUT(I,2,NMAX)    !PRINT OUT EVERY OTHER J i.e. J = 2,4,6 etc
60          DO 5 I = 420,600,20
61       5  CALL OUTPUT(I,5,NMAX)
62          DO 6 I = 510,698,2
```

```
      6  CALL OUTPUT(I,2,NMAX)
         DO 7 I = 700,800,20
      7  CALL OUTPUT(I,5,NMAX)
     20  FORMAT(1X,'HYMASS = ',F11.8,3X,'BODYMASS = ',F11.8)
         END

         SUBROUTINE OUTPUT(I,INC,NMAX)
         COMMON /FIELD/P(1250,101),VR(1250,101),VZ(1250,101),PRESS(1250,101)

         WRITE(2,23)I

         DO 2 JDUM = 2,NMAX,10*INC
         WRITE(2,22)(J,J=JDUM,9*INC+JDUM,INC)
         WRITE(2,21)(P(I,J),J=JDUM,9*INC+JDUM,INC)
         WRITE(2,24)(VR(I,J),J=JDUM,9*INC+JDUM,INC)
         WRITE(2,24)(VZ(I,J),J=JDUM,9*INC+JDUM,INC)
         WRITE(2,21)(PRESS(I,J),J=JDUM,9*INC+JDUM,INC)
      2  CONTINUE

         WRITE(2,102)
         RETURN

     21  FORMAT(1X,10(F7.4,1X))
     22  FORMAT(/,1X,10(2X,'J=',I3,1X))
     23  FORMAT(30X,'I = ',I4)
     24  FORMAT(1X,10(F7.3,1X))
    102        FORMAT(//)
         END
```

BIBLIOGRAPHY

Abramovich, G.N., "Calculation of Air Resistance of Trains when Moving in the Open and in Tunnels," Trudy Tsentr, Aerogedradinam, Inst. 400, 1939.

Barbin, A.R., and Jones, J.B., "Turbulent Flow in the Inlet Region of a Smooth Pipe," Journal of Basic Engineering, Trans. ASME, Vol. 85, Series D, Mar 1963, pp. 29-34.

Becker, E., "Stromungsvorgange In Ringformigen Splaten (Labyrinth-Dichugen)," Zeitschrift V.D.I., vol. 51, 1907, pp. 1133-1141.

Bowlus, D.A., and Brighton, J.A., "Incompressible Turbulent Flow in the Inlet Region of a Pipe", Journal of Basic Engineering, Trans. ASME, Vol. 90, Series D, No. 3, Sept. 1968, pp. 431-433.

CRC Handbook of Tables for Applied Engineering Science, CRC Press, Inc., 2000 Corporate Blvd. N.W., Boca Raton, Florida, 33431, Second Edition, 1985.

CRC Handbook of Chemistry and Physics, CRC Press, Inc., 2000 Corporate Blvd. N.W., Boca Raton, Florida, 33431, 1980.

Cromack, D.E., "Experiments on the Propulsion of Vehicles in Tubes of Varying Porosities," R.P.I. Report TR PT 6803, to Office of High Speed Ground Transportation, U.S. Department of Transportation, June 1968.

Davidson, J.V., "Aerodynamic Drag of Tube Vehicles," Master's Thesis, Duke University, Durham, N.C., 1974.

Deissler, R.G., and Taylor, M.F., "Analysis of Fully Developed Turbulent Heat Transfer and Flow in an Annulus with Various Eccentricities," NACA TN 3451, 1951.

Ferziger, J.H., "Simulation of Incompressible Turbulent Flows," Journal of Computational Physics, Vol. 69, No. 1, March 1987, pp. 1-48.

FLUENT release 2.81, Licensed by and the property of CREARE Inc., P.O. Box 71, Hanover, New Hampshire, 03755, phone (603) 643-3800.

Fukuchi, G., and Nischizawa, S., "Estimate of Aerodynamic Drag of a Train in a Long Tunnel," Quarterly Report of Railroad Technology Research Inst., Japanese National Railways, Vol. 8, No. 1, 1967, pp. 30-33.

Fukuchi, G., "A Method of Aerodynamic Drag Abatement for High-Speed Train in Single-Tracked Tunnel," Railroad Technology Research Inst., Japanese National Railways, 1967.

Goodman, T.R., "The Aerodynamic Characteristics of a Slender Body Traveling in a Tube," U.S. Dept. of Commerce Report, Contract No. C-265-66.

Gouse, S.W., et al., "Aerodynamic Drag on a Body Traveling in a Tube," U.S. Dept. of Transportation Report, Contract No. C-85-65, October 1967, NTIS No. PB 177 211.

Gouse, S.W., and Nwude, J., "Aerodynamic Drag on Vehicles in Enclosed Guideways," M.I.T., Engineering Projects Laboratory Report No. DSR 76108-1, Mech. Engr. Dept., December 1966, NTIS No. PB 173 646.

Gregorek, G.M., and Engle, J.H., "An Experimental Study of Aerodynamics of Vehicles Traveling at High Speeds Through Long Tubes," The Ohio State Univ., Columbus, Ohio. Presented at the International Conf. on Vehicle Mechanics at Wayne State Univ., July 1968.

Hammitt, Andrew G., The Aerodynamics of High Speed Ground Transportation, published by Western Periodicals Co., 13000 Raymer St., North Hollywood, California, 1973.

Hammitt, Andrew G., "High Speed Ground Transportation System Engineering Program," T.R.W. Rept. No. 06818-6026-R000, for the Office of High Speed Ground Transportation, U.S. Dept. of Transportation, April 15, 1968.

Hara, Tomoshige, "Method of Measuring the Aerodynamic Drag of Trains," Bulletin of JSME, Vol. 8, No. 31, 1965.

Hara, T., "Aerodynamic Force on a High Speed Train at Tunnel Entrance," Bull. of JSME, Vol. 4, No. 15, 1961, pp. 547-553.

Hara, T. and Okushi, J., "Model Tests on Aerodynamical Phenomena of a High Speed Train Entering a Tunnel," Quarterly Report of Railroad Technology Research Inst., Japanese National Railways, Vol. 3, No. 4, 1962, pp. 6-10.

Hara, T., Ohkushi, J. and Nishimura, B., "Aerodynamic Drag of Trains," Quarterly Report of Railroad Technology Research Inst., Japanese National Railways, Vol. 8, No. 4, 1967, pp. 226-229.

Hara, T., "Aerodynamic Drag of Trains in Tunnels," Quarterly Report of Railroad Technology Research Inst., Japanese National Railways, Vol. 8, No. 4, 1967, pp. 229-235.

Hoerner, S.F., Fluid Dynamic Drag, published by the author, 148 Busteed Drive, Midland Park, New Jersey, 07432, pp. 3 - 19.

Hoppe, R.G., and Gouse, S.W., "Fluid Dynamic Drag on Vehicles Traveling Through Tubes," Carnegie-Mellon University Report No. 1-59076-1, August 1969, NTIS No. PB 188 451.

Kawaguti, M., "Effects of the Ground and a Tunnel on the Frictional Drag of High-Speed Trains," Quarterly Report of Railroad Technology Research Inst., Japanese National Railways, Vol. 2, No. 4, 1961, pp. 1-6.

Kotlow, D.A., "Aerodynamic Drag of Vehicles in Long Tubes," Master's Thesis, University of Rhode Island, Kingston, R.I., 1985.

Kurtz, Donald W., et al., "Experimental Aerodynamic Characteristics of Vehicles in Confined Spaces," Caltech Technical Report No. UMTA-DC-06-0010-72-14, Contract No. DC-290, December 1972, NTIS No. PB 231 386.

Langer, R.E., "Versuche an einem Schnellbahnwagen," Ergebnisse der Aerodynamischen Versuchstalt zu Gottingen, 111, Lieferung, 1927.

Mark's Standard Handbook for Mechanical Engineers, McGraw-Hill Book Co., New York, Eighth Edition, 1978.

Miki, N., "Research Report on the New Japanese National Railways, Tokaido Line," Vol. 3, 1962, pp. 12.

Nayak, U.S.L., et al., "The Aerodynamic Drag of Tube Vehicles Traveling at Low Subsonic Speeds," BHRA Fluid Engineering Second International Symposium on Aerodynamics and Ventilation of Vehicle Tunnels, Paper E1, held at Churchill College, Cambridge, England, 23rd-25th March, 1976.

Nixon, D., "A Report on a Workshop on Turbulence Research," prepared for Air Force Office of Scientific Research, Bolling Air Force Base, Washington D.C. 20332, dated March 28, 1986, covering the period, August 8, 1985 to April 12, 1986, NEAR TR-361.

Nouvion, F., "The Train Drag at High Speed," Paper presented at the International Conf. on Vehicle Mechanics Wayne State University, July 1968.

Ono, Ito, Nishimura, and Kawamura, Memo. Railroad Technology Research Inst., No. 253, Japanese National Railways, 1959.

Patankar, S.V., Numerical Heat Transfer and Fluid Flow, Hemisphere Publishing Corp., McGraw-Hill Book Co., 1980.

Quarmby, A., "An Analysis of Turbulent Flow in Concentric Annuli," Applied Scientific Research, Vol. 19, July 1968, pp. 250-293.

Rodi, W., "Turbulence Models and Their Application in Hydraulics - A State of the Art Review," International Association for Hydraulic Research, The Netherlands, June, 1980.

Skinner, J.H., "Tube-Vehicle Drag," General Electric Co., Research and Development Center, Schenectady, New York, 1969.

Streeter, V.L., Handbook of Fluid Dynamics, McGraw-Hill Book Company, Inc., 1961, pp. 3-21.

Sud, I., and Chaddock, J.B., "Drag Calculations for Vehicles in Very Long Tubes from Turbulent Flow Theory," Journal of Fluids Engineering, Vol. 103, June 1981, pp. 361-366.

Sutter, K., "Der Luftwiderstand auf Eisenbahnzuge in Tunneln," Munchen, 1930.

Tanaka, T., et al., "Research Report on the New Tokaido Line," Vol. 4, 1963, p. 142.

Tollmein, Walter, "Luftwiderstand und Druckverlauf bei der Fahrt von Zugen in einem Tunnel," Zeitschrift des Verines Deutscher Ingerieure, Vol. 71, No. 6, Feb 5, 1927, pp. 199-202.

Van Driest, E.R., "On Turbulent Flow Near a Wall," Journal Aero. Science, vol. 23, 1956, pp. 1007-1012.

Weismann C., "Die Kunsliche Luftung in Stollen und Tunnelbau," 1919.

White, F.M., Fluid Mechanics, McGraw-Hill Inc., New York, 1979.

White, F.M., Viscous Fluid Flow, McGraw-Hill Inc., New York, 1974.

Wilson, N.W., and Medwell, J.O., "An Analysis of the Developing Turbulent Hydrodynamic and Thermal Boundary Layers in an Internally Heated Annulus," ASME Journal of Heat Transfer, Vol. 64, February 1971, pp. 25-32.

INITIAL DISTRIBUTION LIST

Addressee	No. of Copies
CNO (OP-22T)	1
CNR (OCNR-23--E. Remmers)	1
NAVSEA (SEA-56W1--P. Crabb)	1
DTIC	2
CNA	1
URI (Attn: Drs. F. White, R. Lessman, T. Kim, M. Sadd)	4